proteins, which act in a feedback loop to inhibit cytokine responses by terminating the activation of the JAK/STAT and other signaling pathways.[14–16] The SOCS family, characterized by a central src homology 2 (SH2) domain and a conserved C-terminus SOCS box, is composed of eight structurally related proteins. Among these, SOCS-1 is known as the *most potent negative regulator of proinflammatory cytokine* signaling.[17] SOCS-1 interacts with phosphorylated tyrosine residues on proteins such as JAK kinases[18,19] to interfere with the activation of STAT proteins or other signaling intermediates. SOCS-1 also recruits the elongin BC-containing E3 ubiquitin-ligase complex *via* the conserved SOCS box to promote the degradation of target proteins.[20] Studies on SOCS-1 deficient mice have indicated that SOCS-1 is essential for the inhibition of excessive immune responses and also are involved in the suppression of tumor development.[17,21] In accordance with this notion, epigenetic silencing of *SOCS-1* by methylation of the CpG island is detected in human cancers, such as hepatocellular carcinoma (HCC), multiple myeloma and pancreatic ductal neoplasm[22–25] and is implicated in cancer development.

Like other cancers, a variety of epigenetic alterations are involved in the development of GC.[26–30] Two groups have recently reported that transcriptional inactivation of *SOCS-1* gene by hypermethylation is frequently observed in GC cell lines[31] and primary GC samples.[32,33] In particular, Oshimo *et al.* have reported that *SOCS-1* gene hypermethylation is not detectable in normal gastric mucosa but is detected in 44% of primary GC tissues and 12% of corresponding non-neoplastic mucosa and is correlated with the progression and lymph node metastasis of GC.[33] However, it remains to be clarified whether the inactivation of *SOCS-1* gene is truly important for the oncogenesis of GC or which signaling pathways targeted by SOCS-1 are important for GC cell proliferation.

In our study, we demonstrate that SOCS-1 is silenced in GC cell lines and is involved in enhanced STAT3 activation in these cells. We also demonstrate that gene delivery of *SOCS-1* in GC cells has a potent antiproliferative effect *via* the suppression of not only JAK/STAT activation but also inhibition of p38 MAPK signaling pathway. Our results provide new insights into the pathogenesis of GC and may highlight potential molecular targets for therapeutic intervention in patients with GC.

Material and Methods

Cell lines

Four human GC cell lines NUGC3 (*JCRB0822*), *MKN45* (JCRB0254), NUGC4 (JCRB0834) and MKN7 (JCRB1025) were obtained from the Japanese Collection of Research Bioresources (Osaka, Japan), and AGS was purchased from the American Type Culture Collection (ATCC, Manassas, VA). All cell lines were maintained in RPMI 1640 medium supplemented with 10% fetal bovine serum (FBS) (HyClone Laboratories, Logan, UT) and 1% penicillin–streptomycin (Nacalai Tesque, Kyoto, Japan) at 37°C under a humidified atmosphere of 5% CO_2.

Enzyme-linked immunosorbent assay

Cell lines were cultured in six-well plates at a density of 1×10^5 cells per well and incubated in RPMI 1640 containing 1% FCS. The concentrations of IL-6, soluble IL-6 receptor (sIL-6R) in the cell culture supernatant was measured at 48-hr time points using Quantikine enzyme-linked immunosorbent assay (ELISA) kits (R&D Systems, Minneapolis, MN) according to the manufacturer's instructions. The ELISA sensitivities for the detection of IL-6 and sIL-6R, as reported by the manufacturer, were 0.7 and 6.5 pg/ml, respectively.

IL-6 and anti-IL-6R antibody treatment of GC cells

After 24 hr of serum starvation, GC cell lines were treated with 20 ng/ml of recombinant IL-6 (PeproTech, Rocky Hill, NJ) and 20 ng/ml of sIL-6R (R&D Systems) and proteins were extracted 15 min after IL-6 stimulation for further analysis. For antibody treatment, 25 and 50 μg/ml of MRA (humanized monoclonal anti-human IL-6R antibody; Chugai Pharmaceutical Co., Tokyo, Japan) was added to cell culture medium with recombinant 20 ng/ml IL-6 and 20 ng/ml sIL-6R. Purified human IgG (Sigma, St. Louis, MO) was used as control. Cells were then harvested for the determination of the phosphorylation status of STAT3.

Methylation-specific PCR

Bisulfite modification of genomic DNA was carried out as described previously.[22,31,33] The bisulfite-treated DNA was amplified with either a methylation-specific or unmethylation-specific primer set using EpiTect methylation-specific PCR (MSP) Kit (Qiagen, Valencia, CA) according to the manufacturer's instructions. The methylation-specific primer sequences in the exon 1 of *SOCS-1* CpG island were 5′-TC GTTCGTACGTCGATTATC-3′ (forward) and 5′-AAAAAA ATACCCACGAACTCG-3′ (reverse); sequences of corresponding unmethylation-specific primer sequences were 5′-TATTTTGTTTGTATGTTGATTATTG-3′ (forward) and 5′-AAACTCAACACACAACCACTC-3′ (reverse). The length of PCR products were 132 bp for methylated reaction, and 122 bp for the unmethylated reaction. PCR products were resolved in 2.5% agarose gels, stained with ethidium bromide and visualized under UV illumination. To ensure that the PCR primers are specific for the detection of methylated or unmethylated bisulfite converted DNA, completely methylated or unmethylated bisulfite converted DNAs, and *untreated, unmethylated genomic DNA (EpiTect control* DNA, Qiagen), were used for control experiments.

Real-time PCR analysis

After 12 hr of serum starvation, GC cell lines (NUGC3, AGS, MKN45, NUGC4 and MKN7) and human PBMC were treated with 10 ng/ml of recombinant human IFN-γ (PeproTech, Rocky Hill, NJ) for 15 min. Total RNA was prepared from cells using an RNeasy Mini Kit (Qiagen) and cDNAs were synthesized from 500 ng of each total RNA preparation using a Quantitect Reverse Transcription Kit (Qiagen), all according to the manufacturers' instructions. The forward and reverse primers were as follows: for human SOCS-1 forward primer, 5′-AGACCCCTTCTCACCTCTTG-3′ and *reverse primer*, 5′-GCACAGCAGAAAAATAAAGC-3′; for β-actin, 5′-GTGGGGCGCCCCAGGCACCA-3′ and 5′-CTCC TTAATGTCACGCACGATTTC-3′.[34] Primers and cDNA were added to SYBR green premix (Invitrogen), which contained all the reagents required for PCR. The PCR conditions of SOCS-1 consisted of 1 cycle at 95°C for 10 min followed by 40–50 cycles of 96°C for 10 sec, 68°C for 15 sec and 72°C for 15 sec; β-actin cycling conditions consisted of 1 cycle at 95°C for 10 min followed by 40–50 cycles of 96°C for 10 sec, 67°C for 30 sec and 72°C for 30 sec. PCR products were measured continuously using the My IQ™ Single-Color Real-Time Detection System (Bio-Rad Laboratories).

Adenoviral vectors

Replication-defective recombinant adenoviral vector expressing the mouse SOCS-1 gene was provided by Dr. Hiroyuki Mizuguchi (Osaka University, Osaka, Japan), which was constructed by an improved *in vitro* ligation method, as described previously.[35,36] An adenoviral vector expressing the LacZ gene was constructed using similar methods. Expression of these genes was regulated by CMV promoter/enhancer and intron A. The viruses were amplified in 293 cells. Viruses were purified by $CsCl_2$ step gradient ultracentrifugation followed by $CsCl_2$ linear gradient ultracentrifugation. The purified viruses were dialyzed against a solution containing 10 mM Tris-HCl (pH 7.5), 1 mM $MgCl_2$ and 10% glycerol and were stored at −80°C. Viral particle and biological titers were determined by a spectrophotometrical method[37] and by using QuickTiter (Adenovirus Titer Immunoassay Kit, Cell Biolabs, San Diego, CA), respectively. After 24-hr incubation of GC cells in culture medium containing 10% FCS, adenoviral vectors were infected by distributing suspensions onto cells at a multiplicity of infection (*MOI*) of *10–160*. Adenoviral vectors containing the genes for HA-tagged Y705F dominant-negative STAT3 (AddnSTAT3) were kindly provided by Dr. Akihiko Yoshimura (Keio University, Tokyo, Japan).

Western-blotting analysis

Cells and tumor tissues from xenograft model were lysed in RIPA buffer (10 mM Tris-HCl, pH 7.5, 150 mM NaCl, 1% Nonidet P-40, 0.1% sodium deoxycholate, 0.1% SDS, 1× *phosphatase inhibitor cocktail (Nacalai Tesque)* and 1× protease inhibitor cocktail (Nacalai Tesque) followed by centrifugation (13,200 rpm, 4°C, 15 min), after which the supernatants were stored at −80°C until use. Protein concentrations were determined with the DC Protein Assay kit (Bio-Rad Laboratories), using BSA as the concentration standard. Extracted proteins were used for SDS-PAGE or immunoprecipitation assay. For immunoprecipitation assay, extracted proteins were incubated with primary antibody coupled Protein G-Sepharose (BioVision, Mountain View, CA) for several hours at 4°C with rotating. The samples were washed several times with RIPA buffer, and proteins were extracted using SDS sample buffer (0.125 M Tris-HCl, pH 6.8, 10% 2-mercaptoethanol, 4% SDS, 10% glycerol and 0.004% bromophenol blue). Proteins were resolved using 5–20% gradient SDS-PAGE gels (Wako Pure Chemical Industries, Osaka, Japan) and subsequently transferred to PVDF membranes (Millipore, Bedford, MA). The membranes were blocked with 1% BSA in PBS containing 0.1% Tween 20 (PBST) and incubated with the respective antibodies against different targets. The following antibodies were used: anti-SOCS-1, 1:500 (IBL, Fujioka, Japan), anti-HA (Sigma), anti-phospho-STAT3, 1:1,000 (Cell Signaling Technology, Danvers, MA); anti-STAT3, 1:1,000; anti-GAPDH, 1:2,000 (all from Santa Cruz Biotechnology, Santa Cruz, CA).

Next, the membranes were incubated with horseradish peroxidase-conjugated sheep anti-mouse IgG or horseradish peroxidase-conjugated donkey anti-rabbit IgG (GE Healthcare, Little Chalfont, Buckinghamshire, UK). Finally, the signals were visualized by means of an enhanced chemiluminescence (ECL) reaction system (Perkin-Elmer Life Sciences, Boston, MA).

Cell proliferation assay

NUGC3 and AGS cells were plated in 96-well plates at a density of 5×10^2 cells per well and incubated in RPMI 1640 supplemented with 10% FCS for 24 hr. Then, cells were treated with 2.5 μM (NUGC3) and 5.0 μM (AGS) of JAK inhibitor I (Jak inhibitor; Calbiochem, San Diego, CA), with 10 μM (NUGC3) and 20 μM (AGS) of SB203580 (p38 MAP kinase inhibitor; Calbiochem), MRA (anti-human IL-6R antibody; Chugai Pharmaceutical Co.) and dimethyl sulfoxide (DMSO) or human IgG (Sigma) alone, followed by incubation at 37°C in RPMI 1640 supplemented with 5% FBS. Cell proliferation was evaluated with the WST-8 [2-(2-methoxy-4-nitrophenyl)-3-(4-nitrophenyl)-5-(2,4-disulfophenyl)-2H-tetrazolium, monosodium salt] assay (*Cell Counting Kit-SF;* Nacalai Tesque, Kyoto, Japan) at indicated period after treatment. The absorption of WST-8 was measured at a wavelength of 450 nm with a reference wavelength of 630 nm using a microplate reader Model 680 (Bio-Rad Laboratories, Hercules, CA). Growth rate was expressed as the percentage of absorbance reading for treated cells *vs.* control cells. Each value is the average ± standard deviation (SD) of triplicate wells.

Measurement of p38 MAP kinase and ERK activation

Kinase assays of p38MAPK were performed using commercial kits (Cell Signaling Technology). Cells were seeded 24 hr before the assay in a 100×100 mm^2 polystyrene nonpyrogenic dish at a density of 5×10^5 cells per dish. Cells were harvested at 48 hr after infection of adenoviral vectors and lysed with buffer (20 mM Tris, pH 7.5, 150 mM NaCl, 1

mM EDTA, 1% Triton X-100, 1 mM Na_3VO_4, 1 mg/ml leupeptin and 1 mM PMSF). Five hundred microliters of cell lysates containing 200 μg total protein were incubated with 20 μL of immobilized phospho-p38MAPK monoclonal antibody for p38MAPK assay. The mixtures were then incubated at 4°C overnight and centrifuged to obtain a cell pellet. The pellet was then washed two times with wash buffer and further two times with a kinase buffer (5 mM Tris, pH 7.5, 10 mM $MgCl_2$, 2 mM DTT and 0.1 mM Na_3VO_4). Kinase reactions were carried out in kinase buffer supplemented with 100 mM ATP and 2 μg activating transcription factor-2 (ATF-2) fusion protein as a substrate for p38MAPK assay. Reactions were performed at 30°C for 30 min and terminated by adding 5× SDS-PAGE sample buffer. Total ATF2 and phosphorylated substrates were analyzed by Western-blotting analysis using phospho-ATF-2 (Cell signaling Technology) antibody for kinase assay of p38MAPK.

Mouse xenograft model

All animal experiments were conducted according to the institutional ethical guidelines for animal experimentation of the National Institute of Biomedical Innovation (Osaka, Japan). Male ICR nu/nu mice, 4–5 weeks of age, were obtained from Charles River Japan (Yokohama, Japan). For subcutaneous xenograft experiments, we injected 2×10^6 cells in a total volume of 100 μL of 1/1 (v/v) PBS/Matrigel (Becton Dickinson, Bedford, MA) in the flank of ICR nu/nu mice. After 1 week when the tumor sizes reached to ~100 mm^3, 2×10^8 plaque-forming units (pfu)/50 μL of AdSOCS1 or AdLacZ was injected intratumorally twice per week. Tumor volumes were determined weekly by measuring in two dimensions, length (L) and width (W), and calculating volume as $(W^2 \times L)/2$.

Statistical analysis

Statistical analyses were performed using the StatView 5.0 software package (Abacus Concepts, Berkeley, CA). One-way ANOVA followed by a Scheffe's test or Mann–Whitney U tests were used to evaluate the significance of differences. In all analyses, $p < 0.05$ was considered statistically significant.

Results

Methylation status of SOCS-1 CpG islands in GC cell lines

Since it was reported that *SOCS-1* gene methylation is frequently observed in primary GC,[33] we initially screened five GC cell lines for methylation of the *SOCS-1* gene. By MSP analysis using primers selected from the CpG islands inside exon 1 of the *SOCS-1* gene, we detected *SOCS-1* methylation in all five (NUGC3, AGS, MKN45, NUGC4 and MKN7) GC cell lines (Fig. 1*a*). By real-time PCR analysis, we also found that these five GC cell lines, but not human PBMC, failed to upregulate *SOCS-1* expression in response to IFN-γ, indicating that transcription of the *SOCS-1* gene is inhibited by gene methylation (Fig. 1*b*).

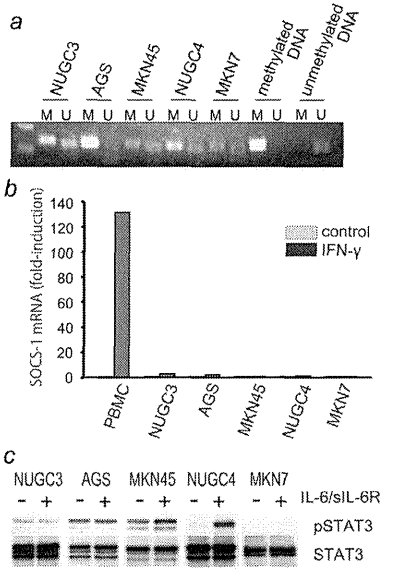

Figure 1. Methylation of *SOCS-1* CpG islands and activation of STAT3 in GC cells. (*a*) MSP of *SOCS-1* gene CpG islands. A visible PCR product in lane-M indicates the presence of methylated gene; the presence of product in lane-U indicates the presence of unmethylated gene. (*b*) Induction of the expression of *SOCS-1* gene with or without stimulation with IFN-γ was analyzed by real-time PCR. (*c*) The phosphorylation of STAT3 was analyzed by Western blotting. Cells were stimulated with 20 ng/ml recombinant IL-6 and 20 μg/ml sIL-6R for 10 min, and protein extracts were subjected to immunoblotting.

Constitutive activation of STAT3 in GC cell lines

We then evaluated the activation status of signal transducer and activator of transcription 3 (STAT3), since STAT3 acts as an important transcriptional mediator of proinflammatory cytokine signaling pathways and contributes to oncogenesis by both preventing apoptosis and enhancing cell proliferation.[11] STAT3 was constitutively phosphorylated in three of five GC cell lines, NUGC3, AGS and MKN45 cells (Fig. 1*c*), raising the possibility that epigenetic silencing of *SOCS* genes may lead to the aberrant activation of the JAK/STAT pathway in these GC cells. In other cell lines, STAT3 phosphorylation was induced strongly in NUGC4 cells after the stimulation with IL-6, but it was not induced in MKN7 cells (Fig. 1*c*).

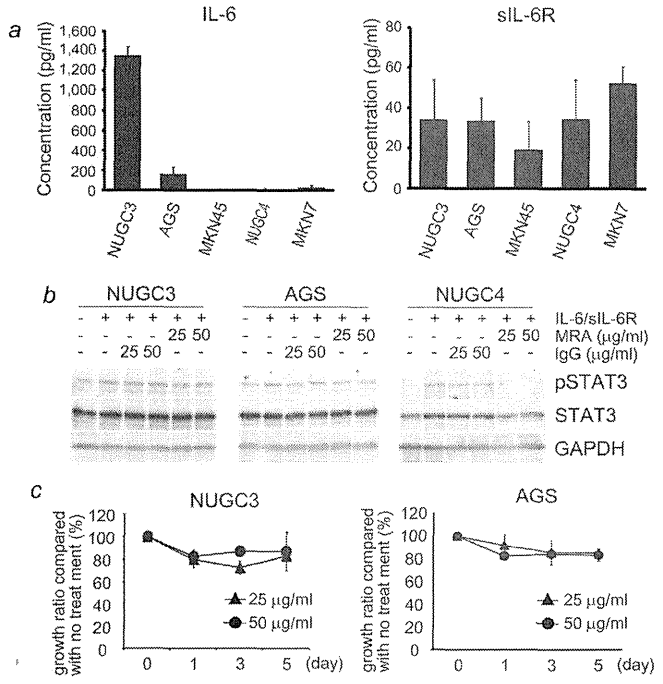

Figure 2. The role of IL-6 production in STAT3 phosphorylation and cell proliferation of GC cells. (*a*) ELISA of IL-6, soluble IL-6 receptor (sIL-6R) protein levels in conditioned media of six GC cell lines. Results are shown as mean ± SD from three independent experiments. (*b*) Effect of anti-IL-6R antibody (MRA) treatment on phosphorylation of STAT3 (Tyr705) was examined by Western-blot analysis in NUGC3, AGS and NUGC4 cell lines. Cell extracts were harvested 15 min after treatment with 20 ng/ml IL-6, 20 μg/ml sIL-6R and 25–50 μg/ml MRA or control IgG, and subjected for immunoblotting with phosphospecific STAT3 (Tyr705) antibody. (*c*) Cell proliferation curves of NUGC3 and AGS cells treated with MRA. Cells were cultured in medium containing 2% FCS with 25 and 50 μg/ml MRA or control human IgG. Cell proliferation was determined by WST-8 assay at 24, 72 and 120 hr after treatment. Percent of cell growth (percent of control) was expressed as mean ± SD value of percentage of absorbance reading from treated cells *vs.* control cells from triplicate wells.

No inhibitory effect of anti-IL-6R antibody on GC cell growth

Previous studies have revealed that IL-6 levels are elevated in cancer tissues[38] and in sera[39,40] of GC patients. We next quantitated levels of IL-6 and soluble IL-6 receptor (sIL-6R) in 48-hr culture supernatants of GC cell lines by sandwich ELISA. As shown in Figure 2*a*, elevated IL-6 levels were observed in NUGC3 cells (1348.6 ± 91.2 pg/ml) and AGS cells (166.3 ± 68.1 pg/ml), while sIL-6R secretion was comparable among all the cell lines tested (Fig. 2*b*). These results suggest that spontaneous production of IL-6 may be crucial for aberrant STAT3 phosphorylation in NUGC3 and AGS cells.

We then assessed the impact of IL-6 blockade on STAT3 phosphorylation and proliferation of NUGC3 and AGS cells, which have demonstrated constitutive STAT3 activation concomitant with high level of IL-6 production (Figs. 1*c* and 2*a*). Western-blot analysis confirmed that humanized anti-IL-6R monoclonal antibody (MRA), which inhibits IL-6 function by competing for the membrane bound and the soluble forms of the human IL-6 receptor,[41] effectively inhibited IL6-induced phosphorylation of STAT3 in NUGC4 cells. However, the

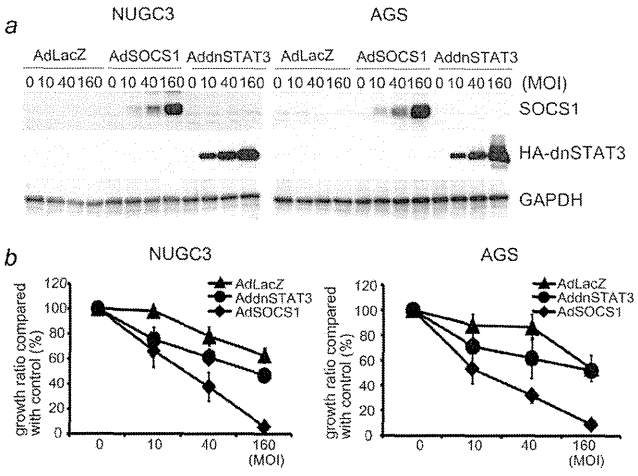

Figure 3. Antiproliferative effect of SOCS-1 in GC cells. (*a*) Western-blot analysis of whole cell extracts to confirm SOCS-1 expression in AdSOCS-1 transfected cells. Cells were infected with AdLacZ, AdSOCS-1 or AddnSTAT3 at an MOI of 10–160. Cell extracts were harvested 24 hr after transfection and subjected for immunoblotting. The expression of SOCS-1 and dnSTAT3 were determined by using anti-SOCS-1 antibody (SOCS-1) and anti-HA antibody (dnSTAT3). (*b*) Cells were infected with AdSOCS-1, AddnSTAT3 or AdLacZ at an MOI of 10–160. Cell proliferation was determined by WST-8 assay at 72 hr after treatment. Growth ratio of AdLacZ-, AdSOCS-1- or AddnSTAT3-infected cells was calculated as the percentage of absorbance reading for infected cells relative to that for nontreated cells. Each value is the average ± SD of triplicate wells.

same treatment could not reduce STAT3 phosphorylation in NUGC3 and AGS cells (Fig. 2*b*). In addition, cell proliferation assay using WST-8 showed that treatment with MRA did not suppress cell proliferation of IL6-producing GC cell lines (Fig. 2*c*). These *in vitro* results suggest that cell proliferation and constitutive STAT3 phosphorylation in NUGC3 and AGS cells occur independently of autocrine IL-6 production, and that signaling pathways other than IL-6 signaling may be involved in cell proliferation of these cells.

Antiproliferative effect of *SOCS-1* gene delivery in GC cells

We next investigated the role of SOCS-1 in regulation of intracellular signaling cascades and GC cell proliferation. For this purpose, we used replication-defective recombinant adenoviral vectors carrying SOCS-1 in cell proliferation assays. Given the established role of STAT3 in tumor development, we also assessed the effect of the inhibition of STAT3-depended pathways, using an adenoviral vector expressing dominant negative STAT3 (dnSTAT3). Immunoblotting analysis showed that adenovirus-mediated gene delivery could induce dose dependent expression of SOCS-1 and dnSTAT3 in both NUGC3 and AGS cells (Fig. 3*a*). As shown in Figure 3*b*, WST-8 assay revealed that adenovirus-mediated *SOCS-1* gene delivery markedly decreased cell proliferation of IL-6 producing NUGC3 and AGS cells. In addition, the magnitude of antiproliferative effects of AdSOCS-1 on GC cells was higher than that of AddnSTAT3. These results suggest that both SOCS-1 and dnSTAT3 can suppress proliferation of NUGC3 and AGS cells, but SOCS-1 is likely to exert additional effects on these GC cells.

Effect of *SOCS-1* gene delivery on JAK/STAT3, MAPK and PI3K pathways

We next determined the activation status of signaling molecules in GC cells infected with AdLacZ, AdSOCS-1 and AddnSTAT3. As shown in Figure 4*a*, immunoblotting analysis showed that phosphorylation levels of STAT3 were effectively decreased in NUGC3 and AGS cells treated with either AdSOCS-1 or AddnSTAT3. Since AdSOCS-1 inhibited GC cell proliferation more effectively than AddnSTAT3, we next investigated if AdSOCS-1 also downregulates STAT3-independent signaling pathway(s) in these cells. Our screening analyses indicated that AKT, SAPK/JNK and p44/p42 MAPK pathways were not affected by AdSOCS-1 infection, although these molecules were constitutively phosphorylated in NUGC3 and AGS cell lines (data not shown). We therefore

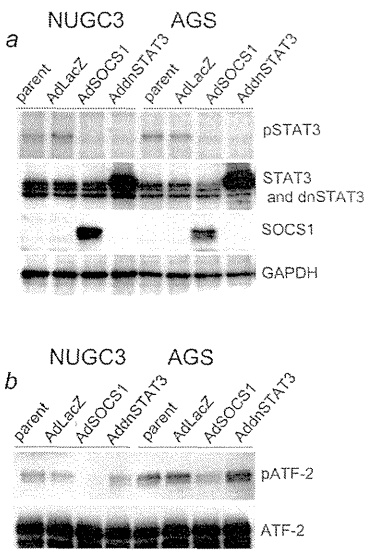

Figure 4. SOCS-1 suppressed the activation of STAT3 and p38 MAPK. (*a*) Cells were infected with AdLacZ, AdSOCS-1 or AddnSTAT3 at an MOI of 40. Cell lysates were prepared at 48 hr after infection, and immunoblotted with SOCS-1, phospho-STAT3 (p-STAT3) and STAT3 antibodies. (*b*) To investigate p38 MAP kinase activity, p38 MAPK was immunoprecipitated and used in an *in vitro* kinase assay with recombinant ATF2 as a substrate. Phosphorylated-ATF2 was determined by immunoblot analysis.

examined another MAPK pathway, the p38MAPK pathway, by evaluating kinase assays with ATF-2 as substrate. Interestingly, the activation of ATF2 in NUGC3 and AGS cells was reduced by AdSOCS-1 infection but not by AddnSTAT3 infection (Fig. 4*b*). Our results indicate that forced expression of SOCS-1 suppresses both JAK/STAT3 and p38 MAPK pathway in NUGC3 and AGS cells.

Inhibition of JAK kinase- and p38 MAP kinase-induced suppression of cell proliferation in GC cells

To confirm whether the activities of JAK/STAT and p38 MAP kinase signaling pathways regulate proliferation of these GC cancer cells, cells were treated with the JAK inhibitor (JAK Inhibitor I), p38 MAP kinase inhibitor (SB203580) or both. Cell proliferation assays revealed that JAK inhibitor I markedly suppressed proliferation in NUGC3 cells (Fig. 5*a*), and moderately suppressed proliferation in AGS cells (Fig. 5*b*). SB203580 suppressed cell proliferation of both NUGC3 and AGS cells more effectively than JAK inhibitor I (Figs. 5*a*

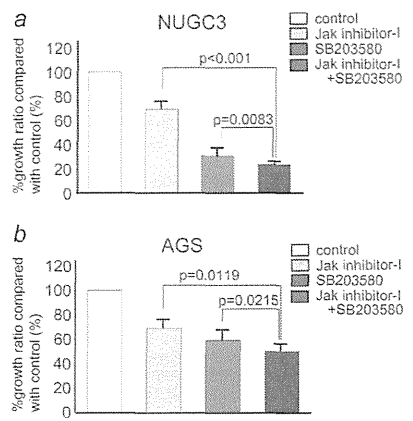

Figure 5. Inhibitors of JAK/STAT and the p38 MAPK signaling pathways suppressed cell growth in GC cells. (*a*) NUGC3 cells and (*b*) AGS cells were cultured in RPMI 1640 medium containing 5% FBS with JAK inhibitor (JAK inhibitor I), with p38 MAPK inhibitor (SB203580) or with JAK inhibitor I and SB203580. Cell proliferation activity was assessed by WST-8-based assay at 72 hr after treatment. Growth ratio (mean ± SD) was calculated as the percentage of absorbance reading for treated cells relative to that for control (DMSO) cells from three independent experiments.

and 5*b*). In both NUGC3 and AGS cells, combined treatment with JAK inhibitor I and SB203580 further suppressed the proliferation of these GC cell lines (Figs. 5*a* and 5*b*). Thus, our results suggest that both JAK/STAT3 and p38 MAPK signaling pathways play crucial roles in the proliferation of NUGC3 and AGS cells.

SOCS-1 exhibits antitumor activity in a GC xenograft model

We also evaluated the therapeutic effect of AdSOCS-1 injection on the growth of GC cells *in vivo*. For this purpose, we established a xenograft model of ICR nu/nu mice in which NUGC3 cells were subcutaneously implanted. Injection of AdSOCS-1 vector (1×10^8 pfu/50 μL) intratumorally twice per week suppressed tumor growth compared to tumor volumes in control AdLacZ-injected animals (Figs. 6*a* and 6*b*). AdSOCS-1 *in vivo* could modulate intracellular signaling in GC cells *as in vitro*, since Western-blot analysis showed that phosphorylation levels of STAT3 were decreased in the NUGC3 tissues from AdSOCS-1 injected animals (Fig. 6*c*).

Discussion

Proinflammatory cytokines induced by *H. pylori* infection are critical for both chronic inflammation in gastric mucosa and

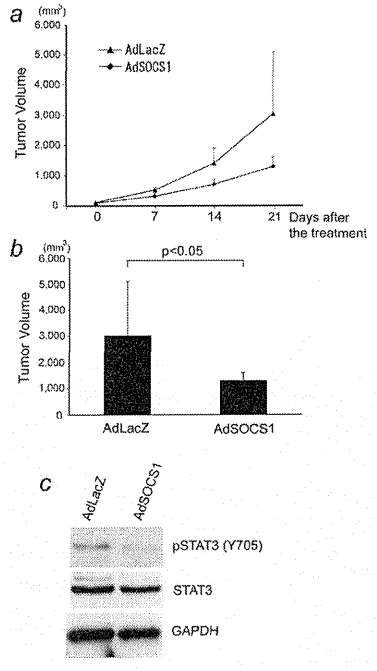

Figure 6. SOCS-1 exhibits antitumor activity in a GC xenograft model. (*a*) Male ICR nu/nu mice, 1 week after the subcutaneous implantation of 2×10^6 NUGC3 cells in their flank, were intratumorally treated with 2×10^8 pfu of AdSOCS1 or AdLacZ twice per week. Tumor volumes were determined weekly. Figures show the average (points) ± SD (bars) for four animals. (*b*) Twenty-eight days after tumor cell inoculation, each tumor volume was calculated. Figures show the average (columns) ± SD (bars) for four animals. (*c*) Western-blot analysis of pSTAT3, STAT3 and GAPDH in NUGC3 tissues from AdSOCS1 or AdLacZ injected animals. NUGC3 tumor-bearing animals were treated once with AdSOCS1 or AdLacZ on day 7 and sacrificed on day 10. Lysates from tumors were analyzed by Western blot.

the initiation and progression of GC. It is thus reasonable to speculate that the changes in sensitivity of gastric epithelial cells to proinflammatory cytokines greatly contribute to the development of GC. In our study, we provide evidence that silencing of *SOCS-1*, a negative regulator of cytokine signaling, is profoundly involved in the development of GC.

We identified *SOCS-1* gene methylation in GC cell lines (Fig. 1*a*). This result is consistent with the previous findings that hypermethylation of the *SOCS-1* gene is detected in GC cell lines and primary GC tissues.[31,33] To *et al.* have previously shown that demethylation treatment can increase SOCS-1 expression and reduce STAT3 activation in GC cell lines.[32] In our study, we demonstrated that forced SOCS-1 expression can inhibit STAT3 activation in GC cells and suppress their proliferation. Our results together with To *et al.* suggest that SOCS-1 functions as a tumor suppressor in GC cells, and its gene silencing should promote GC development and progression.

In our study, we showed that high levels of IL-6 are spontaneously produced in NUGC3 and AGS cell lines. Previous studies have shown that IL-6 facilitates GC cell invasion *in vitro*[42] and serum IL-6 levels correlate well with disease progression and recurrence in GC.[39,40,43] Moreover, the methylation of *SOCS-1* gene is associated with lymph node metastasis and advanced tumor stage in GC.[33] Thus, NUGC3 and AGS cell lines share two features (IL-6 production and *SOCS-1* methylation) of GC with poor prognosis. While the frequency of GC that possesses these two features is currently unknown, future studies on both IL-6-producing capacity and *SOCS-1 gene* methylation status in GC may help to predict the prognosis of GC.

We showed here that STAT3 is persistently activated in several GC cell lines. Similar activation of STAT3 has been reported in other cancer cell lines in which *SOCS-1* gene expression is downregulated by DNA methylation.[22,24,25] One possible mechanism for STAT3 activation in these cells is constitutive production of cytokines such as IL-6. However, in IL-6-producing NUGC3 and AGS cells, anti-IL-6R antibody failed to reduce STAT3 phosphorylation (Fig. 2), suggesting that IL-6 does not act as an autocrine growth factor in these GC cells. Interestingly, conditioned culture media of NUGC3 cells could induce STAT3 phosphorylation in anti-IL-6R antibody-treated human umbilical vein endothelial cells (Supporting Information Fig. 1), suggesting the presence of unknown soluble factor(s) contributing to the STAT3 phosphorylation in NUGC3 cells. However, IL-11, another member of IL-6 family possibly involved in the development of GC,[44] was not elevated in conditioned media of NUGC3 cells (data not shown). These results, nevertheless, suggest that the blockade of IL-6 may have limited therapeutic effects on the growth signals in established GC cells.

In contrast to IL-6 blockade, adenovirus-mediated forced expression of SOCS-1 or dnSTAT3 successfully suppressed cell proliferation of NUGC3 and AGS cells (Fig. 3). The suppressive effect of STAT3 inhibition on GC cell proliferation has been reported previously.[12] Importantly, however, the magnitude of antiproliferative effects of AdSOCS-1 was superior to that of AddnSTAT3, suggesting that AdSOCS-1 has additional mechanism(s) of action distinct from that of AddnSTAT3. Indeed, proliferation of MKN7 cells, in which constitutively phosphorylated STAT3 was not detected (Fig. 1*c*), was successively inhibited by AdSOCS-1, but not by AddnSTAT3 (Supporting Information Fig. 2). Furthermore,

proliferation of MKN45 cells, which exhibited constitutive STAT3 phosphorylation (Fig. 1*c*), was also inhibited by AdSOCS-1 but, surprisingly, not by AddnSTAT3 (Supporting Information Fig. 2). These results indicate that SOCS-1 inhibits not only JAK/STAT3-dependent pathway but also STAT3-independent growth signal pathways. In accordance with this, we found that p38MAPK pathway in GC cells is downregulated by SOCS-1. Moreover, inhibition of these two pathways using JAK inhibitor I and SB203580 had significant antiproliferative effects on GC proliferation. Thus, our results suggest that the potent antiproliferative effect of SOCS-1 is associated with combined inhibition of JAK/STAT3 and p38 MAPK pathways in GC cells.

MAPK family including p38MAPK is activated by a variety of environmental stresses and inflammatory cytokines, and traditionally is thought to play a role in differentiation, growth arrest, inflammation, immune activation and apoptosis. *In vivo*, p38MAPK may function as a tumor suppressor, since mice lacking p38α are sensitized to lung and liver tumors.[45] However, for the development of *H. pylori*-associated GC, p38 MAPK/ATF-2-mediated COX-2 was reported to be necessary.[46] Further studies are needed to elucidate the exact role of p38 MAPK signaling pathway for the growth of GC cells.

In our study, the mechanism by which SOCS-1 suppress the activation of p38 MAPK was not determined. One possible target of SOCS proteins is apoptosis signal-regulating kinase 1 (ASK1), an upstream activator of both the p38 MAPK and JUN N-terminal kinase (JNK) cascades. Supporting this possibility, it has been reported that SOCS-1 regulates the activation of stress-activated MAPKs by binding to ASK1.[47] Moreover, a recent study has shown that ASK1 contributes to tumor growth in GC.[48] SOCS-1 may also target other proteins in GC cells, since SOCS-1 can interact with a variety of tyrosine-phosphorylated proteins *via* their SH2 domain and promote the degradation of target proteins *via* the SOCS box.[21] Recently, we showed that adenoviral gene delivery of SOCS-3, one of the genes of the SOCS family, could inhibit growth of malignant pleural mesothelioma cells *in vitro* and *in vivo via* the modulation of multiple pathways involving JAK/STAT3, ERK, FAK and p53.[41] Although further studies are required, SOCS-1 may also act as an inhibitor of a wide variety of growth signals and may be applicable to the treatment of various types of GC.

In conclusion, we identified *SOCS-1* gene methylation in GC cell lines and highlighted a potent antiproliferative effect of SOCS-1 on GC cells both *in vitro* and *in vivo*, *via* the inhibition of JAK/STAT3 and p38 MAPK activation. Epigenetic silencing of *SOCS-1* may thus represent a critical step in the development of human GC and forced expression of SOCS-1 may represent a novel therapeutic approach for various types of GC through the inhibition of JAK/STAT3 and p38 MAPK signaling pathways.

Acknowledgements

We thank Y. Ito, N. Kawakami and Y. Kanazawa for secretarial assistance, and M. Urase for technical assistance.

References

1. Pisani P, Parkin DM, Ferlay J. Estimates of the worldwide mortality from eighteen major cancers in 1985. Implications for prevention and projections of future burden. *Int J Cancer* 1993; 55:891–903.
2. Dicken BJ, Bigam DL, Cass C, Mackey JR, Joy AA, Hamilton SM. Gastric adenocarcinoma: review and considerations for future directions. *Ann Surg* 2005;241:27–39.
3. Grivennikov SI, Greten FR, Karin M. Immunity, inflammation, and cancer. *Cell* 2010;140:883–99.
4. Peek RM, Jr, Crabtree JE. Helicobacter infection and gastric neoplasia. *J Pathol* 2006;208:233–48.
5. Lacronique V, Boureux A, Valle VD, Poirel H, Quang CT, Mauchauffe M, Berthou C, Lessard M, Berger R, Ghysdael J, Bernard OA. A TEL-JAK2 fusion protein with constitutive kinase activity in human leukemia. *Science* 1997;278: 1309–12.
6. Burke WM, Jin X, Lin HJ, Huang M, Liu R, Reynolds RK, Lin J. Inhibition of constitutively active Stat3 suppresses growth of human ovarian and breast cancer cells. *Oncogene* 2001;20: 7925–34.
7. Bromberg JF, Wrzeszczynska MH, Devgan G, Zhao Y, Pestell RG, Albanese C, Darnell JE, Jr. Stat3 as an oncogene. *Cell* 1999;98:295–303.
8. Rahaman SO, Harbor PC, Chernova O, Barnett GH, Vogelbaum MA, Haque SJ. Inhibition of constitutively active Stat3 suppresses proliferation and induces apoptosis in glioblastoma multiforme cells. *Oncogene* 2002;21:8404–13.
9. Zhang F, Li C, Halfter H, Liu J. Delineating an oncostatin M-activated STAT3 signaling pathway that coordinates the expression of genes involved in cell cycle regulation and extracellular matrix deposition of MCF-7 cells. *Oncogene* 2003;22: 894–905.
10. He B, You L, Uematsu K, Zang K, Xu Z, Lee AY, Costello JF, McCormick F, Jablons DM. SOCS-3 is frequently silenced by hypermethylation and suppresses cell growth in human lung cancer. *Proc Natl Acad Sci USA* 2003;100:14133–8.
11. Yu H, Pardoll D, Jove R. STATs in cancer inflammation and immunity: a leading role for STAT3. *Nat Rev Cancer* 2009;9:798–809.
12. Kanda N, Seno H, Konda Y, Marusawa H, Kanai M, Nakajima T, Kawashima T, Nanakin A, Sawabu T, Uenoyama Y, Sekikawa A, Kawada M, et al. STAT3 is constitutively activated and supports cell survival in association with survivin expression in gastric cancer cells. *Oncogene* 2004; 23:4921–9.
13. Howlett M, Menheniott TR, Judd LM, Giraud AS. Cytokine signalling via gp130 in gastric cancer. *Biochim Biophys Acta* 2009;1793:1623–33.
14. Naka T, Narazaki M, Hirata M, Matsumoto T, Minamoto S, Aono A, Nishimoto N, Kajita T, Taga T, Yoshizaki K, Akira S, Kishimoto T. Structure and function of a new STAT-induced STAT inhibitor. *Nature* 1997;387:924–9.
15. Starr R, Willson TA, Viney EM, Murray LJ, Rayner JR, Jenkins BJ, Gonda TJ, Alexander WS, Metcalf D, Nicola NA, Hilton DJ. A family of cytokine-inducible inhibitors of signalling. *Nature* 1997;387:917–21.
16. Endo TA, Masuhara M, Yokouchi M, Suzuki R, Sakamoto H, Mitsui K, Matsumoto A, Tanimura S, Ohtsubo M, Misawa H, Miyazaki T, Leonor N, et al. A new protein containing an SH2 domain that inhibits JAK kinases. *Nature* 1997;387:921–4.
17. Yoshimura A, Naka T, Kubo M. SOCS proteins, cytokine signalling and immune regulation. *Nat Rev Immunol* 2007;7:454–65.
18. Narazaki M, Fujimoto M, Matsumoto T, Morita Y, Saito H, Kajita T, Yoshizaki K, Naka T, Kishimoto T. Three distinct domains of SSI-1/SOCS-1/JAB protein are required for its suppression of interleukin 6 signaling. *Proc Natl Acad Sci USA* 1998;95:13130–4.
19. Yasukawa H, Misawa H, Sakamoto H, Masuhara M, Sasaki A, Wakioka T, Ohtsuka S, Imaizumi T, Matsuda T, Ihle JN, Yoshimura A. The JAK-binding protein JAB inhibits Janus tyrosine kinase activity through binding in the activation loop. *EMBO J* 1999;18:1309–20.
20. Krebs DL, Hilton DJ. SOCS proteins: negative regulators of cytokine signaling. *Stem Cells* 2001; 19:378–87.
21. Naka T, Fujimoto M, Tsutsui H, Yoshimura A. Negative regulation of cytokine and TLR signalings by SOCS and others. *Adv Immunol* 2005;87:61–122.
22. Yoshikawa H, Matsubara K, Qian GS, Jackson P, Groopman JD, Manning JE, Harris CC, Herman JG. SOCS-1, a negative regulator of the JAK/

STAT pathway, is silenced by methylation in human hepatocellular carcinoma and shows growth-suppression activity. *Nat Genet* 2001;28: 29–35.
23. Nagai H, Kim YS, Konishi N, Baba M, Kubota T, Yoshimura A, Emi M. Combined hypermethylation and chromosome loss associated with inactivation of SSI-1/SOCS-1/JAB gene in human hepatocellular carcinomas. *Cancer Lett* 2002;186:59–65.
24. Fukushima N, Sato N, Sahin F, Su GH, Hruban RH, Goggins M. Aberrant methylation of suppressor of cytokine signalling-1 (SOCS-1) gene in pancreatic ductal neoplasms. *Br J Cancer* 2003;89:338–43.
25. Galm O, Yoshikawa H, Esteller M, Osieka R, Herman JG. SOCS-1, a negative regulator of cytokine signaling, is frequently silenced by methylation in multiple myeloma. *Blood* 2003; 101:2784–8.
26. Yasui W, Oue N, Kuniyasu H, Ito R, Tahara E, Yokozaki H. Molecular diagnosis of gastric cancer: present and future. *Gastric Cancer* 2001;4: 113–21.
27. Yokozaki H, Yasui W, Tahara E. Genetic and epigenetic changes in stomach cancer. *Int Rev Cytol* 2001;204:49–95.
28. Yasui W, Oue N, Aung PP, Matsumura S, Shutoh M, Nakayama H. Molecular-pathological prognostic factors of gastric cancer: a review. *Gastric Cancer* 2005;8:86–94.
29. Yasui W, Yokozaki H, Fujimoto J, Naka K, Kuniyasu H, Tahara E. Genetic and epigenetic alterations in multistep carcinogenesis of the stomach. *J Gastroenterol* 2000;35 (Suppl 12): 111–5.
30. Yasui W, Oue N, Sentani K, Sakamoto N, Motoshita J. Transcriptome dissection of gastric cancer: identification of novel diagnostic and therapeutic targets from pathology specimens. *Pathol Int* 2009;59:121–36.
31. To KF, Chan MW, Leung WK, Ng EK, Yu J, Bai AH, Lo AW, Chu SH, Tong JH, Lo KW, Sung JJ, Chan FK. Constitutional activation of IL-6-mediated JAK/STAT pathway through hypermethylation of SOCS-1 in human gastric cancer cell line. *Br J Cancer* 2004;91:1335–41.
32. Aihara M, Tsuchimoto D, Takizawa H, Azuma A, Wakebe H, Ohmoto Y, Imagawa K, Kikuchi M, Mukaida N, Matsushima K. Mechanisms involved in Helicobacter pylori-induced interleukin-8 production by a gastric cancer cell line, MKN45. *Infect Immun* 1997;65:3218–24.
33. Oshimo Y, Kuraoka K, Nakayama H, Kitadai Y, Yoshida K, Chayama K, Yasui W. Epigenetic inactivation of SOCS-1 by CpG island hypermethylation in human gastric carcinoma. *Int J Cancer* 2004;112:1003–9.
34. Yamana J, Yamamura M, Okamoto A, Aita T, Iwahashi M, Sunahori K, Makino H. Resistance to IL-10 inhibition of interferon gamma production and expression of suppressor of cytokine signaling 1 in CD4+ T cells from patients with rheumatoid arthritis. *Arthritis Res Ther* 2004;6:R567–77.
35. Mizuguchi H, Kay MA. A simple method for constructing E1- and E1/E4-deleted recombinant adenoviral vectors. *Hum Gene Ther* 1999;10: 2013–7.
36. Sakurai H, Tashiro K, Kawabata K, Yamaguchi T, Sakurai F, Nakagawa S, Mizuguchi H. Adenoviral expression of suppressor of cytokine signaling-1 reduces adenovirus vector-induced innate immune responses. *J Immmunol* 2008;180:4931–8.
37. Maizel JV, Jr, White DO, Scharff MD. The polypeptides of adenovirus. I. Evidence for multiple protein components in the virion and a comparison of types 2, 7A, and 12. *Virology* 1968;36:115–25.
38. Yamaoka Y, Kodama T, Kita M, Imanishi J, Kashima K, Graham DY. Relation between cytokines and *Helicobacter pylori* in gastric cancer. *Helicobacter* 2001;6:116–24.
39. Wu CW, Wang SR, Chao MF, Wu TC, Lui WY, P'Eng F K, Chi CW. Serum interleukin-6 levels reflect disease status of gastric cancer. *Am J Gastroenterol* 1996;91:1417–22.
40. Ashizawa T, Okada R, Suzuki Y, Takagi M, Yamazaki T, Sumi T, Aoki T, Ohnuma S. Clinical significance of interleukin-6 (IL-6) in the spread of gastric cancer: role of IL-6 as a prognostic factor. *Gastric Cancer* 2005;8:124–31.
41. Iwahori K, Serada S, Fujimoto M, Nomura S, Osaki T, Lee CM, Mizuguchi H, Takahashi T, Ripley B, Okumura M, Kawase I, Kishimoto T, Naka T. Overexpression of SOCS3 exhibits preclinical antitumor activity against malignant pleural mesothelioma. *Int J Cancer*. 2011;129: 1005–17.
42. Lin MT, Lin BR, Chang CC, Chu CY, Su HJ, Chen ST, Jeng YM, Kuo ML. IL-6 induces AGS gastric cancer cell invasion via activation of the c-Src/RhoA/ROCK signaling pathway. *Int J Cancer* 2007;120:2600–8.
43. Kabir S, Daar GA. Serum levels of interleukin-1, interleukin-6 and tumour necrosis factor-alpha in patients with gastric carcinoma. *Cancer Lett* 1995; 95:207–12.
44. Howlett M, Giraud AS, Lescesen H, Jackson CB, Kalantzis A, van Driel IR, Robb L, van der Hoek M, Ernst M, Minamoto T, Boussioutas A, Oshima H, et al. The interleukin-6 family cytokine interleukin-11 regulates homeostatic epithelial cell turnover and promotes gastric tumor development. *Gastroenterology* 2009;136:967–77.
45. Cuadrado A, Nebreda AR. Mechanisms and functions of p38 MAPK signalling. *Biochem J* 2010;429:403–17.
46. Li Q, Liu N, Shen B, Zhou L, Wang Y, Sun J, Fan Z, Liu RH. Helicobacter pylori enhances cyclooxygenase 2 expression via p38MAPK/ATF-2 signaling pathway in MKN45 cells. *Cancer Lett* 2009;278:97–103.
47. He Y, Zhang W, Zhang R, Zhang H, Min W. SOCS1 inhibits tumor necrosis factor-induced activation of ASK1-JNK inflammatory signaling by mediating ASK1 degradation. *J Biol Chem* 2006;281:5559–66.
48. Hayakawa Y, Hirata Y, Nakagawa H, Sakamoto K, Hikiba Y, Kinoshita H, Nakata W, Takahashi R, Tateishi K, Tada M, Akanuma M, Yoshida H, et al. Apoptosis signal-regulating kinase 1 and cyclin D1 compose a positive feedback loop contributing to tumor growth in gastric cancer. *Proc Natl Acad Sci USA* 2011;108:780–5.

Suppressor of Cytokine Signaling 1 DNA Administration Inhibits Inflammatory and Pathogenic Responses in Autoimmune Myocarditis

Kazuko Tajiri,*,† Kyoko Imanaka-Yoshida,‡,§ Akihiro Matsubara,*,¶ Yusuke Tsujimura,* Michiaki Hiroe,‖ Tetsuji Naka,# Nobutake Shimojo,† Satoshi Sakai,† Kazutaka Aonuma,† and Yasuhiro Yasutomi*,¶

Myocarditis and subsequent dilated cardiomyopathy are major causes of heart failure in young adults. Myocarditis in humans is highly heterogeneous in etiology. Recent studies have indicated that a subgroup of myocarditis patients may benefit from immune-targeted therapies, because autoimmunity plays an important role in myocarditis as well as contributing to the progression to cardiomyopathy and heart failure. Suppressor of cytokine signaling (SOCS) 1 plays a key role in the negative regulation of both TLR- and cytokine receptor-mediated signaling, which is involved in innate immunity and subsequent adaptive immunity. In this study, we investigated the therapeutic effect of SOCS1 DNA administration on experimental autoimmune myocarditis (EAM) in mice. EAM was induced by s.c. immunization with cardiac-specific peptides derived from α myosin H chain in BALB/c mice. In contrast to control myocarditis mice, SOCS1 DNA-injected mice were protected from development of EAM and heart failure. SOCS1 DNA administration was effective for reducing the activation of autoreactive CD4⁺ T cells by inhibition of the function of Ag-presenting dendritic cells. Our findings suggest that SOCS1 DNA administration has considerable therapeutic potential in individuals with autoimmune myocarditis and dilated cardiomyopathy. *The Journal of Immunology*, **2012, 189: 2043–2053.**

Dilated cardiomyopathy (DCM) is a potentially lethal disorder of various etiologies for which no treatment is currently satisfactory (1); it often results from enteroviral myocarditis (2, 3). Many patients show heart-specific autoantibodies (3, 4), and immunosuppressive therapy can improve cardiac function in DCM patients who show no evidence of viral or bacterial genomes in heart biopsy samples (5). These observations suggest that autoimmunity plays an important role in myocarditis as well as contributing to the progression to cardiomyopathy and heart failure (6).

Experimental autoimmune myocarditis (EAM) is a model of postinfectious myocarditis and cardiomyopathy (7). A number of proinflammatory cytokines, including IL-1β, IL-6, IL-12, TNF-α, and GM-CSF, have been shown to contribute to the development of autoimmune myocarditis in animal models and human cases (8–13). EAM is a CD4⁺ T cell-mediated disease (7, 14), and activation of self-Ag–loaded dendritic cells (DCs) is critical for expansion of autoreactive CD4⁺ T cells. Activation of TLRs and IL-1 type I receptor and their common downstream signaling adaptor molecule, MyD88, in self-Ag–presenting DCs is also critical for the development of EAM (11, 15, 16). Compared with inhibition of a single cytokine, a more effective treatment might be inhibition of various signaling pathways to induce production of cytokines through both innate and adaptive immunity. One strategy that could accomplish this would be to target shared cytokine and TLR signal transduction pathways using suppressor of cytokine signaling (SOCS) molecules.

Recent lines of evidence indicate that SOCS proteins, originally identified as negative-feedback regulators in cytokine signaling, are involved in the regulation of TLR-mediated immune responses (17, 18). The SOCS family is composed of eight members: cytokine-inducible Src homology 2 domain-containing protein and SOCS1 to SOCS7 (19, 20). SOCS1 plays a key role in the negative regulation of both TLR-mediated signaling and cytokine receptor-mediated signaling, which are involved in innate immunity and subsequent adaptive immunity (21). The expression of SOCS1 is induced by various cytokines, including IFN-γ, IL-4, and IL-6, and also by TLR ligands, such as LPS and CpG-DNA (22). Several studies have demonstrated that SOCS1 is a negative regulator of LPS-induced macrophage activation and plays an essential role in suppression of systemic autoimmunity mediated by DCs (23–25). Thus, SOCS1 regulates not only adaptive immunity

*Laboratory of Immunoregulation and Vaccine Research, Tsukuba Primate Research Center, National Institute of Biomedical Innovation, Tsukuba, Ibaraki 305-0843, Japan; †Department of Cardiovascular Medicine, Majors of Medical Sciences, Graduate School of Comprehensive Human Sciences, University of Tsukuba, Tsukuba, Ibaraki 305-8575, Japan; ‡Department of Pathology and Matrix Biology, Mie University Graduate School of Medicine, Tsu, Mie 514-8507, Japan; §Mie University Matrix Biology Research Center, Mie University Graduate School of Medicine, Tsu, Mie 514-8507, Japan; ¶Division of Immunoregulation, Department of Molecular and Experimental Medicine, Mie University Graduate School of Medicine, Tsu, Mie 514-8507, Japan; ‖Department of Cardiology, National Center for Global Health and Medicine, Shinjuku, Tokyo 162-8655, Japan; and #Laboratory of Immune Signal, National Institute of Biomedical Innovation, Ibaragi, Osaka 565-0871, Japan

Received for publication December 13, 2011. Accepted for publication June 5, 2012.

This work was supported by Health Science Research grants from the Ministry of Health, Labor and Welfare of Japan and the Ministry of Education, Culture, Sports, Science and Technology of Japan.

Address correspondence and reprint requests to Dr. Yasuhiro Yasutomi, Laboratory of Immunoregulation and Vaccine Research, Tsukuba Primate Research Center, National Institute of Biomedical Innovation, 1-1 Hachimandai, Tsukuba, Ibaraki 305-0843, Japan. E-mail address: yasutomi@nibio.go.jp

The online version of this article contains supplemental material.

Abbreviations used in this article: BMDC, bone marrow-derived dendritic cell; DC, dendritic cell; dnSOCS1, dominant-negative suppressor of cytokine signaling 1; EAM, experimental autoimmune myocarditis; FS, fractional shortening; KO, knockout; LV, left ventricular; LVEDd, left ventricular end-diastolic dimension; LVESd, left ventricular end-systolic dimension; MyHC-α, cardiac myosin-specific peptide; pdnSOCS1, plasmid vector encoding dominant-negative suppressor of cytokine signaling 1; pSOCS1, plasmid vector encoding suppressor of cytokine signaling 1; QRT-PCR, quantitative real-time RT-PCR; SOCS, suppressor of cytokine signaling.

www.jimmunol.org/cgi/doi/10.4049/jimmunol.1103610

but also innate immunity by suppressing hyperactivation of macrophages and DCs.

In this study, we describe the therapeutic effect of SOCS1 DNA administration using plasmid DNA encoding SOCS1 for EAM. SOCS1 DNA therapy reduces myocarditis by regulating DC populations during EAM.

Materials and Methods

Animals

BALB/c mice and CB17.SCID mice were purchased from CLEA Japan. We used 5–7-wk-old male mice. All animals were cared for according to ethical guidelines approved by the Institutional Animal Care and Use Committee of the National Institute of Biomedical Innovation.

Immunization protocols

Mice were immunized with 100 μg cardiac myosin-specific peptide (MyHC-$\alpha_{614-629}$) Ac-RSLKLMATLFSTYASADR-OH (Toray Research Center) emulsified 1:1 in PBS/CFA (1 mg/ml; H37Ra; Sigma-Aldrich) on days 0 and 7 as described previously (12). For DC immunization, bone marrow-derived DCs (BMDCs) were generated as described (26). BMDCs were pulsed overnight with 10 μg/ml MyHC-α peptide and stimulated for another 4 h with 0.1 μg/ml LPS (Sigma-Aldrich) and 5 μg/ml anti-CD40 (BD Pharmingen) (15). Recipient mice received 2.5×10^5 pulsed and activated BMDCs i.p. on days 0, 2, and 4 and were killed 10 d after the first injection.

Plasmid construction and DNA transfection

Mouse SOCS1 cDNA and dominant-negative SOCS1 (dnSOCS1) cDNA were subcloned into the mammalian vector pcDNA3.1-myc/His(-) using oligonucleotide primers containing restriction sites for XhoI and EchoRI at the 5′ and 3′ ends, respectively. MyHC-α/CFA-immunized mice were injected i.p. with 100 μg of plasmid DNA in 200 μl PBS on days 0, 5, and 10. BMDC-transferred mice and $CD4^+$ T cell adoptive-transferred SCID mice were treated with plasmid DNA on days 0 and 5.

Histopathologic examination

Myocarditis severity was scored on H&E-stained sections using grades from 0–4: 0, no inflammation; 1, <25% of the heart section involved; 2, 25–50%; 3, 50–75%; and 4, >75%. To quantify the fibrotic area, ventricular sections were stained with Sirius Red. The fibrotic area was calculated as the sum of all areas stained positive for Sirius Red divided by the sum of all myocardial areas in each mouse. Two independent researchers scored the slides separately in a blinded manner.

Flow cytometry

Heart inflammatory cells were isolated and processed as described (15, 27). Cells were stained using fluorochrome-conjugated mouse-specific Abs against CD45, CD4, CD3e, CD44, CD62L, and CD40L (BD Biosciences). Samples were analyzed on an FACSCalibur cell sorter (BD Biosciences).

Measurements of cytokines and chemokines

Hearts were homogenized in media containing 2.5% FBS. Supernatants were collected after centrifugation and stored at −80°C. For in vitro stimulation assay of primary $CD4^+$ T cells, naive $CD4^+CD62L^+$ T cells were isolated from the spleens by MACS ($CD4^+CD62L^+$ T Cell Isolation Kit II; Miltenyi Biotec). A total of 1.5×10^7 $CD4^+CD62L^+$ cells were then stimulated with recombinant mouse IL-2 (R&D Systems) or recombinant mouse IL-12 (R&D Systems). Concentrations of cytokines and chemokines in the heart homogenates or culture supernatants were measured with Quantikine ELISA kits (R&D Systems).

Proliferative responses of T cells

Proliferation of T cells was assessed as previously described (28). Briefly, mice were immunized as described above, and the spleens collected on day 14. Cells were cultured with 5 μg/ml MyHC-α for 72 h and pulsed with 0.5 μCi [^{3}H]thymidine 8 h before being measured with a β counter. For in vitro stimulation assay of primary $CD4^+$ T cells, naive $CD4^+CD62L^+$ T cells were isolated from the spleens by MACS ($CD4^+CD62L^+$ T Cell Isolation Kit II; Miltenyi Biotec). A total of 10^5 $CD4^+CD62L^+$ cells were then stimulated with 5 μg/ml anti-CD3ε, 5 μg/ml anti-CD3ε, 1 μg/ml anti-CD28, 50 ng/ml PMA, and 500 ng/ml ionomycin or with 1 μg/ml Con A together with 0.25×10^5 DCs. Proliferative responses were assessed after 48 h in 2.5% RPMI 1640 medium by measurement of the [^{3}H]thymidine incorporation.

Western blot analysis

Total lysates from $CD4^+$ T cells or DCs were immunoblotted and probed with Abs directed against STAT1 (Santa Cruz Biotechnology) and p-STAT1 protein (Cell Signaling Technology). HRP-conjugated goat anti-rabbit IgG (Bio-Rad) was used to identify the binding sites of the primary Ab.

Adoptive transfer of T cells

Splenocytes were collected from diseased mice and cultured with 5 μg/ml MyHC-α for 48 h. A total of 5×10^6 $CD4^+$ T cells were purified by using anti-CD4 magnetic beads (Miltenyi Biotec) and injected i.p. into the SCID mice. The mice were killed 10 d after the injection.

Quantitative real-time RT-PCR

Total RNA was prepared using TRIzol reagent (Invitrogen) according to the manufacturer's instructions. cDNA was synthesized from 1 μg total RNA by reverse transcriptase (Takara). Quantitative real-time RT-PCR (QRT-PCR) *analysis was performed with LightCycler (Roche Diagnostics).* Primers for mouse *Socs1* were 5′-GTGGTTGTGGAGGGTGAGAT-3′ (sense) and 5′-CCTGAGAGGTGGGATGAGG-3′ (antisense). Primers for mouse *Hprt* were 5′-TCCTCCTCAGACCGCTTTT-3′ (sense) and 5′-CCTGGTTCATCATCGCTAATC-3′ (antisense). Data were normalized by the level of *Hprt* expression in each sample.

Echocardiography

Transthoracic echocardiography was performed on animals on day 35 by using a Prosound α6 with a 10-MHz transducer (Aloka). The left ventricular (LV) chamber dimensions were measured from the M-mode. Two independent investigators who conducted the echocardiography were unaware of the treatment status.

Statistical analysis

All data were expressed as means ± SEM. Statistical analyses were performed using the two-tailed *t* test or Mann–Whitney *U* test for experiments comparing two groups. The *p* values <0.05 were considered statistically significant.

Results

SOCS1 DNA administration inhibits the development of EAM

To examine the effect of in vivo gene delivery of *Socs1* on the pathogenesis of EAM, BALB/c mice were injected with a mammalian expression plasmid vector encoding SOCS1 (pSOCS1) during the course of EAM induction (Fig. 1A). QRT-PCR analysis revealed elevated expression of *Socs1* in the control EAM heart (Fig. 1B). Importantly, in the SOCS1 DNA-administered mice, *Socs1* was strongly expressed in the heart. By day 28, *Socs1* gene expression was significantly elevated in the pSOCS1-treated heart as compared with the controls (Supplemental Fig. 1). Gross cardiac enlargement and edema were reduced in mice with EAM that received pSOCS1 as compared with those in control empty plasmid DNA-administered EAM mice (Fig. 1C). The heart-to-body weight ratio in the pSOCS1-injected mice was significantly decreased as compared with that in the control plasmid-administered mice (Fig. 1D). The pSOCS1-injected EAM mice had a significantly lower myocarditis severity score and fewer infiltrating inflammatory cells than did the control plasmid-injected mice (Fig. 1E–G). The empty vector [pcDNA3.1-myc/His(-)] was used as the control and did not have any effects on EAM in our experiments (data not shown).

Recently, Hanada et al. (29) demonstrated that dnSOCS1, which has a point mutation (F59D) in a functionally critical kinase inhibitory region of SOCS1, strongly augmented cytokine-dependent JAK-STAT activation both in vivo and in vitro as an antagonist of SOCS1. We examined the effect of dnSOCS1 on the clinical course of EAM. Mice administered a plasmid vector

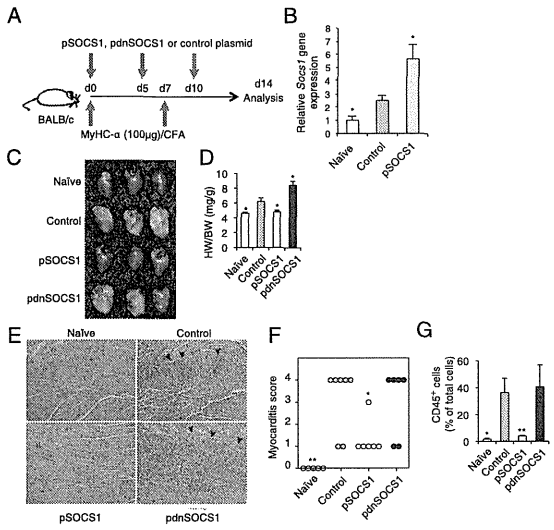

FIGURE 1. Amelioration of EAM and heart failure by SOCS1 DNA administration. (**A**) BALB/c mice were immunized twice, on days 0 and 7, with 100 μg of MyHC-α and treated with pSOCS1, pdnSOCS1, or control plasmid on days 0, 5, and 10. (**B**) QRT-PCR for the *Socs1* gene. RNA samples were obtained from hearts of immunized mice on day 14 and used as a template for QRT-PCR. Results represent the average gene induction in five independent heart samples. (**C**) Representative gross hearts (day 14) of naive and EAM mice treated with the indicated plasmid. (**D**) Heart-to-body weight ratios of naive and EAM mice with indicated treatment ($n = 5$ mice/group). (**E**) Representative H&E-stained sections of hearts from naive and immunized mice. Arrowheads indicate infiltrating cells. Scale bar, 50 μm. (**F**) Myocarditis severity in heart sections stained with H&E ($n = 5$–7 mice/group). (**G**) Flow cytometry analysis of $CD45^+$ heart infiltrates of naive and immunized mice ($n = 5$–7 mice/group). Data are representative of at least two independent experiments. Error bars represent means ± SEM. $^*p < 0.05$, $^{**}p < 0.01$ compared with control.

encoding dnSOCS1 (pdnSOCS1) showed augmentation of gross heart enlargement, edema, and heart-to-body weight ratio (Fig. 1C, 1D). However, the myocardial leukocyte infiltration and myocarditis scores were not significantly different between the pdnSOCS1- and control plasmid-administered mice (Fig. 1E–G).

To clarify the adverse effect of dnSOCS1 DNA administration on the development of EAM, we used mice immunized with a tithe amount (10 μg) of MyHC-α instead of the usual amount of peptide for EAM development (Fig. 2A). Those MyHC-α–immunized mice injected with the control plasmid or pSOCS1 did not develop myocarditis (Fig. 2B–F). However, immunized mice injected with pdnSOCS1 developed myocarditis with inflammatory infiltrates (Fig. 2B–F). Thus, administration of pSOCS1 is effective against the development of EAM, and the inhibition of SOCS1 by use of a SOCS1 antagonist adversely affects myocarditis.

SOCS1 DNA administration prevents progression of heart failure and fibrosis after myocarditis

Some patients diagnosed with myocarditis after viral, bacterial, or protozoal infection develop heart failure (2). On day 35 of the present experiment, mice immunized with MyHC-α showed increased LV end-diastolic dimensions (LVEDd) and LV end-systolic dimensions (LVESd) and decreased fractional shortening (FS); however, pSOCS1-injected mice showed almost normal chamber size and LV function (Fig. 3A, 3B). In contrast, LV dysfunction and chamber dilatation in pdnSOCS1-administered mice were manifested as significant increases in LVEDd and LVESd and decrease in FS (Fig. 3A, 3B). In these EAM models, on day 35, hearts from myocarditis mice showed interstitial fibrosis without active leukocyte infiltration. The fibrotic area in mice administered pSOCS1 was significantly smaller than that in control plasmid-injected mice (Fig. 3C, 3D). Although pdnSOCS1-injected mice developed severe cardiac fibrosis, the difference between the fibrotic areas in pdnSOCS1- and control plasmid-injected mice was not statistically significant (Fig. 3C, 3D). These inhibitory effects of pSOCS1 on the development of fibrosis and heart failure were considered to be the result of inhibition of myocardial inflammation because myocarditis developed mice injected with pSOCS1 on day 14, 21, and 28 did not show inhibitory effects on fibrosis and heart failure (data not shown).

Cardiac myosin-specific $CD4^+$ T cell response and cytokine production

Autoimmune myocarditis is a $CD4^+$ T cell-mediated disease (7, 15). Proliferative responses of $CD4^+$ T cells after in vitro restimulation with MyHC-α were not clearly seen in pSOCS1-injected mice; however, the proliferation of $CD4^+$ T cells from pdnSOCS1-injected mice was enhanced (Fig. 4A). Production of IL-2, IL-6, IL-10, IL-17, IL-22, IFN-γ, TNF-α, CCL2, CCL3, CCL5, CCL17, and CXCL10 by $CD4^+$ T cells from EAM mice was enhanced by in vitro restimulation with the MyHC-α epitope peptide. This cardiac-Ag–specific cytokine production by $CD4^+$ T cells was decreased in the supernatants of in vitro MyHC-α–restimulated $CD4^+$ T cells from pSOCS1-administered mice but

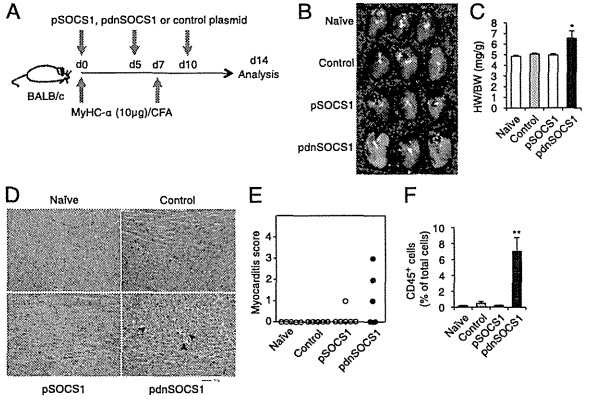

FIGURE 2. Increased susceptibility to EAM induced by inhibition of SOCS1. (**A**) Mice were immunized twice, on days 0 and 7, with 10 μg of MyHC-α emulsified 1:1 in PBS/CFA and treated with pSOCS1, pdnSOCS1, or control plasmid on days 0, 5, and 10. (**B**) Representative gross hearts (day 14) of naive and 10 μg of MyHC-α–immunized mice treated with the indicated plasmid. (**C**) Heart-to-body weight ratios of naive and immunized mice ($n = 5$ to 6 mice/group). (**D**) Representative H&E-stained sections of hearts from naive and immunized mice. Arrowheads indicate infiltrating cells. Scale bar, 50 μm. (**E**) Myocarditis severity in heart sections stained with H&E ($n = 5$ to 6 mice/group). (**F**) Flow cytometry analysis of $CD45^+$ heart infiltrates of naive and immunized mice ($n = 5$ mice/group). Data are representative of at least two independent experiments. Error bars represent means ± SEM. $^*p < 0.05$, $^{**}p < 0.01$ compared with control.

was increased in the supernatants of these cells from pdnSOCS1-administered mice (Fig. 4B). In contrast, cardiac-Ag–specific production of IL-1β, IL-10, and CXCL1 was not detected in the culture supernatants of in vitro-restimulated $CD4^+$ T cells from control plasmid-, pSOCS1-, or pdnSOCS1-injected mice (data not shown). Taken together, these results indicate that SOCS1 DNA

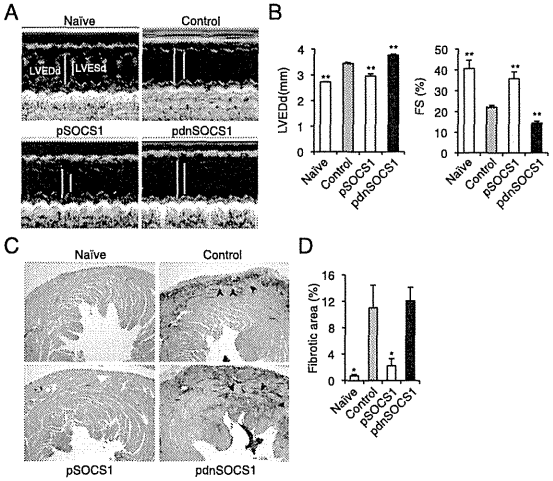

FIGURE 3. SOCS1 DNA administration prevents progression to heart failure. (**A** and **B**) Echocardiography was performed on naive and immunized mice on day 35. (A) Representative M-mode echocardiograms. Bars indicate LVESd and LVEDd. Bar graphs (B) represent LVEDd and percentage of FS from the indicated animals ($n = 9$ mice/group). The percentage FS was calculated according to the following formula: FS (%) = (LVEDd − LVESd)/LVEDd. (**C** and **D**) Heart tissue sections were stained with Sirius Red and analyzed for fibrosis at day 35. Representative Sirius Red-stained sections of hearts. Scale bar, 50 μm. (C) Arrowheads indicate fibrotic area. (D) The degree of fibrosis was calculated as the percentage of the fibrotic area in relation to the total heart area ($n = 5$ mice/group). Data are representative of at least two independent experiments. Error bars represent means ± SEM. $^*p < 0.05$, $^{**}p < 0.01$ compared with control.

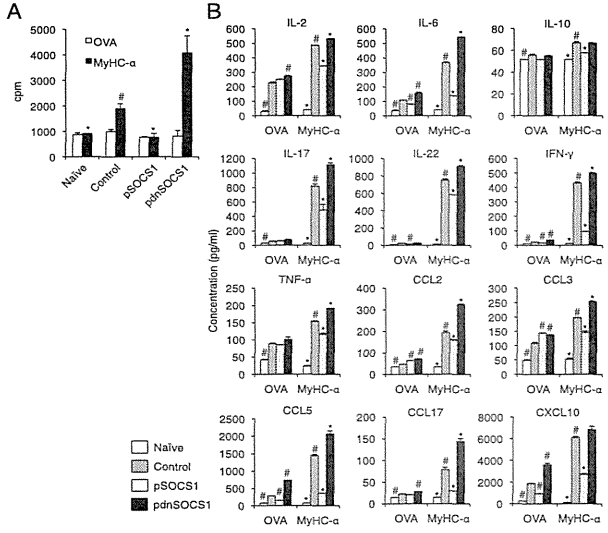

FIGURE 4. Impaired expansion of heart-specific $CD4^+$ T cells in pSOCS1-treated mice. (**A**) Splenocytes were isolated from naive and EAM mice treated with pSOCS1, pdnSOCS1, or control plasmid on day 14 and restimulated in vitro with MyHC-α or OVA peptide for 72 h. Proliferation was assessed by measurement of $[^3H]$thymidine incorporation. Data represent means ± SEM of triplicates from one of three independent experiments. (**B**) Cytokines and chemokines in the culture supernatants of splenocytes were measured by ELISA after 48 h of restimulation with MyHC-α or OVA peptide. Data are expressed as mean ± SEM from triplicate culture wells. Results of one of two representative experiments are shown. $^*p < 0.05$ compared with MyHC-α–stimulated control, $^{\#}p < 0.05$ compared with OVA-stimulated control.

delivery inhibits the activation of myosin-specific $CD4^+$ T cells and strongly suggest that impaired $CD4^+$ Th cell function prevents EAM development in pSOCS1-injected mice after immunization with cardiac self-Ag.

To evaluate whether pSOCS1 administration affects Ag-specific $CD4^+$ T cell function in other models, we injected plasmid DNA into an autoimmune gastritis model and an OVA-immunized model. In the autoimmune gastritis model, gastric-Ag–specific production of IL-2, IL-6, IL-13, IL-17, IL-22, IFN-γ, TNF-α, CCL2, CCL5, CCL17, and CXCL10 by $CD4^+$ T cells was decreased in pSOCS1-administered mice but increased in pdnSOCS1-administered mice (Supplemental Fig. 2). Lower amounts of cytokines (including IL-2, IL-6, IL-13, IFN-γ, TNF-α, CCL2, CCL3, CCL5, CCL17, and CXCL10) were also produced in $CD4^+$ T cells from pSOCS1-injected OVA-immunized mice (Supplemental Fig. 3). These results suggest that pSOCS1 administration may suppress Ag-specific $CD4^+$ T cell activation in various autoimmune diseases and foreign body infections.

SOCS1 DNA administration inhibits the production of proinflammatory cytokines and $CD4^+$ T cell differentiation in the heart

We also examined whether SOCS1 DNA administration has an effect on cytokine and chemokine milieu in the heart. On day 14 after MyHC-α immunization, heart homogenates from pSOCS1-injected mice had significantly decreased amounts of proinflammatory cytokines, including IL-1β and IL-6, and of myelotropic chemokines, including CCL5, CXCL1, and CXCL10 (Fig. 5A). In contrast, hearts from mice injected with pdnSOCS1 showed greatly increased amounts of proinflammatory cytokines and chemokines (Fig. 5A). SOCS1 protein has been shown to regulate T cell differentiation (17, 18). To determine the differentiation of $CD4^+$ T cells during EAM, we examined the heart-infiltrating $CD4^+$ T cell populations by FACS analysis. Activated $CD4^+$ T cells ($CD4^+CD40L^+$) and effector memory $CD4^+$ T cells ($CD44^+CD62L^-$) were reduced in the pSOCS1-injected mice (Fig. 5B). Thus, protection from EAM in pSOCS1-administered mice is associated with abrogation of proinflammatory cytokines, chemokines, and $CD4^+$ T cell differentiation in the heart.

SOCS1 DNA injection does not have a direct suppressive effect on $CD4^+$ T cell activation

To gain new insights into the mechanism of protection from myocarditis, we investigated whether pSOCS1 therapy directly affects $CD4^+$ T cell activation. Naive T cells ($CD4^+CD62L^+$ cells) were isolated from non-EAM mice injected with pSOCS1, pdnSOCS1, or control plasmid, and their primary responses to various stimuli were compared (Fig. 6A). As shown in Fig. 6B, there were no differences in IFN-γ–induced STAT1 activation among these $CD4^+$ T cells. There were also no differences in primary responses to stimulation with anti-CD3ε, anti-CD3ε/anti-CD28, PMA/ionomycin, or Con A presented by mitomycin C-treated wild-type DCs among pSOCS1-, pdnSOCS1-, and control plasmid-treated $CD4^+$ T cells (Fig. 6C). Chong et al. (30) demonstrated that SOCS1-deficient T cells produced substantially greater levels of IFN-γ in response to IL-2 or IL-12. From these findings, we assessed the production of IFN-γ from $CD4^+$ T cells by using the same experiments. In the culture supernatants of

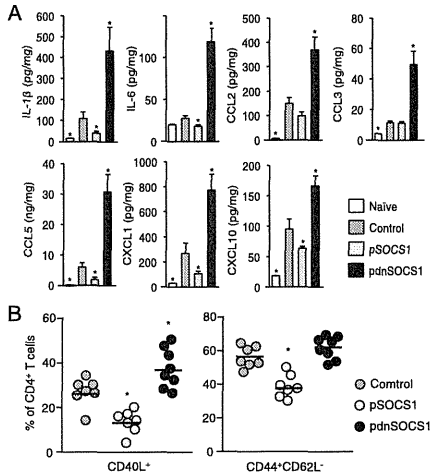

FIGURE 5. Cytokine and chemokine responses and $CD4^+$ T cell differentiation in the heart. (**A**) Myocardial tissues were homogenated and processed by ELISA to detect cytokines and chemokines on day 14. Bar graphs show group means ± SEM of 8–16 mice/group. Results of one of three representative experiments are shown. (**B**) Heart-infiltrating cells were isolated from EAM mice treated with indicated plasmid DNA. Cells were stained for CD4, CD40L, CD44, and CD62L. CD44 and CD62L expression are based on gates set from total $CD4^+$ T cells. Bar graphs show group means ± SEM of 5–9 mice/group. Data are representative of two independent experiments. *$p < 0.05$ compared with control.

$CD4^+$ T cells stimulated with IL-2 or IL-12, there were also no differences in IFN-γ production (Fig. 6*D*). These results indicate that in vivo administration of pSOCS1 does not directly affect $CD4^+$ T cell activation.

In vivo SOCS1 DNA administration inhibits DC function

Although $CD4^+$ T cell differentiation was inhibited in pSOCS1-treated mice (Fig. 5B), our results suggested that in vivo *Socs1* gene administration has no direct effect on $CD4^+$ T cell activation (Fig. 6). We therefore investigated whether in vivo pSOCS1 administration inhibits the function of Ag-presenting DCs by stimulation through the TLR pathway. DCs from mice administered pSOCS1, pdnSOCS1, or control plasmid were stimulated with LPS for 24 h (Fig. 7A). STAT1 phosphorylation was attenuated in DCs from pSOCS1-injected mice and enhanced in DCs from pdnSOCS1-injected mice (Fig. 7B). The production of proinflammatory cytokines, including IL-6, TNF-α, and IFN-γ, was inhibited in DCs from pSOCS1-injected mice and enhanced in DCs from pdnSOCS1-injected mice (Fig. 7C). These results indicate that in vivo administration of *Socs1* affects DC function. In the current study, the cardiac-Ag–specific proliferative response and cytokine production of $CD4^+$ T cells were inhibited in pSOCS1-injected EAM mice (Fig. 4). We next assessed the functional capability of DCs to prime and expand autoreactive $CD4^+$ T cells from mice injected with each plasmid as a measure of Ag-specific proliferative responses of $CD4^+$ T cells from MyHC-α–immunized mice. Myosin-specific $CD4^+$ T cells were cocultured with MyHC-α–pulsed DCs from pSOCS1-, pdnSOCS1-, and control plasmid-treated mice (Fig. 7D). Interestingly, the proliferative responses of $CD4^+$ T cells cocultured with DCs from pSOCS1-treated mice were much weaker than those of cells cultured with DCs from control plasmid-treated mice, and these proliferative responses of $CD4^+$ T cells were enhanced by coculturing with DCs from pdnSOCS1-administered mice (Fig. 7E). These results suggest that in vivo gene delivery of *Socs1* suppresses the functional capability of DCs to prime and expand autoreactive $CD4^+$ T cells.

SOCS1 DNA administration inhibits the development of myocarditis induced by cardiac myosin peptide-loaded BMDC transfer but not by $CD4^+$ T cell transfer

Functionally interposed SOCS1 is induced in various cell populations, including leukocytes, vascular cells, and cardiomyocytes (18, 31, 32). A mouse model of EAM was established by cell transfer using peptide-pulsed DCs or cardiac epitope-specific $CD4^+$ T cells (7, 14). The effects of pSOCS1 administration in mice transferred with $CD4^+$ T cells from mice with EAM were assessed. pSOCS1, pdnSOCS1, or control plasmid was injected into mice transferred with cardiac myosin-specific $CD4^+$ T cells (Fig. 8A). All mice transferred with $CD4^+$ T cells developed myocarditis, and no therapeutic effects were seen in pSOCS1-injected mice (Fig. 8B–D). Furthermore, pdnSOCS1 administration showed no adverse effect on the status of myocarditis induced by $CD4^+$ T cell transfer (Fig. 8B–D). These findings suggest that systemic injection of pSOCS1 is not effective for inhibition of autoreactive $CD4^+$ T cell activation and recruitment to the heart during myocarditis development. Next, we administered pSOCS1, pdnSOCS1, or control plasmid into mice transferred with MyHC-α–loaded BMDCs (Fig. 8E). Interestingly, pSOCS1 injection inhibited the development of myocarditis after MyHC-α–loaded BMDC transfer, and myocarditis deteriorated after administration of pdnSOCS1 (Fig. 8F–H). These results indicate that the therapeutic effects of SOCS1 DNA administration on EAM contribute to professional APCs such as DCs and also provide evidence for the potential utility of SOCS1 DNA inoculation as an approach to gene therapy for myocarditis.

Discussion

There have been no effective fundamental therapies for acute myocarditis; therefore, supportive care for LV dysfunction is the first line of treatment. Because patients generally present days to weeks after the initial viral infection, antiviral therapy has limited applicability in patients with acute viral myocarditis. The long-term sequelae of viral myocarditis appear to be related to abnormal cellular and humoral immunity; therefore, many clinicians believe that immunosuppression is beneficial for myocarditis treatment (2). In this study, we showed that administration of SOCS1 DNA is effective for inhibiting the development of EAM in BALB/c mice, suggesting a novel immunotherapy for myocarditis. To our knowledge, this is the first report showing that gene delivery of *Socs1* prevents autoimmune disease.

Animal models have greatly advanced our knowledge of the pathogenesis of myocarditis and inflammatory cardiomyopathy. Infection of BALB/c mice with either Coxsackievirus or murine CMV results in the development of acute myocarditis from days 7–14 postinfection that is characterized by myocyte damage due to viral cytotoxicity, and the infectious virus cannot be detected past day 14 of the infection (7). After elimination of viruses, mice showed autoimmune myocarditis, which is associated with mononuclear infiltration of the myocardium and production of autoantibodies to cardiac myosin (7), similar to the pathogenesis of autoimmune myocarditis in humans (3, 4, 33). These autoimmune responses are thought to be elicited by two mechanisms. One is molecular mimicry: responses to microbial Ags could result in the activation of T cells that are cross-reactive with self-Ags. Another possibility is bystander activation of autoreactive cells. APCs that have become activated in the inflammatory milieu of a pathogenic infection can stimulate the activation and proliferation of autoreactive T or B cells in a process known as bystander activation (reviewed in Ref. 34). Thus, immune responses to myocytes involving various innate and adaptive immune pathways were recognized during myocarditis development. The cardiac myosin peptide-immunized mouse EAM model reflects human autoimmune myocarditis and heart failure after elimination of infectious pathogens.

Recent studies have indicated that various microbes use the host's SOCS proteins for manipulating cytokine receptor signaling as one of the strategies to evade immune responses (35, 36). Coxsackievirus usually infects cardiomyocytes and induces the expression of SOCS1 and SOCS3 in cardiomyocytes, which can result in evasion of immune responses and facilitation of virus replication by inhibition of JAK–STAT signaling (32, 37). These findings indicate that it may be harmful to administer SOCS1 DNA in the acute phase of infectious myocarditis because it may augment viral replication by inhibition of IFN signaling. The effect of SOCS1 transduction on viral myocarditis has been examined by Yasukawa et al. (32). The SOCS1-transgenic mice infected with CVB3 showed increased myocardial injury, virus replication, and mortality. In contrast, they also showed that SOCS1 inhibition in the heart through adeno-associated virus-mediated expression of dnSOCS1 increased resistance to the acute cardiac injury caused by CVB3 infection. These results were acceptable because SOCS proteins have emerged as frequent targets of viral exploitation. Furthermore, when administrating JAK inhibitors, such as SOCS, active serious infections should have been resolved before the start of treatment. It is considered to be inappropriate to use JAK inhibitors for a person with infectious disease or their possibility with consideration for complication of infection (38–40). In contrast, the overactive autoimmune responses triggered by microbial pathogens can persist after elimination of infectious pathogens (7). Therefore, we examined the efficacy of SOCS1 transfection by using EAM induced by cardiac autoantigen immunization in the absence of viral infection. In the current study, we clearly showed the efficacy of *Socs1* gene transfer as an immunosuppressive therapy for myocarditis under infectious pathogen-free conditions in an EAM mice model. The results of a recent randomized, double-blind, placebo-controlled study showed that immunosuppressive therapy, including prednisone and azathioprine, was effective in patients with myocarditis and inflammatory cardiomyopathy and without evidence of the myocardial viral genome (41). These findings indicate that *Socs1* gene transfer can be effective to treat some clinical

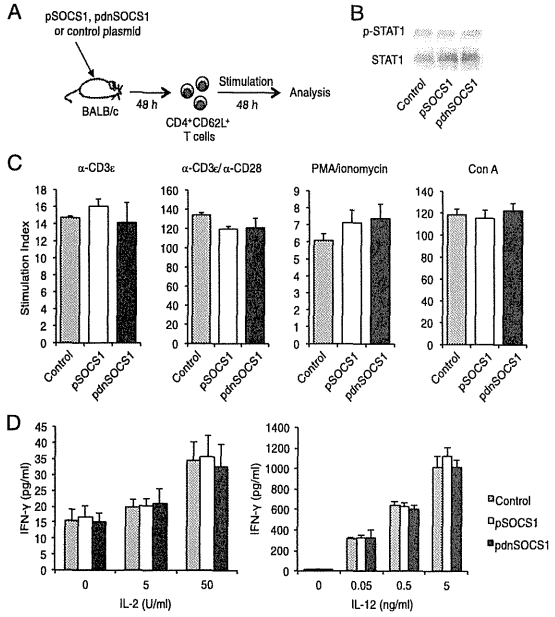

FIGURE 6. Primary responses of $CD4^+$ T cells from pSOCS1-, pdnSOCS1-, and control plasmid-treated mice. (**A**) $CD4^+CD62L^+$ T cells from mice injected with pSOCS1, pdnSOCS1, or control plasmid were stimulated with IFN-γ, anti-CD3ε, anti-CD3ε, anti-CD28, PMA/ionomycin, and Con A in the presence of wild-type DCs, IL-2, or IL-12. (**B**) STAT1 phosphorylation of $CD4^+$ T cells after IFN-γ treatment (10 ng/ml) was assessed by Western blotting. (**C**) T cell proliferation was measured after 48 h of culture. (**D**) IFN-γ in the culture supernatants was measured by ELISA. Values are expressed as means ± SEM of triplicate culture wells. Results of one of at least two representative experiments are shown.

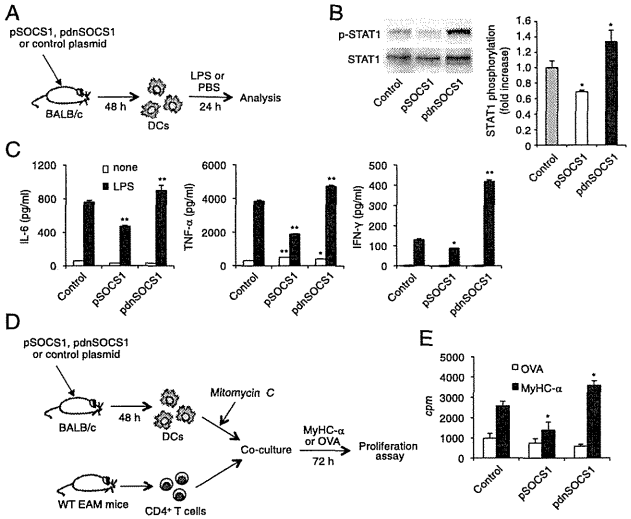

FIGURE 7. Functional capacities of DCs from pSOCS1-, pdnSOCS1-, and control plasmid-treated mice. (**A**) DCs from mice treated with pSOCS1, pdnSOCS1, or control plasmid were stimulated with LPS for 24 h. (**B**) STAT1 phosphorylation of DCs was assessed by Western blotting. Densitometry ratios of pSTAT1/STAT1 are shown as fold induction, the ratio for DCs from control plasmid-injected mice being set at 1. Results are means of five independent experiments ± SEM. Blots are representative of experiments performed a minimum of three times. (**C**) IL-6, TNF-α, and IFN-γ in the culture supernatants were measured by ELISA. Values indicate means ± SEM of triplicate culture wells from one of three independent experiments. (**D** and **E**) Heart-specific $CD4^+$ T cells from EAM mice were restimulated with MyHC-α or OVA peptide on DCs from mice treated with control plasmid, pSOCS1, or pdnSOCS1 for 72 h before measurement of $[^3H]$thymidine incorporation. Each value represents mean ± SEM cpm values of six different culture wells. Results of one of three representative experiments are shown. $*p < 0.05$, $**p < 0.01$ compared with control.

cases of myocarditis and inflammatory cardiomyopathy associated with autoimmunity and without the virus genome in the myocardium, as well as EAM in mice.

In the current study, we demonstrated that the administration of plasmid DNA encoding SOCS1 did not affect autoreactive $CD4^+$ T cell function (Fig. 6) and adoptive transfer of autoreactive $CD4^+$ T cells was able to induce myocarditis in SOCS1 DNA-administered SCID mice (Fig. 8*A–D*), suggesting that SOCS1 DNA does not suppress either $CD4^+$ T cell recruitment or accumulation of other inflammatory cells in the heart. In contrast, the introduced SOCS1 DNA inhibited the activation of DCs producing proinflammatory cytokines (Fig. 7C). In fact, inhibition of the phosphorylation of STAT1 molecules was observed in DCs from mice injected with SOCS1 DNA (Fig. 7B). In addition, the proliferative responses of $CD4^+$ T cells cocultured with DCs from pSOCS1-treated mice were much weaker than those of cells cultured with DCs from control plasmid-injected mice (Fig. 7E). These results suggest that the inoculated SOCS1 DNA may have been transfected into DCs and impaired DC function in vivo. Contrary to expectations, we could not find evidence of direct transfection of inoculated DNA into DCs in the heart, spleen, peritoneal cavity, or lymph nodes. Although the introduced DNA is expressed predominantly by somatic cells (e.g., cardiomyocytes, keratinocytes, and fibroblasts), it is known that relatively small but biologically significant numbers of DCs are transfected with the inoculated DNA (42–44). Based on this fact, the inoculated SOCS1 DNA may have inhibited DC activation through the direct transfection into DCs; however, our data do not exclude the possibility of another indirect mechanisms.

In the EAM model, activation of TLRs on self-Ag–presenting DCs is essential for the expansion of autoreactive $CD4^+$ T cells to induce myocarditis and heart failure (15). We previously reported that *Tlr4* mutant C3H/HeJ mice are resistant to development of EAM (45). Furthermore, IL-1 type 1 receptor signaling on DCs is critical for autoimmune myocarditis development (11). MyD88 is a crucial common adaptor molecule that mediates both TLRs and IL-1 type 1 receptor activation (46, 47), and MyD88 signaling in DCs is critical for the induction of EAM (16). SOCS1 negatively regulates the MyD88-dependent pathway by interacting with both IL-1R–associated kinase and NF-κB (17), which results in a decrease in the induction of inflammatory cytokines such as TNF-α and IL-6. In fact, production of these inflammatory cytokines was inhibited by the administration of SOCS1 DNA in the current study (Fig. 7C). Although nearly all TLRs recruit MyD88, other specific adaptor proteins function downstream of particular TLRs. One such adaptor molecule is Toll/IL-1R domain-containing adaptor protein/Mal. SOCS1 also binds to tyrosine-phosphorylated Mal through its interaction with Bruton's tyrosine kinase, leading to the suppression of Mal-dependent p65 phosphorylation and transactivation of NF-κB (48). Another important mechanism of the suppression of APC activation by SOCS1 is inhibition of the secondary activated JAK–STAT pathway (49, 50). The Toll/IL-1R domain-containing adaptor protein-inducing IFN-β–IFN-regulatory factor 3 pathway rapidly induces IFN-β, which in turn activates JAK–STAT1 and contributes to the expression of IFN-

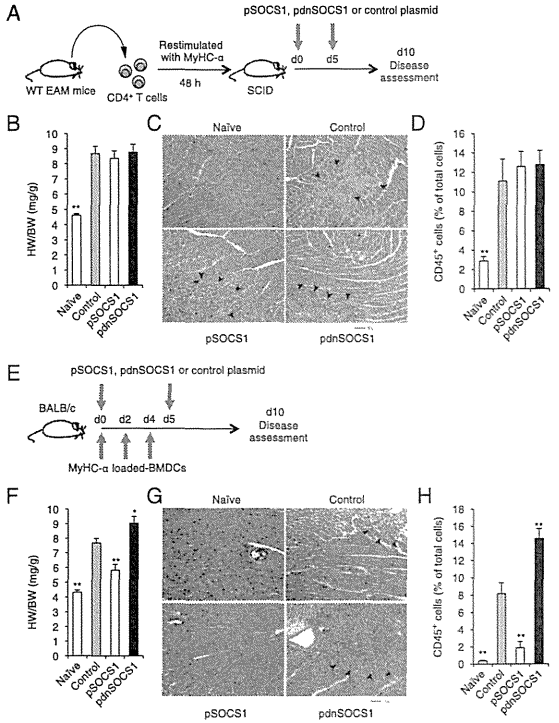

FIGURE 8. pSOCS1 administration inhibited the development of myocarditis induced by cardiac Ag-loaded BMDC injection but not by heart-specific $CD4^+$ T cells. (**A–D**) $CD4^+$ T cells were purified from diseased mice and restimulated in vitro with MyHC-α for 48 h before transfer into SCID recipients. pSOCS1, pdnSOCS1, or control plasmid was injected on days 0 and 5 after the transfer. Heart-to-body weight ratios (B; $n = 5$ mice/group), representative H&E-stained sections of hearts (C), and results of flow cytometry analysis of $CD45^+$ heart infiltrates (D; $n = 5$ mice/group) of naive and adoptive transferred mice at day 10. Arrowheads indicate infiltrating cells. Scale bar, 50 μm. (**E–H**) Mice were immunized with activated MyHC-α– or control OVA peptide-pulsed DCs on days 0, 2, and 4. Mice immunized with MyHC-α–pulsed DCs were treated with pSOCS1, pdnSOCS1, or control plasmid on days 0 and 5. Heart-to-body weight ratios (F; $n = 6–12$ mice/group), representative H&E-stained sections of hearts (G), and results of flow cytometry analysis of $CD45^+$ heart infiltrates (H; $n = 5$ mice/group) of naive and transferred mice at day 10. Arrowheads indicate infiltrating cells. Scale bar, 50 μm. Data are expressed as means ± SEM. Data are representative of at least two independent experiments. $*p < 0.05$, $**p < 0.01$ compared with control.

inducible genes (51). Moreover, Kimura et al. (52) showed that LPS can activate JAK2 and STAT5, which are involved in IL-6 induction, and that SOCS1 selectively inhibits this process. Thus, SOCS1 negatively regulates several activation pathways in DCs. The present study indicates that pSOCS1 administration is a possible therapy against various diseases caused by overshooting of DCs.

IFN-γ has been shown to be a downregulatory cytokine, as evidenced by exacerbated myocarditis in IFN-γR knockout (KO), IFN-γ KO, and T-bet KO mice (9, 53, 54). In contrast, Th17 cells have recently been implicated in the pathogenesis of various types of autoimmune diseases (reviewed in Ref. 55); however, IL-17 deficiency did not significantly impact the severity of EAM (56). Though these gene-ablated mice provided us with much important information, these studies do not necessarily lead to an effective therapy. In this study, we showed that SOCS1 DNA administration inhibited a broad array of cytokine production from $CD4^+$ T cells (Fig. 4B) and effectively reduced myocardial inflammation (Fig. 1). Compared with inhibition of a single cytokine, SOCS1 DNA therapy could be a more useful therapy that inhibits various signaling pathways to induce production of cytokines.

In the current study, SOCS1 DNA administration was efficacious against EAM development, and inhibition of SOCS1 molecules by SOCS1 antagonist DNA administration enhanced the severity of myocarditis. We demonstrated that SOCS1 DNA administration inhibits the stimulation of self-Ag–presenting DCs inducing cardiac myosin-specific $CD4^+$ T cell responses in peripheral compartments in vivo. Given the availability of clinically effective drugs targeting SOCS1, our findings show new therapeutic perspectives for the treatment of autoimmune myocarditis and cardiomyopathy.

Acknowledgments

We thank T. Okamura, Y. Shiogama, T. Wada, K. Watanabe, H. Shibata, and M. Namikata for technical support and valuable discussion and F. Miyamasu of the Medical English Communications Center, University of Tsukuba, for grammatical revision of this manuscript.

Disclosures

The authors have no financial conflicts of interest.

References

1. Brown, C. A., and J. B. O'Connell. 1995. Myocarditis and idiopathic dilated cardiomyopathy. *Am. J. Med.* 99: 309–314.
2. Feldman, A. M., and D. McNamara. 2000. Myocarditis. *N. Engl. J. Med.* 343: 1388–1398.
3. Caforio, A. L., N. J. Mahon, F. Tona, and W. J. McKenna. 2002. Circulating cardiac autoantibodies in dilated cardiomyopathy and myocarditis: pathogenetic and clinical significance. *Eur. J. Heart Fail.* 4: 411–417.
4. Lauer, B., M. Schannwell, U. Kühl, B. E. Strauer, and H. P. Schultheiss. 2000. Antimyosin autoantibodies are associated with deterioration of systolic and diastolic left ventricular function in patients with chronic myocarditis. *J. Am. Coll. Cardiol.* 35: 11–18.
5. Frustaci, A., C. Chimenti, F. Calabrese, M. Pieroni, G. Thiene, and A. Maseri. 2003. Immunosuppressive therapy for active lymphocytic myocarditis: virological and immunologic profile of responders versus nonresponders. *Circulation* 107: 857–863.
6. Caforio, A. L., J. H. Goldman, A. J. Haven, K. M. Baig, L. D. Libera, and W. J. McKenna; The Myocarditis Treatment Trial Investigators. 1997. Circulating cardiac-specific autoantibodies as markers of autoimmunity in clinical and biopsy-proven myocarditis. *Eur. Heart J.* 18: 270–275.
7. Fairweather, D., Z. Kaya, G. R. Shellam, C. M. Lawson, and N. R. Rose. 2001. From infection to autoimmunity. *J. Autoimmun.* 16: 175–186.
8. Eriksson, U., M. O. Kurrer, W. Sebald, F. Brombacher, and M. Kopf. 2001. Dual role of the IL-12/IFN-gamma axis in the development of autoimmune myocarditis: induction by IL-12 and protection by IFN-gamma. *J. Immunol.* 167: 5464–5469.
9. Afanasyeva, M., Y. Wang, Z. Kaya, E. A. Stafford, K. M. Dohmen, A. A. Sadighi Akha, and N. R. Rose. 2001. Interleukin-12 receptor/STAT4 signaling is required for the development of autoimmune myocarditis in mice by an interferon-gamma-independent pathway. *Circulation* 104: 3145–3151.
10. Eriksson, U., M. O. Kurrer, N. Schmitz, S. C. Marsch, A. Fontana, H. P. Eugster, and M. Kopf. 2003. Interleukin-6-deficient mice resist development of autoimmune myocarditis associated with impaired upregulation of complement C3. *Circulation* 107: 320–325.
11. Eriksson, U., M. O. Kurrer, I. Sonderegger, G. Iezzi, A. Tafuri, L. Hunziker, S. Suzuki, K. Bachmaier, R. M. Bingisser, J. M. Penninger, and M. Kopf. 2003. Activation of dendritic cells through the interleukin 1 receptor 1 is critical for the induction of autoimmune myocarditis. *J. Exp. Med.* 197: 323–331.
12. Sonderegger, I., G. Iezzi, R. Maier, N. Schmitz, M. Kurrer, and M. Kopf. 2008. GM-CSF mediates autoimmunity by enhancing IL-6-dependent Th17 cell development and survival. *J. Exp. Med.* 205: 2281–2294.
13. Satoh, M., G. Tamura, I. Segawa, A. Tashiro, K. Hiramori, and R. Satodate. 1996. Expression of cytokine genes and presence of enteroviral genomic RNA in endomyocardial biopsy tissues of myocarditis and dilated cardiomyopathy. *Virchows Arch.* 427: 503–509.
14. Eriksson, U., and J. M. Penninger. 2005. Autoimmune heart failure: new understandings of pathogenesis. *Int. J. Biochem. Cell Biol.* 37: 27–32.
15. Eriksson, U., R. Ricci, L. Hunziker, M. O. Kurrer, G. Y. Oudit, T. H. Watts, I. Sonderegger, K. Bachmaier, M. Kopf, and J. M. Penninger. 2003. Dendritic cell-induced autoimmune heart failure requires cooperation between adaptive and innate immunity. *Nat. Med.* 9: 1484–1490.
16. Marty, R. R., S. Dirnhofer, N. Mauermann, S. Schweikert, S. Akira, L. Hunziker, J. M. Penninger, and U. Eriksson. 2006. MyD88 signaling controls autoimmune myocarditis induction. *Circulation* 113: 258–265.
17. Dimitriou, I. D., L. Clemenza, A. J. Scotter, G. Chen, F. M. Guerra, and R. Rottapel. 2008. Putting out the fire: coordinated suppression of the innate and adaptive immune systems by SOCS1 and SOCS3 proteins. *Immunol. Rev.* 224: 265–283.
18. Yoshimura, A., T. Naka, and M. Kubo. 2007. SOCS proteins, cytokine signalling and immune regulation. *Nat. Rev. Immunol.* 7: 454–465.
19. Shuai, K., and B. Liu. 2003. Regulation of JAK-STAT signalling in the immune system. *Nat. Rev. Immunol.* 3: 900–911.
20. Croker, B. A., H. Kiu, and S. E. Nicholson. 2008. SOCS regulation of the JAK/STAT signalling pathway. *Semin. Cell Dev. Biol.* 19: 414–422.
21. Fujimoto, M., and T. Naka. 2010. SOCS1, a Negative Regulator of Cytokine Signals and TLR Responses, in Human Liver Diseases. *Gastroenterol. Res. Pract.* 2010: 2010.
22. Naka, T., M. Fujimoto, H. Tsutsui, and A. Yoshimura. 2005. Negative regulation of cytokine and TLR signalings by SOCS and others. *Adv. Immunol.* 87: 61–122.
23. Hanada, T., H. Yoshida, S. Kato, K. Tanaka, K. Masutani, J. Tsukada, Y. Nomura, H. Mimata, M. Kubo, and A. Yoshimura. 2003. Suppressor of cytokine signaling-1 is essential for suppressing dendritic cell activation and systemic autoimmunity. *Immunity* 19: 437–450.
24. Kinjyo, I., T. Hanada, K. Inagaki-Ohara, H. Mori, D. Aki, M. Ohishi, H. Yoshida, M. Kubo, and A. Yoshimura. 2002. SOCS1/JAB is a negative regulator of LPS-induced macrophage activation. *Immunity* 17: 583–591.
25. Nakagawa, R., T. Naka, H. Tsutsui, M. Fujimoto, A. Kimura, T. Abe, E. Seki, S. Sato, O. Takeuchi, K. Takeda, et al. 2002. SOCS-1 participates in negative regulation of LPS responses. *Immunity* 17: 677–687.
26. Lutz, M. B., N. Kukutsch, A. L. Ogilvie, S. Rössner, F. Koch, N. Romani, and G. Schuler. 1999. An advanced culture method for generating large quantities of highly pure dendritic cells from mouse bone marrow. *J. Immunol. Methods* 223: 77–92.
27. Valaperti, A., R. R. Marty, G. Kania, D. Germano, N. Mauermann, S. Dirnhofer, B. Leimenstoll, P. Blyszczuk, C. Dong, C. Mueller, et al. 2008. CD11b+ monocytes abrogate Th17 CD4+ T cell-mediated experimental autoimmune myocarditis. *J. Immunol.* 180: 2686–2695.
28. Cihakova, D., J. G. Barin, M. Afanasyeva, M. Kimura, D. Fairweather, M. Berg, M. V. Talor, G. C. Baldeviano, S. Frisancho, K. Gabrielson, et al. 2008. Interleukin-13 protects against experimental autoimmune myocarditis by regulating macrophage differentiation. *Am. J. Pathol.* 172: 1195–1208.
29. Hanada, T., T. Yoshida, I. Kinjyo, S. Minoguchi, H. Yasukawa, S. Kato, H. Mimata, Y. Nomura, Y. Seki, M. Kubo, and A. Yoshimura. 2001. A mutant form of JAB/SOCS1 augments the cytokine-induced JAK/STAT pathway by accelerating degradation of wild-type JAB/CIS family proteins through the SOCS-box. *J. Biol. Chem.* 276: 40746–40754.
30. Chong, M. M., D. Metcalf, E. Jamieson, W. S. Alexander, and T. W. Kay. 2005. Suppressor of cytokine signaling-1 in T cells and macrophages is critical for preventing lethal inflammation. *Blood* 106: 1668–1675.
31. Ortiz-Muñoz, G., J. L. Martin-Ventura, P. Hernandez-Vargas, B. Mallavia, V. Lopez-Parra, O. Lopez-Franco, B. Muñoz-Garcia, P. Fernandez-Vizarra, L. Ortega, J. Egido, and C. Gomez-Guerrero. 2009. Suppressors of cytokine signaling modulate JAK/STAT-mediated cell responses during atherosclerosis. *Arterioscler. Thromb. Vasc. Biol.* 29: 525–531.
32. Yasukawa, H., T. Yajima, H. Duplain, M. Iwatate, M. Kido, M. Hoshijima, M. D. Weitzman, T. Nakamura, S. Woodard, D. Xiong, et al. 2003. The suppressor of cytokine signaling-1 (SOCS1) is a novel therapeutic target for enterovirus-induced cardiac injury. *J. Clin. Invest.* 111: 469–478.
33. Kanzaki, Y., F. Terasaki, M. Okabe, T. Hayashi, H. Toko, H. Shimomura, S. Fujioka, Y. Kitaura, K. Kawamura, Y. Horii, et al. 2001. Myocardial inflammatory cell infiltrates in cases of dilated cardiomyopathy as a determinant of outcome following partial left ventriculectomy. *Jpn. Circ. J.* 65: 797–802.
34. Münz, C., J. D. Lünemann, M. T. Getts, and S. D. Miller. 2009. Antiviral immune responses: triggers of or triggered by autoimmunity? *Nat. Rev. Immunol.* 9: 246–258.
35. Baetz, A., S. Zimmermann, and A. H. Dalpke. 2007. Microbial immune evasion employing suppressor of cytokine signaling (SOCS) proteins. *Inflamm. Allergy Drug Targets* 6: 160–167.
36. Akhtar, L. N., and E. N. Benveniste. 2011. Viral exploitation of host SOCS protein functions. *J. Virol.* 85: 1912–1921.
37. Yajima, T., H. Yasukawa, E. S. Jeon, D. Xiong, A. Dorner, M. Iwatate, M. Nara, H. Zhou, D. Summers-Torres, M. Hoshijima, et al. 2006. Innate defense mechanism against virus infection within the cardiac myocyte requiring gp130-STAT3 signaling. *Circulation* 114: 2364–2373.
38. Pesu, M., A. Laurence, N. Kishore, S. H. Zwillich, G. Chan, and J. J. O'Shea. 2008. Therapeutic targeting of Janus kinases. *Immunol. Rev.* 223: 132–142.
39. Yamaoka, K., B. Min, Y. J. Zhou, W. E. Paul, and J. J. O'shea. 2005. Jak3 negatively regulates dendritic-cell cytokine production and survival. *Blood* 106: 3227–3233.
40. Changelian, P. S., D. Moshinsky, C. F. Kuhn, M. E. Flanagan, M. J. Munchhof, T. M. Harris, D. A. Whipple, J. L. Doty, J. Sun, C. R. Kent, et al. 2008. The specificity of JAK3 kinase inhibitors. *Blood* 111: 2155–2157.
41. Frustaci, A., M. A. Russo, and C. Chimenti. 2009. Randomized study on the efficacy of immunosuppressive therapy in patients with virus-negative inflammatory cardiomyopathy: the TIMIC study. *Eur. Heart J.* 30: 1995–2002.
42. Tüting, T., W. J. Storkus, and L. D. Falo, Jr. 1998. DNA immunization targeting the skin: molecular control of adaptive immunity. *J. Invest. Dermatol.* 111: 183–188.
43. Condon, C., S. C. Watkins, C. M. Celluzzi, K. Thompson, and L. D. Falo, Jr. 1996. DNA-based immunization by in vivo transfection of dendritic cells. *Nat. Med.* 2: 1122–1128.
44. Porgador, A., K. R. Irvine, A. Iwasaki, B. H. Barber, N. P. Restifo, and R. N. Germain. 1998. Predominant role for directly transfected dendritic cells in antigen presentation to CD8+ T cells after gene gun immunization. *J. Exp. Med.* 188: 1075–1082.
45. Nishikubo, K., K. Imanaka-Yoshida, S. Tamaki, M. Hiroe, T. Yoshida, Y. Adachi, and Y. Yasutomi. 2007. Th1-type immune responses by Toll-like receptor 4 signaling are required for the development of myocarditis in mice with BCG-induced myocarditis. *J. Autoimmun.* 29: 146–153.
46. Akira, S., and H. Hemmi. 2003. Recognition of pathogen-associated molecular patterns by TLR family. *Immunol. Lett.* 85: 85–95.
47. Li, X., and J. Qin. 2005. Modulation of Toll-interleukin 1 receptor mediated signaling. *J. Mol. Med.* 83: 258–266.
48. Mansell, A., R. Smith, S. L. Doyle, P. Gray, J. E. Fenner, P. J. Crack, S. E. Nicholson, D. J. Hilton, L. A. O'Neill, and P. J. Hertzog. 2006. Suppressor of cytokine signaling 1 negatively regulates Toll-like receptor signaling by mediating Mal degradation. *Nat. Immunol.* 7: 148–155.
49. Gingras, S., E. Parganas, A. de Pauw, J. N. Ihle, and P. J. Murray. 2004. Re-examination of the role of suppressor of cytokine signaling 1 (SOCS1) in the regulation of toll-like receptor signaling. *J. Biol. Chem.* 279: 54702–54707.
50. Baetz, A., M. Frey, K. Heeg, and A. H. Dalpke. 2004. Suppressor of cytokine signaling (SOCS) proteins indirectly regulate toll-like receptor signaling in innate immune cells. *J. Biol. Chem.* 279: 54708–54715.

51. Qin, H., C. A. Wilson, S. J. Lee, and E. N. Benveniste. 2006. IFN-beta-induced SOCS-1 negatively regulates CD40 gene expression in macrophages and microglia. *FASEB J.* 20: 985–987.
52. Kimura, A., T. Naka, T. Muta, O. Takeuchi, S. Akira, I. Kawase, and T. Kishimoto. 2005. Suppressor of cytokine signaling-1 selectively inhibits LPS-induced IL-6 production by regulating JAK-STAT. *Proc. Natl. Acad. Sci. USA* 102: 17089–17094.
53. Eriksson, U., M. O. Kurrer, R. Bingisser, H. P. Eugster, P. Saremaslani, F. Follath, S. Marsch, and U. Widmer. 2001. Lethal autoimmune myocarditis in interferon-gamma receptor-deficient mice: enhanced disease severity by impaired inducible nitric oxide synthase induction. *Circulation* 103: 18–21.
54. Rangachari, M., N. Mauermann, R. R. Marty, S. Dirnhofer, M. O. Kurrer, V. Komnenovic, J. M. Penninger, and U. Eriksson. 2006. T-bet negatively regulates autoimmune myocarditis by suppressing local production of interleukin 17. *J. Exp. Med.* 203: 2009–2019.
55. Ghoreschi, K., A. Laurence, X. P. Yang, K. Hirahara, and J. J. O'Shea. 2011. T helper 17 cell heterogeneity and pathogenicity in autoimmune disease. *Trends Immunol.* 32: 395–401.
56. Baldeviano, G. C., J. G. Barin, M. V. Talor, S. Srinivasan, D. Bedja, D. Zheng, K. Gabrielson, Y. Iwakura, N. R. Rose, and D. Cihakova. 2010. Interleukin-17A is dispensable for myocarditis but essential for the progression to dilated cardiomyopathy. *Circ. Res.* 106: 1646–1655.

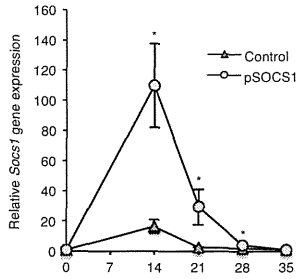

Supplementary Figure 1. *Socs1* gene expression in the heart. RNA samples were obtained from EAM hearts on days 0, 14, 21, 28 and 35, and used as a template for QRT-PCR. Results represent the average gene induction in five to six independent heart samples. Results of one of two representative experiments are shown. $*P < 0.05$ compared to control.

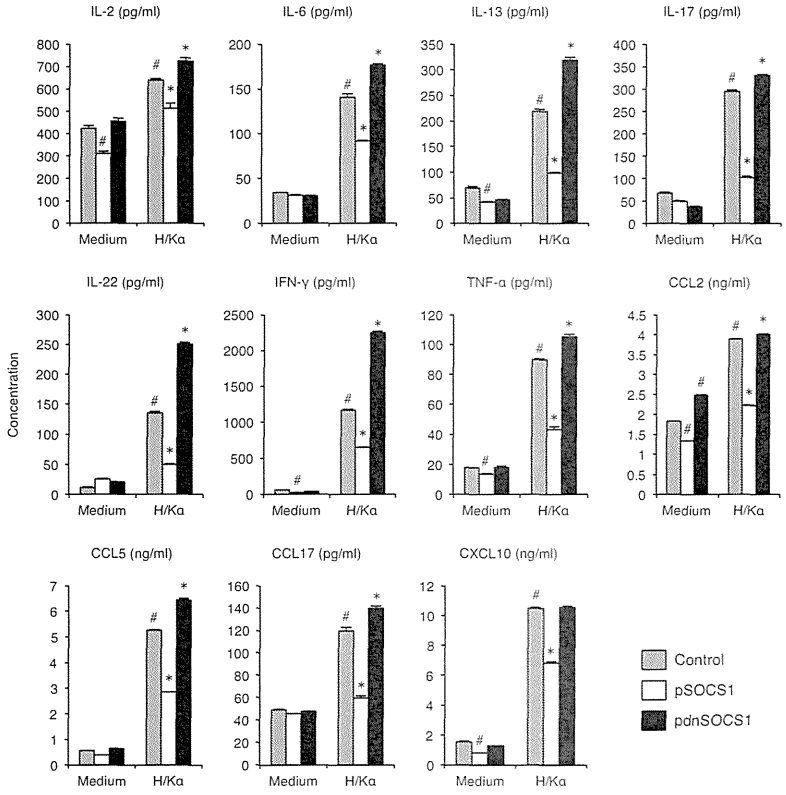

Supplementary Figure 2. Impaired cytokine production by H^+/K^+ ATPase α (H/Kα)-specific $CD4^+$ T cells in pSOCS1-treated mice. BALB/c mice were immunized twice, on days 0 and 7, with 100 μg of H/Kα p253-277 in an emulsion with CFA and treated with pSOCS1, pdnSOCS1 or control plasmid on days 0, 5 and 10. Splenocytes were isolated from mice on day 14 and cultured in the absence or presence of H/Kα peptide (1 μg/ml) for 72 h. Cytokines and chemokines in the culture supernatants were measured by ELISA. Data are expressed as mean ± SEM from triplicate culture wells. Results of one of two representative experiments are shown. $*P < 0.05$ compared to H/Kα stimulated control and $\#P < 0.05$ compared to unstimulated control.

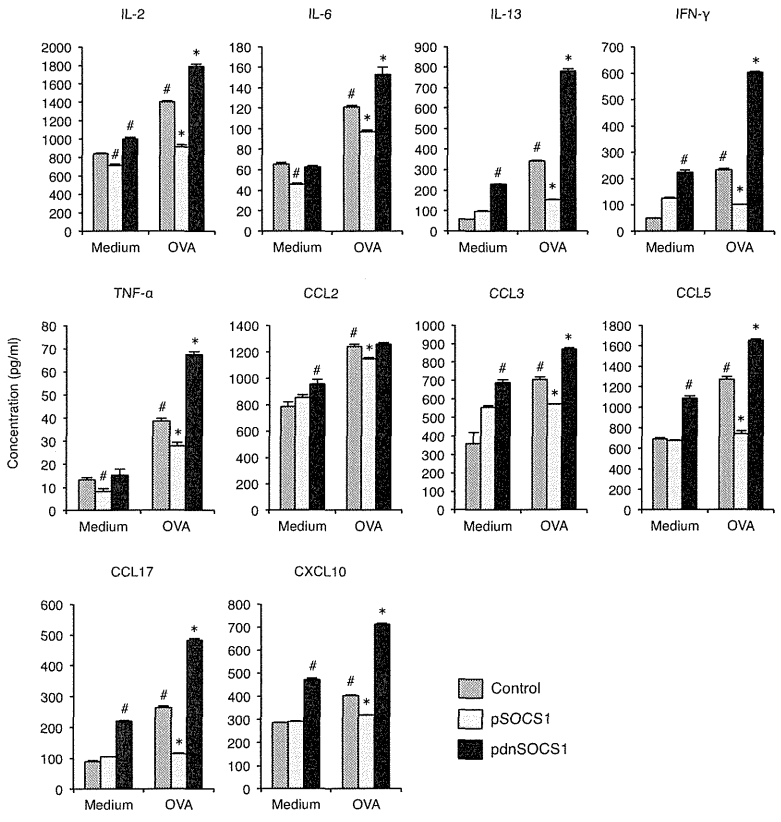

Supplementary Figure 3. Impaired cytokine production by OVA-specific CD4$^+$ T cells in pSOCS1-treated mice. BALB/c mice were immunized twice, on days 0 and 7, with 100 μg of OVA p323-339 in an emulsion with alum and treated with pSOCS1, pdnSOCS1 or control plasmid on days 0, 5 and 10. Splenocytes were isolated from mice on day 14 and cultured in the absence or presence of OVA peptide (5 μg/ml) for 72 h. Cytokines and chemokines in the culture supernatants were measured by ELISA. Data are expressed as mean ± SEM from triplicate culture wells. Results of one of two representative experiments are shown. *$P < 0.05$ compared to OVA stimulated control and #$P < 0.05$ compared to unstimulated control.

OPEN ACCESS Freely available online

PLoS one

Involvement of SIK3 in Glucose and Lipid Homeostasis in Mice

Tatsuya Uebi[1], Yumi Itoh[1], Osamu Hatano[2], Ayako Kumagai[1,3], Masato Sanosaka[1], Tsutomu Sasaki[4], Satoru Sasagawa[5], Junko Doi[6], Keita Tatsumi[7], Kuniko Mitamura[8], Eiichi Morii[9], Katsuyuki Aozasa[9], Tomohiro Kawamura[10], Meinoshin Okumura[10], Jun Nakae[11], Hajime Takikawa[12], Toshio Fukusato[13], Minako Koura[14], Mayumi Nish[2], Anders Hamsten[15], Angela Silveira[15], Alejandro M. Bertorello[16], Kazuo Kitagawa[4], Yasuo Nagaoka[3], Hidehisa Kawahara[3], Takeshi Tomonaga[17], Tetsuji Naka[18], Shigeo Ikegawa[8], Noriyuki Tsumaki[5,19], Junichiro Matsuda[14], Hiroshi Takemori[1]*

1 Laboratory of Cell Signaling and Metabolic Disease, National Institute of Biomedical Innovation, Ibaraki, Osaka, Japan, **2** Department of Anatomy, Nara Medical University, Nara, Japan, **3** Department of Life Science and Biotechnology, Kansai University, Suita, Osaka, Japan, **4** Department of Neurology, Osaka University Graduate School of Medicine, Osaka, Japan, **5** Department of Bone and Cartilage Biology, Osaka University Graduate School of Medicine, Osaka, Japan, **6** Food and Nutrition, Senri Kinran University, Osaka, Japan, **7** Department of Laboratory Medicine, Osaka University Graduate School of Medicine, Osaka, Japan, **8** Faculty of Pharmaceutical Sciences, Kinki University, Osaka, Japan, **9** Department of Pathology, Osaka University Graduate School of Medicine, Osaka, Japan, **10** Department of General Thoracic Surgery, Osaka University Graduate School of Medicine, Osaka, Japan, **11** Frontier Medicine on Metabolic Syndrome, Keio University School of Medicine, Tokyo, Japan, **12** Department of Medicine, Teikyo University School of Medicine, Tokyo, Japan, **13** Department of Pathology, Teikyo University School of Medicine, Tokyo, Japan, **14** Animal Models for Human Diseases, National Institute of Biomedical Innovation, Ibaraki, Osaka, Japan, **15** Cardiovascular Genetics and Genomics, Atherosclerosis Research Unit, Karolinska Institutet, CMM, Karolinska University Hospital-Solna, Stockholm, Sweden, **16** Membrane Signaling Networks, Atherosclerosis Research Unit, Karolinska Institutet, CMM, Karolinska University Hospital-Solna, Stockholm, Sweden, **17** Laboratory of Proteome Research, National Institute of Biomedical Innovation, Ibaraki, Osaka, Japan, **18** Laboratory for Immune Signal, National Institute of Biomedical Innovation, Ibaraki, Osaka, Japan, **19** Department of Cell Growth and Differentiation, Center for iPS Cell Research and Application, Kyoto University, Kyoto, Japan

Abstract

Salt-inducible kinase 3 (SIK3), an AMP-activated protein kinase-related kinase, is induced in the murine liver after the consumption of a diet rich in fat, sucrose, and cholesterol. To examine whether SIK3 can modulate glucose and lipid metabolism in the liver, we analyzed phenotypes of SIK3-deficient mice. *Sik3*$^{-/-}$ mice have a malnourished the phenotype (*i.e.*, lipodystrophy, hypolipidemia, hypoglycemia, and hyper-insulin sensitivity) accompanied by cholestasis and cholelithiasis. The hypoglycemic and hyper-insulin-sensitive phenotypes may be due to reduced energy storage, which is represented by the low expression levels of mRNA for components of the fatty acid synthesis pathways in the liver. The biliary disorders in *Sik3*$^{-/-}$ mice are associated with the dysregulation of gene expression programs that respond to nutritional stresses and are probably regulated by nuclear receptors. Retinoic acid plays a role in cholesterol and bile acid homeostasis, wheras ALDH1a which produces retinoic acid, is expressed at low levels in *Sik3*$^{-/-}$ mice. Lipid metabolism disorders in *Sik3*$^{-/-}$ mice are ameliorated by the treatment with 9-cis-retinoic acid. In conclusion, SIK3 is a novel energy regulator that modulates cholesterol and bile acid metabolism by coupling with retinoid metabolism, and may alter the size of energy storage in mice.

Citation: Uebi T, Itoh Y, Hatano O, Kumagai A, Sanosaka M, et al. (2012) Involvement of SIK3 in Glucose and Lipid Homeostasis in Mice. PLoS ONE 7(5): e37803. doi:10.1371/journal.pone.0037803

Editor: Jean-Marc A. Lobaccaro, Clermont Université, France

Received February 10, 2012; **Accepted** April 24, 2012; **Published** May 25, 2012

Funding: This study was supported by Grants-in-aid for Scientific Research from the Ministry of Education, Culture, Sports, Science, and Technology, Japan; Natural Scientists and the Strategic Project to Support the Formation of Research Bases at Private Universities; and a grant from the Sumitomo Foundation. The funders had no role in study design, data collection and analysis, decision to publish, or preparation of the manuscript.

Competing Interests: The authors have declared that no competing interests exist.

* E-mail: takemori@nibio.go.jp

Introduction

Cholesterol has diverse functions in eukaryotes, *e.g.*, as a cell membrane component and a source of hormones and bile acid (BA). Dysregulation of cholesterol metabolism is involved in a variety of disease, such as dyslipidemia, cardiovascular disease, and obesity [1]. The liver X receptor (LXR) is a nuclear receptor that binds to target DNA elements by forming a heterodimer complex with the retinoid X receptor (RXR) [2,3]. Excess cholesterol is sensed by LXRs as their ligands, and active LXR-RXR complexes promote the gene expression of cholesterol-catabolic enzymes (*e.g.*, cytochrome P450 family 7A [CYP7A], which catabolizes cholesterol to BA in the liver) and cholesterol transporters, *e.g.*, ATP-cassette G5 (ABCG5) and G8 in the liver and ABCA1 in the peripheral tissues. LXR also up-regulates hepatic fatty acid (FA) synthesis by inducing the expression of sterol regulatory element-binding protein 1c (SREBP1c) [4].

BA is also multifunctional molecules with a role in the digestive tract. The impairment of bile flow by bile duct lesions and cholelithiasis causes the retention of excess amounts of BA (cholestasis) and leads to chronic hepatitis. The farnesoid X

receptor (FXR) senses BA as its ligand, forms a complex with RXR, and up-regulates gene expression to lower the level of BA in the liver [5] by inducing the bile salt export pump (BSEP) and small heterodimer partner (SHP), which suppresses *Cyp7a* expression [6]. Excess levels of the BA pool also enhance energy expenditure and suppression of FA synthesis [7]. Meanwhile, a reduction of the BA pool by the activation of FXR induces obesity and hyperglycemia [8], suggesting that cholesterol-BA homeostasis is important for lipid and glucose metabolism.

9-*Cis* retinoic acid (9-cis-RA), an endogenous RXR ligand, is synthesized from vitamin A [9]. Vitamin A deficiency or RXR inhibition results in reduced LXR and FXR activity, which can lead to hepatic cholestasis [1]. Conversely, dysregulation of the metabolism of vitamin A to 9-cis-RA induces resistance to diet-induced obesity and type 2 diabetes in mice [10]. Because vitamin A absorption by enterocytes requires BA, BA homeostasis is tightly coupled with vitamin A metabolism [11].

Salt-inducible kinase (SIK), a member of the 5′-AMP-activated protein kinase (AMPK)-related kinase family, has 3 isoforms and regulates gene expression in various cells [12]. For example, SIK1 inhibits steroidogenic gene expression in the adrenal glands and gluconeogenic gene expression programs in the liver by repressing the cAMP response element (CRE)-binding protein (CREB) transcription factor [13,14] [15–16]. Meanwhile, SIK2 suppresses insulin-dependent thermogenic gene expression in brown adipose tissue [17]. In addition, in mice with a disrupted *Sik2* gene, downregulation of SIK2 expression confers resistance to oxidative stresses after brain ischemia [18] and enhances melanogenesis in melanocytes after ultraviolet irradiation [19,20]. These SIK2-dependent physiological events are also explained by the modulation of CREB activity.

When CREB is phosphorylated at Ser133 in its kinase-inducible domain by upstream activating kinases, such as protein kinase A (PKA) and Ca^{2+}/calmodulin-dependent kinase I/IV (CaMKI/IV), it recruits coactivators, *e.g.*, CREB-binding protein and p300 and induces CRE-dependent transcription [21]. The other CREB-specific coactivator, *i.e.*, CREB regulated transcription coactivator (CRTC or TORC), also activates CREB in response to PKA and CaMKI/IV [22,23]. In contrast to CREB, CRTC is inactivated by phosphorylation and is sequestered in the cytoplasm of unstimulated cells [24]. SIK1 and SIK2 are among the CRTC kinases that are involved in SIK-mediated inhibition of CREB [25]. Recently, p300 was also reported to be a mediator of SIK signaling in hepatocytes [26]. SIK2 inhibits the coactivation activity of p300 by phosphorylating Ser89, which prevents carbohydrate response element-binding protein-dependent hepatic steatosis in mice.

In addition to CREB and p300 repression, SIK1 induces hypertrophic action in the muscles by inhibiting class 2a histone deacetylase (HDAC) and then upregulating MEF2C transcription activity [27]. Recently, SIK2 was also found to inactivate class 2a HDAC in *Drosophila*, which results in the accumulation of FA in the fat body of insects and confers resistance to starvation [28]. These observations suggest that like AMPK, SIK1 and SIK2 may play important roles in the regulation of metabolic or stress responses.

SIK3 is also capable of regulating CREB activity in cultured cells under overexpression [29] or *in vitro* conditions [30]. Recently, we found that mice with a disrupted *Sik3* gene showed dwarfism because of the impairment of chondrocyte hypertrophy during skeletal development, which was accompanied by disinactivation of class 2a HDAC in the cartilage [31]. However, SIK3 phenotypes in adult mice, especially those related to energy metabolism, have not yet been elucidated.

Here, we report the induction of *Sik3* mRNA in the mouse liver after the consumption of a high-fat diet supplemented with excess cholesterol. Phenotyping of adult $Sik3^{-/-}$ mice suggested that SIK3 is a novel regulator of glucose-lipid metabolism in the liver that maintains cholesterol-BA homeostasis along with the regulation of lipid storage size.

Results

Sik3$^{-/-}$ Mice Exhibit a Lipodystrophic Phenotype

Factors affecting body size and longevity in model organisms, such as *Caenorhabditis elegans* and *Drosophila*, often play important roles in the regulation of energy metabolism in mammals. The same may hold true for SIK. The *C. elegans kin-29* (ortholog of SIK) mutant shows increased longevity and small body size [32], while *Drosophila* expressing reduced levels of SIK2 acquired resistance to oxidative stress and starvation [33]. We also found that $Sik2^{-/-}$ mice show resistance to brain ischemia [18]; however, $Sik2^{-/-}$ mice are apparently normal in terms of body weight regulation [19].

To reevaluate individual SIK isoforms in the regulation of nutrient metabolism, normal C57BL/6J mice were fed with a variety of diets, and we examined their mRNA levels were examined. Interestingly, *Sik3* mRNA was strongly induced in the livers of the mice fed a high-fat/high-sucrose/high-cholesterol (HF/HS/HChol) diet. This up-regulation was accompanied by the induction of mRNA for metabolic enzymes such as *FA synthase* (*Fasn*) and *Cyp7a* (Figure 1A). These results led us to investigate of the metabolic profiles of *Sik3* knockout mice [31].

Although $Sik3^{-/-}$ mice were indistinguishable from wild-type mice just after birth, most of the knockout (KO) mice died on the first day (Figure S1A). Caesarean delivery failed to prevent the early death of $Sik3^{-/-}$ mice. Because $Sik3^{-/-}$ mice had skeletal abnormalities, their early death was probably due to respiratory failure caused by thoracic dystrophy [31]. However, the transgenic expression of SIK3 in the cartilage of $Sik3^{-/-}$ mice failed to prevent their early death despite its correction of the skeletal abnormalities (no $Sik3^{-/-}$ mouse survived out of seventeen weanling mice derived from the matings between $Sik3^{-/-}$ females and $Sik3^{-/-}$ :: *Col11a2-hSik3* males).

The $Sik3^{-/-}$ mice that survived the first day could be weaned (Figure S1B), but their body weight was obviously less than that of the wild-type mice (male; Figure 1B). This was also the case with the females. We dissected 1-year-old mice and found that the lean phenotype of $Sik3^{-/-}$ mice was attributed to the liver and adipose tissues, especially mesenteric and perirenal fat (Figure 1C and D). Small but substantial amounts of gonadal and subcutaneous fat and brown adipose tissue were observed in $Sik3^{-/-}$ mice. Hematoxylin and eosin (HE) staining suggested that the small fat pads were probably due to the small size of the adipocytes (Figure 1E and S1C). The low levels of liver TG in $Sik3^{-/-}$ mice might have prevented the development of fatty liver (Figure 1E and F), while total cholesterol levels were low in the serum of $Sik3^{-/-}$ mice. Fast protein liquid chromatography (FPLC) analysis of serum lipids indicated that $Sik3^{-/-}$ mice exhibited hypo-high density lipoprotein (HDL) cholesterolemia (Figure 1G).

To elucidate the causes of the lipodystrophic phenotype of $Sik3^{-/-}$ mice, we compared the energy balance between wild-type and $Sik3^{-/-}$ mice. $Sik3^{-/-}$ mice consumed more food than the wild-type mice (Figure 1H), while the rate of digestion and absorption in the intestine appeared normal (Figure S1D). The rectal temperature of $Sik3^{-/-}$ mice was higher than that of the wild-type mice (Figure 1I), which might correlate with the high levels of the O_2 consumption (VO_2: voluntary O_2 consumption) observed in $Sik3^{-/-}$ mice (Figure 1J). The high respiratory quotient (RQ) value of the $Sik3^{-/-}$ mice was well explained by the insufficient fat storage followed by reduced fat utilization observed in these mice (Figure 1K). These results suggested that the lipodystrophic phenotype of $Sik3^{-/-}$ mice might be a result of their high rates of energy consumption.

We also examined secondary parameters such as blood glucose levels. In the fed condition, the $Sik3^{-/-}$ mice had slightly lower

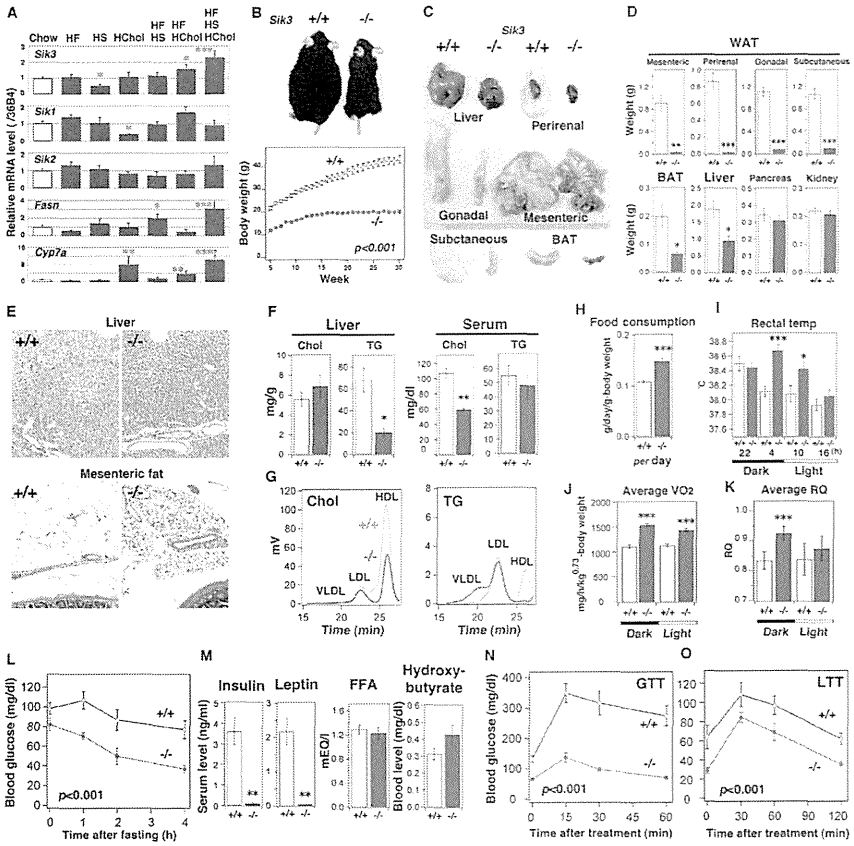

Figure 1. *Sik3*$^{-/-}$ mice are lean, hypolipidemic, and hypoglycemic. (A) C57BL/6 mice (male: n = 4) were fed various diets (HF, high fat; HS, high sucrose; HChol, high cholesterol) for 2 weeks, and liver mRNA was examined by quantitative PCR. *, **, and *** indicate $p<0.05$, <0.01, and <0.001, respectively. Means and SEM are shown. (B) The body weight of male mice (n = 6) was monitored. All data points show $p<0.001$. (C) One-year-old male mice (n = 5) were sacrificed (scale: 1 mm), and the indicated tissues were weighed (D). (E) Histology of liver and mesenteric fatty tissue is shown. Each magnification is the same. (F) Cholesterol (Chol) and triglycerides (TG) in the liver and serum were measured (n = 5). (G) Serum cholesterol and TG were separated using FPLC. (H) The food consumption of each group (n = 12). (I) Rectal temperature (n = 12). (J) Oxygen consumption (VO_2, voluntarily O_2 consumption) and (K) average respiratory quotient (RQ) during the day and night (n = 5). (L) Mice (n = 5) were fasted and their blood glucose levels were monitored at the indicated time points. All data points show $p<0.001$. (M) After 4-h fasting, the serum levels of insulin, leptin, free fatty acid (FFA), and ß-hydroxybutyrate were measured. (N) After 4-h fasting, glucose (1.5 g/kg) was intraperitoneally injected (GTT, glucose tolerance test) and blood glucose levels were monitored (n = 5). (O) After 24-h fasting, lactate (1.5 g/kg) was injected intraperitoneally (LTT, lactate tolerance test; n = 5).
doi:10.1371/journal.pone.0037803.g001

blood glucose levels than the wild-type mice, and the levels quickly decreased after fasting (Figure 1L). After a 4-h fast, the *Sik3*$^{-/-}$ mice had significantly lower serum insulin and leptin levels than the wild-type mice (Figure 1M), while no obvious differences were observed in free FA or ketone body (ß-hydroxybutyrate) levels. Given the enhanced food-consumption of *Sik3*$^{-/-}$ mice, the apparently enhanced insulin- and leptin-action may be restricted to the peripheral tissues. Although we suspected thyrotoxicosis, the levels of circulating thyroid hormones did not differ between the 2 genotypes (Figure S1E).

Sik3$^{-/-}$ mice exhibited enhanced glucose tolerance (GTT) (Figure 1N). When *Sik3*$^{-/-}$ mice were treated with insulin (ITT), their blood glucose levels decreased like those of the wild-type mice (Figure S1F). Once the *Sik3*$^{-/-}$ mice were supplied exogenously with an energy source, such as lactate (lactate tolerance test), they were able to produce glucose efficiently (Figure 1O), suggesting that the hypoglycemia of *Sik3*$^{-/-}$ mice may be due to a lack of energy storage followed by an enhanced insulin response. This was also the case under the high-fat diet feeding condition (Figure 2A–J). Of particular note is that accumulation of cholesterol was suppressed in the livers of *Sik3*$^{-/-}$ mice (Figure 2I), and the ratio of LDL-cholesterol to HDL-cholesterol was decreased in the serum of *Sik3*$^{-/-}$ mice with a reduction of TG content in the very low-density lipoprotein (VLDL) fraction (Figure 2J).

Which tissue is responsible for the phenotypes of the *Sik3*$^{-/-}$ mice? To address this question, we measured the body weight of heterozygous (*Sik3*$^{+/-}$) mice. The body weight curve of the *Sik3*$^{+/-}$ mice overlapped with that of the wild-type mice (Figure S2A). Curiously, the mRNA and protein levels of SIK3 in the livers of *Sik3*$^{+/-}$ mice were as high as those in wild-type mice (Figure S2B), though the specific levels of *Sik3* mRNA did not differ between parenchymal and non-parenchymal cells (Figure S2C). Given that parenchymal cells are the major population of the liver, we surmised that the liver, probably parenchymal cells, may be one of the responsible tissues/cells for the phenotypes of the *Sik3*$^{-/-}$ mice.

Mice with disrupted genes for *Mark2* [34] or *Mark3* [35], which are other members of the AMPK family, have been found to be resistant to diet-induced obesity due to enhanced glucose-utilization in the brown adipose tissue. However, the mRNA expression levels of genes related to energy expenditure, such as *Ppargc1a* and *Ucp1*, in brown adipose tissue were not different between wild-type and *Sik3*$^{-/-}$ mice.

Moreover, an *in vitro* adipocyte differentiation experiment using gonadal fat indicated that the preadipocytes of *Sik3*$^{-/-}$ mice possessed a higher capability to differentiate into adipocytes than those from wild-type mice (Figure S2D), which might correlate with the high serum level of adiponectin in *Sik3*$^{-/-}$ mice (Figure S2E). Given the expression level of *Sik3* mRNA (Figure S2B), we surmised that the lipodystrophic phenotype of *Sik3*$^{-/-}$ mice might be caused by the impairments of the liver rather than the adipose tissues.

Signaling States in the Livers of Sik3$^{-/-}$ Mice

The gene expression profile of the liver (Figure 3A) indicated that the pathway from glycolysis to FA synthesis was down-regulated in *Sik3*$^{-/-}$ mice, while the glyconeogenic pathway was up-regulated. *Sik3*$^{-/-}$ mice expressed high levels of *Fgf21* mRNA, suggesting an adaptive response to starvation; however, its promoting pathway, *i.e.*, the peroxisome proliferator-activated receptor alpha (PPARα) pathway, was down-regulated. Lack of FA storage and the uncoupling of FGF21 from the PPARα pathway in *Sik3*$^{-/-}$ mice may result in the failure to induce ß-oxidation followed by ketogenesis [36].

We also examined the state of signaling molecules. The high level of PGC-1α protein in the liver of *Sik3*$^{-/-}$ mice was accompanied by the dephosphorylation of CRTC2 (Figure 3B) despite there being no significant difference in the status of CREB. Interestingly, the level of another CRTC2 kinase, AMPK [15], and of its activated phosphorylated form (pThr172) were also high in the livers of *Sik3*$^{-/-}$ mice. Immunohistochemical analyses revealed the enhanced accumulation of CRTC2 in the nuclei of *Sik3*$^{-/-}$ mice hepatocytes (Figure 3C). In addition, HDAC5, another SIK/AMPK substrate [37,38], also accumulated in the nuclei of liver cells in *Sik3*$^{-/-}$ mice, suggesting that AMPK is unable to compensate for the deficiency of SIK3 in hepatocytes.

Sik3$^{-/-}$ Mice are Unable to Adapt to Cholesterol

Adiponectin had been found to promote fat accumulation in adipose tissues and to improve insulin sensitivity in leptin-resistant mice [39], which could explain the hypoglycemic phenotype of *Sik3*$^{-/-}$ mice, but not their lipodystrophy. What are the unknown factors? Interestingly, little, if any, changes were found in the mRNA levels of the cholesterol and BA metabolic genes in *Sik3*$^{-/-}$ mice (Figure 3A) and irregular expression patterns were observed, *i.e.*, *ApoA1* and *Abcg5* were up-regulated, while *Cyp8b* was strongly suppressed. Moreover, hepatic *Sik3* mRNA expression is induced by a high-fat diet supplemented with high-cholesterol (Figure 1A). Therefore, we decided to examine effects of cholesterol (with fat) on *Sik3*$^{-/-}$ mice by challenging the mice with a high-cholesterol diet (HF/HS/HChol).

After 4 months, the wild-type mice developed fatty liver, while the livers of *Sik3*$^{-/-}$ mice had surface asperity and turned yellow (Figure 4A). HE staining revealed the enhanced formation of a dilated canalicular structure in the livers of *Sik3*$^{-/-}$ mice (Fig 4B, *upper* and *lower left*), and these structures were highly positive for BSEP-immunoreactive signals (*green signals* in Figure 4B *lower right*). Liver and serum lipid levels were increased after feeding with the HF/HS/HChol diet; however, they were not significantly different from the levels observed when wild-type and *Sik3*$^{-/-}$ mice were fed a chow diet (compare Figure 1F to Figure 4C). The ratio of LDL-cholesterol to HDL-cholesterol in *Sik3*$^{-/-}$ mice was reversed after feeding with the cholesterol-containing diet (compare Figure 1G to Figure 4D), and was accompanied by an increase in TG content in the LDL fraction in *Sik3*$^{-/-}$ mice.

The fluctuations in serum alanine amino transferase (ALT) levels suggested that the livers of *Sik3*$^{-/-}$ mice were damaged soon after feeding and lost their normal function, *e.g.*, ALT production, after 5 weeks (Figure 4E). While liver injury in the wild-type mice progressed gradually, probably due to fatty liver, the degree of latent liver injury after 4-month of receiving the high-cholesterol diet was higher in *Sik3*$^{-/-}$ mice, possibly because of the higher mRNA expression levels of inflammatory factors in the livers of *Sik3*$^{-/-}$ mice (Figure 4F).

To focus on effects of cholesterol alone, *Sik3*$^{-/-}$ mice were challenged with a high-cholesterol (2%) diet according to the same schedule as the HF/HS/HChol diet. The liver abnormalities of *Sik3*$^{-/-}$ mice were barely visible on the surface (Figure 5A); however, a number of foci that were negative for eosin-staining (Figure 5B, arrows) were detected in the livers of *Sik3*$^{-/-}$ mice. These foci might be enriched in cholesterol derivatives, because we observed strong autofluorescence in the frozen sections (Figure 5B *lower right*), and the level of hepatic cholesterol was higher in *Sik3*$^{-/-}$ mice than in wild-type mice (Figure 5C). A small numbers of dilated canalicular structures were again observed in the *Sik3*$^{-/-}$ mice liver (Figure 5B *lower left*).

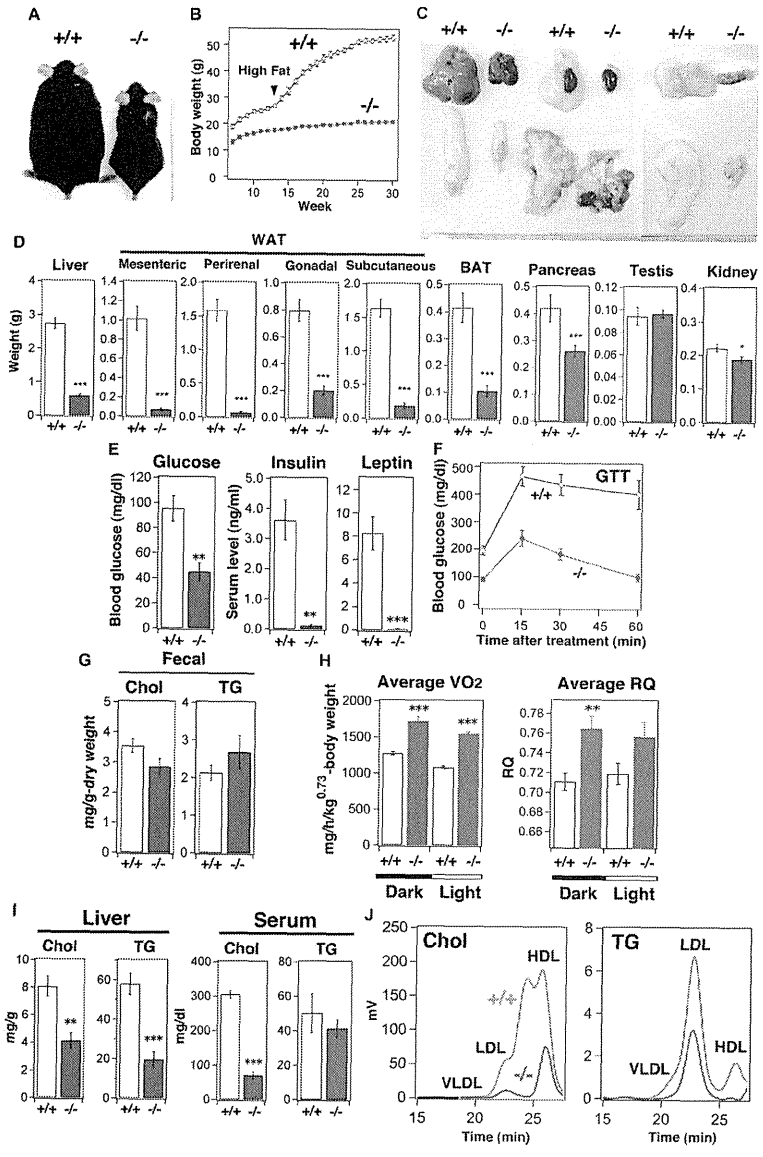

Figure 2. *Sik3*$^{-/-}$ mice are resistant to a high-fat diet. (A) A representative image of male mice after high-fat (60% of calories) feeding. Mice (n = 6) were fed with a high-fat diet for 12–30 weeks and their body weights were monitored every week (B). Means and SEM are shown. All data points indicate $p<0.001$. (C) Representative photos of tissues (scale, 1 mm). (D) Tissue weights are shown. *, **, and *** indicate $p<0.05$, <0.01, and <0.001, respectively. (E) Levels of blood glucose, insulin, and leptin measured after 4-h fasting. (F) Glucose tolerance test (1.5 g/kg) performed after 4-h fasting. (G) Cholesterol and triglyceride content in feces (n = 3 cages). (H) Oxygen consumption (VO_2, voluntarily O_2 consumption) of each group (n = 6) was monitored. Respiration quotient (RQ) during the day and night. (I) Cholesterol (Chol) and triglycerides (TG) in the liver and serum were measured (n = 6). (J) Serum Chol and TG were separated using FPLC.
doi:10.1371/journal.pone.0037803.g002

The patterns of serum lipids in *Sik3*$^{-/-}$ mice fed with the high-cholesterol diet were almost the same as those of *Sik3*$^{-/-}$ mice fed with the HF/HS/HChol diet. Liver injury in *Sik3*$^{-/-}$ mice progressed gradually (Figure 5E), and we observed high mRNA expression levels of inflammatory factors in the liver of *Sik3*$^{-/-}$ mice (Figure 5F).

Why were the livers of *Sik3*$^{-/-}$ mice injured after the consumption of the high-cholesterol diet? Are there any hints to explain the lipodystrophic phenotype of these mice? To address these questions, we reevaluated blood biochemical markers for the liver and biliary duct systems. Even when *Sik3*$^{-/-}$ mice were fed a chow diet, their serum ALT levels gradually increased with age (Figure 6A). However, the high-fat diet (as evidenced by the dissection of a 30-week-old mouse) protected the livers of *Sik3*$^{-/-}$ mice from the injuries caused by aging as well as by fatty liver. Conversely, once cholesterol is added to the diet, this protection may become invalid. As the serum alkaline phosphatase (ALP) and BA levels were continuously high in *Sik3*$^{-/-}$ mice, except when under the high-fat diet, we hypothesized that the dysregulation of BA metabolism followed by hepatic cholestasis (Figure 6B) might be the cause of the hepatic injuries.

In addition, to test whether high levels of BA could suppress body weight gain, the mice were fed a high-cholic acid (CA) diet for 1 month. As shown in Figure 6C, the high-CA diet completely suppressed the weight gain of wild-type mice and reduced the body weight of *Sik3*$^{-/-}$ mice, suggesting that dysregulation of BA metabolism might be one of the causes of the lipodystrophic phenotype of *Sik3*$^{-/-}$ mice.

Sik3$^{-/-}$ Mice are Unable to Adapt to CA

To examine the details of the dysregulation of BA metabolism in *Sik3*$^{-/-}$ mice, we dissected these mice. Their gallbladders of *Sik3*$^{-/-}$ mice were enlarged, and their livers had become yellow-brown (Figure 7A). HE staining identified hypertrophic hepatocytes with lipid droplets (Figure 7B). The gallbladders of *Sik3*$^{-/-}$ mice (Figure 7C) were accompanied by hyperplastic mucosal epithelia (Figure 7E).

The volume of bile in the gallbladders of *Sik3*$^{-/-}$ mice was large, but its color was light (Figure 7D). A good amount of bile sand was also found in the gallbladders of *Sik3*$^{-/-}$ mice (Figure 7D, *right*). Like FXR-KO mice [40], the deposition of bile sand might be a result of the presence of cholesterol crystals

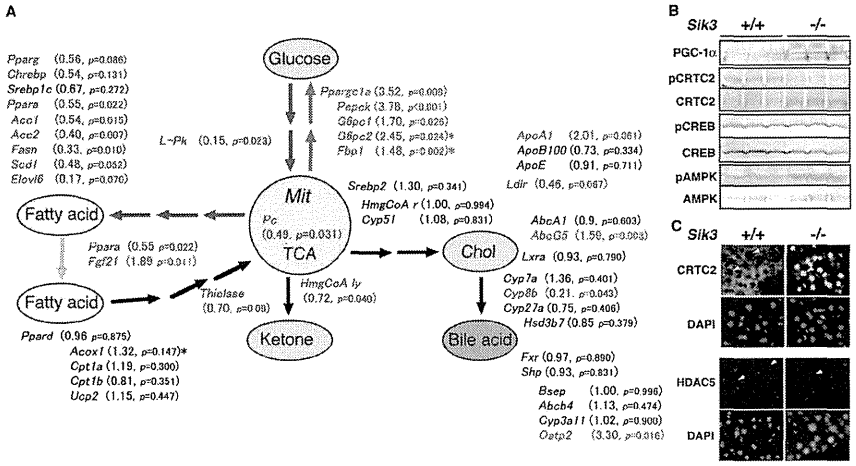

Figure 3. Gene expression profile in the liver. (A) One-year-old male mice (n = 5) were fasted for 4 h, and the liver mRNA levels were measured using quantitative polymerase chain reaction (qPCR). Red and blue indicate the up- and down-regulated genes in *Sik3*$^{-/-}$ mice, respectively. +, fold increase; -, fold decrease. The threshold is set at $p = 0.1$. The values marked with an asterisk (*) were obtained using PCR-array kits (n = 3). The abbreviations for the genes and the PCR primers used are listed in Table S2. Mit, mitochondria; TCA, tricarboxylic acid cycle. (B) Intracellular signaling molecules and their activation status in the liver were examined by western blot analysis. (C) Immunohistochemical analysis of SIK3 substrates (CRTC2 and HDAC5) in the liver.
doi:10.1371/journal.pone.0037803.g003

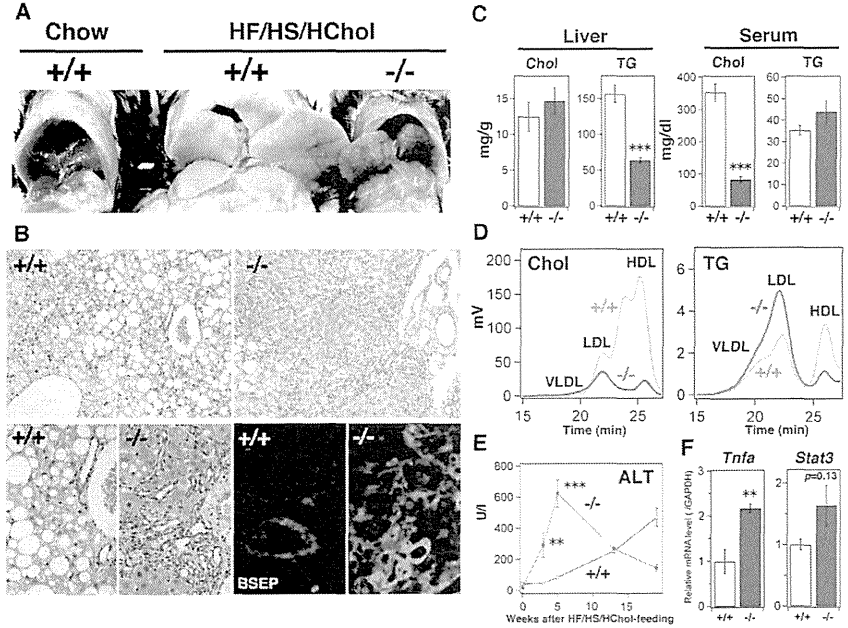

Figure 4. *Sik3*$^{-/-}$ mice are less tolerant to a cholesterol-containing high-fat diet. (A) Male mice were fed a high-fat and high-sucrose diet supplemented with 2% cholesterol (HF/HS/HChol) for 4 months (12–30 weeks) and then sacrificed (n = 6). (B) HE staining of the liver (sets at the *upper* and *lower left*), BSEP-staining (*lower right*: BSEP is green and nuclei are blue (DAPI)). The magnification is the same in each set. (C) Cholesterol and TG levels in the liver and serum were measured (n = 6). *** indicates $p<0.001$. Means and SEM are shown. (D) FPLC analysis of serum lipids. (E) Serum levels of alanine aminotransferase (ALT) were monitored at the indicated time points. ** indicates $p<0.01$. (F) Quantitative polymerase chain reaction analysis of inflammatory molecules (tumor necrosis factor-α and STAT3) in the liver.
doi:10.1371/journal.pone.0037803.g004

because cholesterol was depleted from the bile of *Sik3*$^{-/-}$ mice (Figure 7F); this could have been caused by the decreased levels of phospholipids followed by the reduced solubility of bile [41].

High serum BA and ALT levels were observed in *Sik3*$^{-/-}$ mice on the high-CA diet (Figure 7G). The levels of ALP and total bilirubin were also high in *Sik3*$^{-/-}$ mice (Figure 7H). The lipid droplets observed in the livers of *Sik3*$^{-/-}$ mice (Figure 7B) might be composed of cholesterol because cholesterol, and not TG, had accumulated in their livers (Figure 7I). The levels and patterns of serum cholesterol and TG in *Sik3*$^{-/-}$ mice were also abnormal (Figure 7J); notably, the levels of cholesterol in the VLDL-LDL fraction of the wild-type mice was enhanced by CA feeding, which was more obvious in *Sik3*$^{-/-}$ mice. Given the severe phenotype caused by CA feeding, we surmised that cholestasis might be the primary phenotype of *Sik3*$^{-/-}$ mice, and this may then lead to or enhance the other phenotypes, *e.g.*, lipodystrophy and dyslipidemia.

Because most of the *Sik3*$^{-/-}$ mice were dead on the day of birth (Figure S1A), we examined the livers of embryos. As shown in Figure S3A, hepatocytes in *Sik3*$^{-/-}$ embryos (E18.5) were not normal; notably, the hepatocytes were of a variable size, and a significant number of multinucleated hepatocytes were observed, suggesting liver damages due to embryonic cholestasis. It was partly true that the BA levels in the livers of *Sik3*$^{-/-}$ embryos were higher than those of wild-type embryos (Figure S3B). However, when the mice were born, the BA content in the liver of the wild-type mice reached levels equivalent to that of *Sik3*$^{-/-}$ mice and decreased thereafter, suggesting that hepatic cholestasis might occur in *Sik3*$^{-/-}$ embryos, but it cannot explain the early death of *Sik3*$^{-/-}$ mice. Alternatively, we suppose that *Sik3*$^{-/-}$ neonates may unable to adapt their metabolism to the environmental changes at birth.

Gene Expression Profile in the Livers of Sik3$^{-/-}$ Mice Fed with Special Diets

We examined mRNA expression in the liver to elucidate the mechanisms involved in the *Sik3*$^{-/-}$ phenotypes. As shown in Table S1, the resistance to diet-induced obesity in *Sik3*$^{-/-}$ mice might be explained by the low levels of lipogenic mRNA, *e.g.*, *Fasn* and *Scd1*. Amelioration of hepatic injury in *Sik3*$^{-/-}$ mice

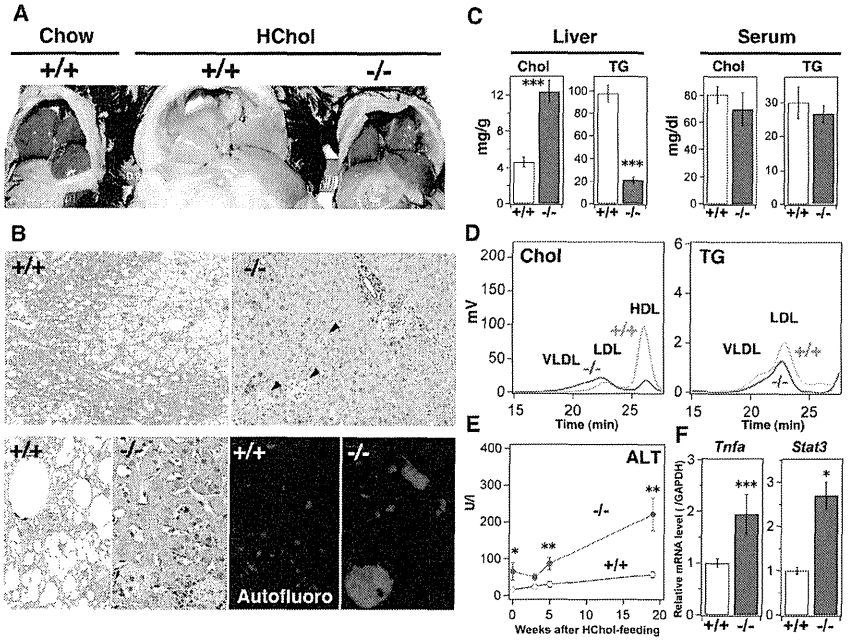

Figure 5. Cholesterol accumulation in the livers of *Sik3*$^{-/-}$ mice after feeding with a high-cholesterol diet. (A) Male mice were fed a 2% cholesterol diet for 4 months (12–30 weeks) and then sacrificed (n = 5). (B) HE staining of the liver (sets at the *upper* and *lower left*). The arrows indicate eosin-negative foci which with autofluorescence (*lower right*: red, and nuclei are blue (DAPI)). The magnification is the same in each set. (C) Cholesterol and TG levels in the liver and serum were measured (n = 5). *** indicates $p<0.001$. Means and SEM are shown. (D) FPLC analysis of serum lipids. (E) Serum levels of alanine aminotransferase (ALT) were monitored at the indicated time points. * and ** indicate $p<0.05$ and $p<0.01$, respectively. (F) Quantitative polymerase chain reaction analysis of inflammatory molecules in the liver.
doi:10.1371/journal.pone.0037803.g005

by the high-fat diet was probably due to the down-regulation of cholesterol (*HmgCoAr*) and BA (*Cyp7a*) synthesis.

However, the mRNA expression patterns of mice fed on the high-cholesterol or high-CA diet could not explain the pathogenesis of *Sik3*$^{-/-}$ *mice*, and some discrepancies remained. When mice were fed with the high-cholesterol diet, no significant difference in the mRNA levels of genes for cholesterol synthesis, *e.g., HmgCoAr*, was observed between wild-type and *Sik3*$^{-/-}$ mice. The level of *Cyp7a* (bile acid synthesis) mRNA was also the same, despite the high expression level of its repressor (*Shp*). Meanwhile, when the mice were fed with the high-CA diet, *Sik3*$^{-/-}$ mice expressed lower levels of *Cyp7a* mRNA than the wild-type mice, despite no changes in the levels of *Shp*.

Here, we have to mention some of the problems associated with these gene expression analyses. For example, the mice that were fed the different diets were of different ages. In addition, the special diets were suspected to produce secondary effects, such as hepatic injury. Therefore, we decided to examine gene expression during the acute phase.

Adaptive Gene Expression is Dysregulated in Sik3$^{-/-}$ Mice

To examine gene expression during the acute phase with a biased diet, 12-week-old mice were fed either a high-cholesterol or high-CA diet for 2 days or a high-fat diet for 2 weeks. As shown in Figure 8A and S3A, the gene expression profile in the livers of young mice under chow-diet feeding was different from that of aged mice (Figure 3A), probably due to differences in the degree of hepatic injury (Figure 6A). Under the acute phase condition, the genes were categorized into 2 groups: (1) mRNA levels not affected by the diets in *Sik3*$^{-/-}$ mice (*e.g., Shp, Bsep, AbcG5, AbcA1, and Fasn*), and (2) mRNA levels that were irregularly affected (*e.g., Cyp7a, Cyp8b,* and *Cyp27a)* (Figure 8A and S4A). Strangely, *Cyp7a* gene expression was lower in *Sik3*$^{-/-}$ mice than in wild-type mice, despite the low expression levels of *Shp*.

The little or no expression of *Cyp7a* observed under the high-cholesterol diet in *Sik3*$^{-/-}$ mice could be explained by LXR dysfunction [3], while the low expression of *Shp* or *Bsep* [6] and hypertrophic gallbladder [40] suggested FXR dysfunction. RXR is activated by 9-cis-RA, which is synthesized from vitamin A [9],

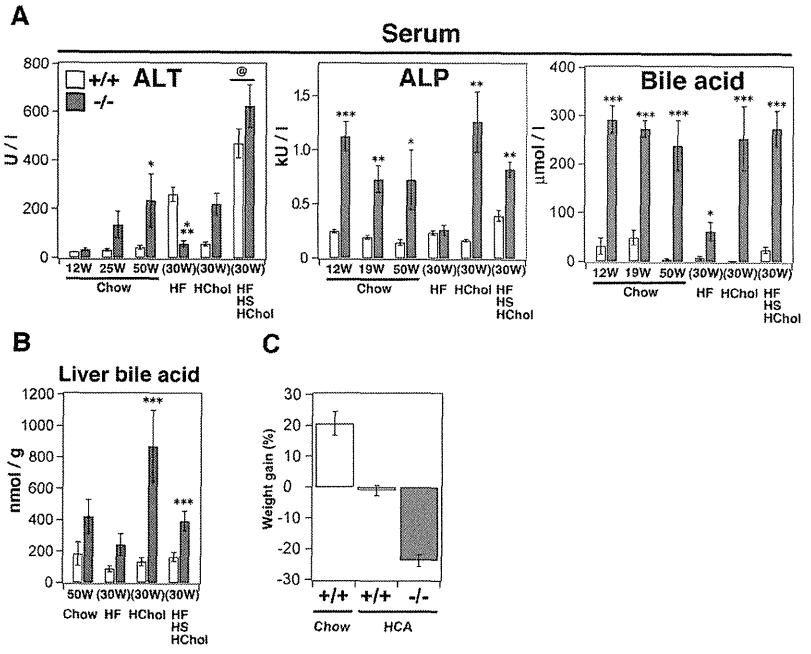

Figure 6. Excess bile acids in the serum and liver of *Sik3*$^{-/-}$ mice. (A) The serum levels of ALT, alkaline phosphatase, and bile acids are shown. The age at serum collection of the mice fed a chow diet (n = 4–6) are shown, while those of mice fed an HF, HChol, or HF/HS/HChol diet (n = 5–6) was 30 weeks (feeding 12–30 weeks). @ in the ALT panel indicates the maximum values for the results shown in Figure 4E. (B) Bile acids were extracted from the liver (n = 3) and normalized by liver weigh. (C) Gain of body weight after feeding mice with a high cholic acid (CA)-containing diet. Wild type (n = 6) and *Sik3*$^{-/-}$ mice (n = 5) were fed a diet supplemented with 0.25% CA for 1 month. For the control group, wild-type mice (n = 9) were fed with a chow diet.
doi:10.1371/journal.pone.0037803.g006

and the impairment of RXR function affects vitamin A metabolism [42], resulting in the proliferation of bile duct epithelial cells (Figure 4B) [43]. Moreover, the livers of *Sik3*$^{-/-}$ mice expressed lower levels of *Rv*αmRNA than the livers of wild-type mice, when the mice were fed with diets rich in cholesterol or CA (Figure S4B). Therefore, we decided to examine vitamin A metabolism in the livers of *Sik3*$^{-/-}$ mice by quantifying mRNA and protein levels.

The mRNA and protein levels of *cellular retinoid-binding protein 1* (*Crbp1*) and *retinal aldehyde dehydrogenase 1a* (*Aldh1a*) were up- and down-regulated, respectively, in *Sik3*$^{-/-}$ mice (Figure S4C and 8B). *Aldh1a* mRNA levels in the livers of *Sik3*$^{-/-}$ mice were also unaffected by the diet (Figure 8C). In addition, the livers of *Sik3*$^{-/-}$ mice contained higher levels of free retinol (vitamin A) than the livers of wild-type mice (Figure 8D). Moreover, treatment with 9-cis-RA rapidly reduced the levels of free retinol in the livers of *Sik3*$^{-/-}$ mice compared to the wild-type mice, suggesting that vitamin A metabolism might be impaired in *Sik3*$^{-/-}$ mice.

To further characterize these findings, the mice were treated with 9-cis-RA for 7 days, and several phenotypic parameters were then examined. Because 9-cis-RA is a pleiotropic compound, we first determined the minimum dose of 9-cis-RA as 4 mg kg^{-1}·day^{-1} by monitoring the body weight and blood glucose levels of wild-type mice (Figure S5A and B). Treatment with 9-cis-RA induced weight gain in *Sik3*$^{-/-}$ mice (Figure 8E) and enabled them to maintain their blood glucose levels after fasting (Figure 8F). In addition, 9-cis-RA substantially decreased the levels of serum ALP and bile acid in *Sik3*$^{-/-}$ mice (Figure S5C). *Sik3*$^{-/-}$ mice treated with 9-cis-RA were also able to respond to nutritional stress by inducing the expression of metabolic markers (compare Figure 8G to 8A and Figure S5D). These results suggest that impaired vitamin A metabolism might be a cause of the phenotypes of *Sik3*$^{-/-}$ mice.

Discussion

Here, we have shown that SIK3 is induced in the liver when mice are fed a diet rich in fat, sucrose, and cholesterol. *Sik3*$^{-/-}$ mice present with a malnourished phenotype due to their reduced adaptation to excess nutrition, especially to cholesterol and CA,

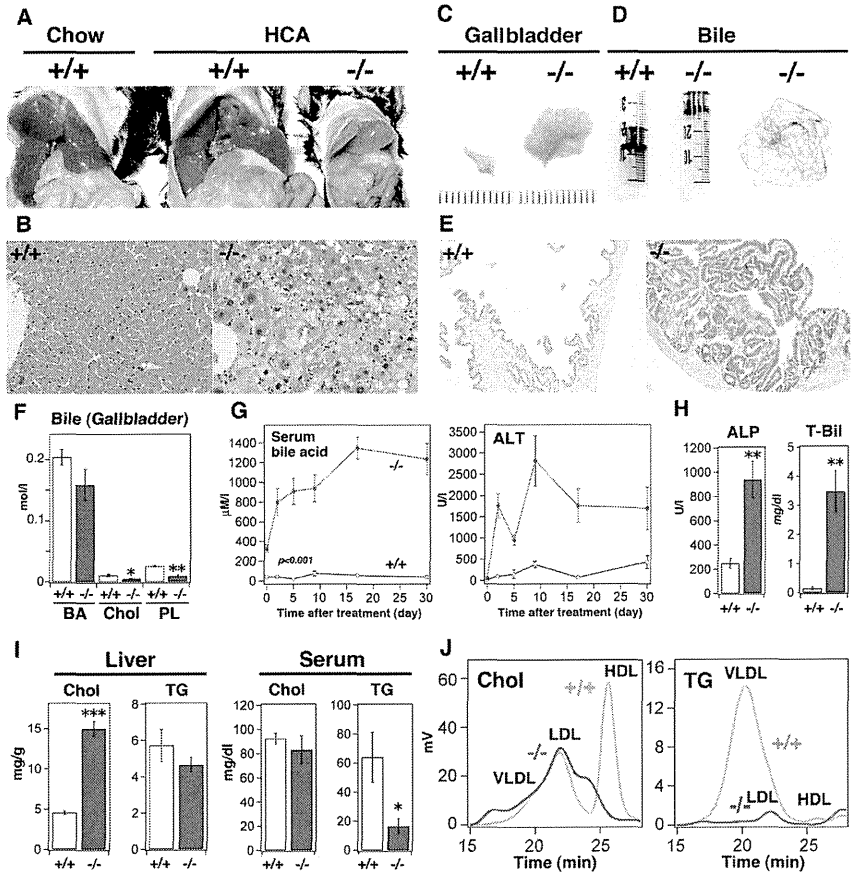

Figure 7. *Sik3*$^{-/-}$ mice are less tolerant to a cholic acid (CA)-containing diet. (A) Mice (n = 6, but *Sik3*$^{-/-}$ mouse died before 1 month) were fed a diet supplemented with 0.25% cholic acid for 1 month (12–16 weeks) and then sacrificed. (B) HE staining of the liver (*left*), BSEP staining (*right*: BSEP is green and nuclei are blue (DAPI)). The magnification is the same in each set. (C) Photographs of gallbladders (scale, 1 mm). (D) The color of bile juice and bile sand in the gallbladder. (E) HE staining of the gallbladder. The magnification is the same in both panels. (F) The levels of bile acid (BA), cholesterol (Chol), and phospholipids (PL) in bile juice from the gallbladder were measured. * and ** indicate $p<0.05$ and <0.01, respectively. *Means and SEM are shown.* (G) *Serum BA and alanine aminotransferase (ALT) levels were monitored at the indicated periods. All ALT data points are* $p<0.001$, except day 0. (H) Serum alkaline phosphatase (ALP) and total bilirubin (T-Bil) levels were measured. (I) Cholesterol and TG levels in the liver and serum were measured. *** indicates $p<0.001$. (J) FPLC analysis of serum lipids.
doi:10.1371/journal.pone.0037803.g007

which eventually leads to severe cholestasis. These phenotypes are continuously observed even after 10 generations of cross-breeding with normal C57BL/6J mice, and we observed no substantial difference between males and females in their response to biased diets. Given these results, we propose that SIK3, in combination with vitamin A metabolism, is a novel regulator of cholesterol-BA homeostasis and lipid-storage size (Figure 9).

Previous studies suggested a direct contribution of RXR to cholesterol-BA homeostasis. Because the RXR ligand 9-*cis*-RA is synthesized from vitamin A, which is absorbed from enterocytes

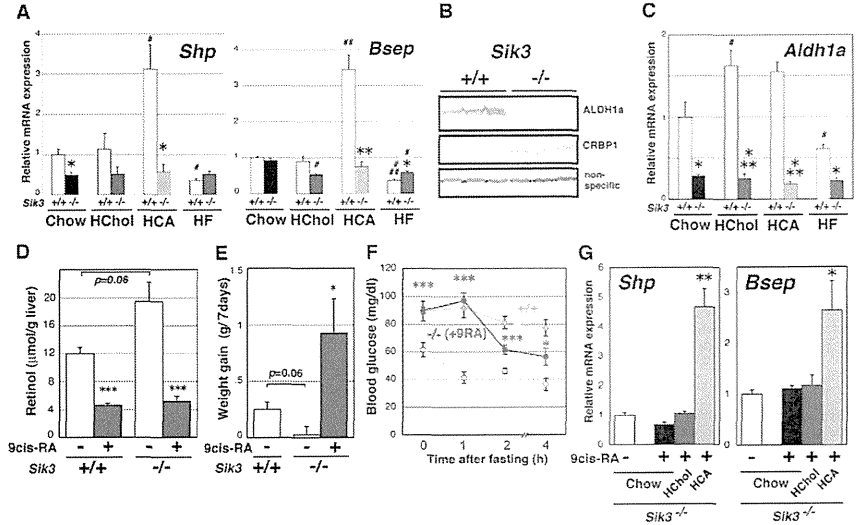

Figure 8. Impairment of cholesterol and bile acid (BA) metabolic gene regulation in *Sik3* $^{-/-}$ mice. (A) Male mice (12 weeks of age, n = 3) were fed diets supplemented with cholesterol (2%) and cholic acid (CA) (0.25%) for 2 days or with fat (60% of calories) for 2 weeks and then sacrificed. The expression of genes for cholesterol and BA metabolism in the liver was examined using qPCR (normalized by glyceraldehyde 3-phosphate dehydrogenase [*Gapdh*] levels). Significant differences between wild-type and *Sik3*$^{-/-}$ mice are shown by *, **, and *** for $p<0.05$, <0.01, and <0.001, respectively. # indicates significant differences between the chow and special diet groups. Means and SEM are shown. (B) Western blot analysis of ALDH1a and CRBP1 levels. (C) The levels of *Aldh1a* mRNA in mouse liver (normalized by *Gapdh* levels). (D) Levels of free retinol (vitamin A) in the livers of wild-type and *Sik3*$^{-/-}$ mice. Mice (12 weeks of age, n = 3) were treated with (+) or without (−) 9-cis-RA (8.3 mg/kg, suspended in 1% ethanol) intraperitoneally. After 6 h, the liver was recovered. (E) Mice (wild type, n = 4; *Sik3*$^{-/-}$ mice, without and with treatment, n = 4 and n = 12, respectively) were treated with 9-cis-RA (4 mg kg^{-1}·d^{-1}) for 7 days and the weight gain during this period is shown. * indicates a significant difference in the *Sik3*$^{-/-}$ groups. (F) After 7 days of treatment, the mice in each group were fasted and their blood glucose levels were monitored. Significance was calculated in the *Sik3*$^{-/-}$ groups. (G) At day 7, the *Sik3*$^{-/-}$ mice that were treated with RA were grouped into sets of 3 (n = 4) and fed a chow, high-cholesterol, or high-CA diet for a further 2 days under continuous RA treatment; mRNA levels in the liver were then examined. Significant differences between the chow and special diet groups are indicated.
doi:10.1371/journal.pone.0037803.g008

with the assistance of BA, its metabolism is tightly coupled to BA homeostasis [44]. A lack of vitamin A stimulates BA synthesis and its transport from hepatocytes to the bile ducts, *e.g.*, via *Cyp7a* and *Bsep* gene expression [45], while excess 9-cis-RA inhibits their expression. The reduced expression of ALDH1a, an RA synthase, in the livers of *Sik3*$^{-/-}$ mice might be one of the causes of the *Sik3*$^{-/-}$ phenotype. All-trans-RA suppresses the expression of *Aldh1a* via an RAR-dependent mechanism [46], but 9-cis-RA does not, suggesting a distinct action for 9-cis-RA from all-trans-RA. Because physiological/endogenous 9-cis-RA has been identified only in the pancreas [47,48], analyses of not only 9-cis-RA, but also its related substances in the liver are required to precisely characterize the *Sik3*$^{-/-}$ phenotype.

The administration of 9-cis-RA to *Sik3*$^{-/-}$ mice recovered the expression of *Cyp7a* and *Bsep* (Figure 7A and 7G), suggesting that the dose used (4 mg kg^{-1}·d^{-1}) may not be excessive for *Sik3*$^{-/-}$ mice. However, we have to mention that the wild-type mice that were fed with a vitamin A-deficient diet for 6 months from weaning did not develop cholestasis (*unpublished observation*), indicating that the levels of vitamin A and its metabolites may be insufficient to explain all of the *Sik3*$^{-/-}$ phenotypes. Meanwhile, free retinol (vitamin A) accumulated in the livers of *Sik3*$^{-/-}$ mice. Vitamin A toxicity is also suspected in hepatic cholestasis [49], suggesting that increased levels of free retinol may also contribute to the dysregulation of cholesterol-BA homeostasis in *Sik3*$^{-/-}$ mice. In addition, retinol aldehyde, a substrate of ALDH1a and a precursor of RA, is found to possess strong anti-obesity actions in mice [10].

Meanwhile, the high-fat diet ameliorated cholestasis in *Sik3*$^{-/-}$ mice (Figure 6A) without FA storage (in the liver and adipose tissues) or restoring the mRNA levels of genes involved in FA synthesis, such as *Fasn* (Figure 2 and Table S1). Interestingly, the high-fat diet up-regulated the expression of *thiolase*, a PPARα target, in the livers of *Sik3*$^{-/-}$ mice. PPARα is known to enhance bile flow [50] and some transcriptional pathways, such as *Shp* [51] (and also compare Table S1 to Figure 3A). Given that RXR is required for PPARα activation, its signaling may also be impaired in *Sik3*$^{-/-}$ mice, as expected from the gene expression profile observed for the chow diet (Figure 3A). These observations suggest that excess fat may stimulate a part of the downstream PPARα

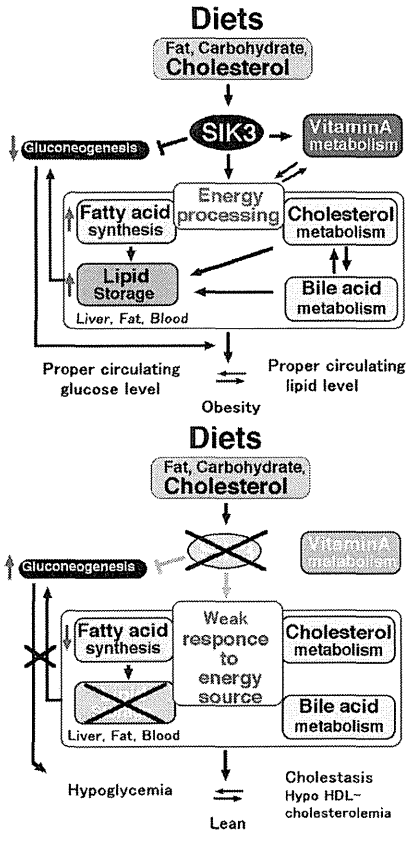

Figure 9. Summary of the metabolic events in wild-type (*upper*) and in *Sik3*$^{-/-}$ mice (*lower*).
doi:10.1371/journal.pone.0037803.g009

pathway (or close the gap downstream from PPARα that is impaired in *Sik3*$^{-/-}$ mice), which can improve BA homeostasis, probably in an SIK3-independent manner.

AMPK-related kinases are activated by the upstream kinase LKB1 [29,52] SIK3 or AMPK–which kinase is important for the LKB1-*mediated suppression of gluconeogenesis in the liver? Loss* of LKB1 in the liver enhances the gluconeogenic program [53]. Since the gluconeogenic program in LKB-defective mice is resistant to the AMPK activator metformin, AMPK is proposed to be the kinase responsible for the LKB1-mediated regulation of gluconeogenesis. However, the livers of *Sik3*$^{-/-}$ mice possessed activated AMPK and an enhanced gluconeogenic program (Figure 3B), suggesting that loss of LKB1 causes a deficiency of SIK3 and subsequent AMPK resistance. In addition to gluconeogenesis, liver-specific LKB-defective mice present with severe cholestasis due to a lack of BSEP membrane-localization in the liver [54], while the apical side of the dilated canalicular structure was positive for BSEP in the livers of *Sik3*$^{-/-}$ mice, suggesting that the cause of cholestasis in these mice may not be identical to that in LKB-defective mice. We would again emphasize that the high-fat diet ameliorated cholestasis in *Sik3*$^{-/-}$ mice, indicating the importance of the process for nutrients rather than developmental defects in BA transportation.

Two recent reports have provided an argument against mechanisms by which SIK3 regulates energy balance. Mihalova *et al.* found that class 2a HDACs activated the FOXO transcription factor via deacetylation, thereby up-regulating gluconeogenesis in the liver [37]. Conversely, Wang *et al.* reported that loss of SIK2 in *Drosophila* (by disrupting the fly's *Sik3* gene) resulted in the dephosphorylation of HDAC4 and the subsequent *activation of FOXO [28]. Activated FOXO induces the lipolytic* programs that reduce the lipid levels in body fat, thereby rendering the fly vulnerable to starvation. These data suggest that disinactivation of class 2a HDACs followed by the constitutive activation of FOXO may be a cause of the phenotypes of *Sik3*$^{-/-}$ mice.

Conversely, *Crebbp*$^{+/-}$ mice, with a mutant allele of the histone acetylase CREB-binding protein, displayed a phenotypes similar to that of *Sik3*$^{-/-}$ mice, *e.g.*, lipodystrophy, increased glucose tolerance, resistance to diet-induced obesity, and hyperadiponectinemia [55], suggesting that SIK3 may regulate energy balance by regulating acetylation states. The levels of adipose tissue and circulating blood lipids may be important for buffering cholesterol and protecting the liver from cholesterol toxicity, which in turn, increases the risk of obesity and hyperlipidemia (Figure 9).

In the present study, profiling the metabolic changes in *Sik3*$^{-/-}$ mice represents a new start to the study SIK and may also provide novel insights into the metabolic diseases caused by Western diets. Another remarkable phenotype of *Sik3*$^{-/-}$ mice is found in the differentiation of chondrocytes [31], and a number of interactions between energy metabolism and skeletal development have been reported, *e.g.*, insulin [56], leptin [57], adiponectin [58], osteocalcin [59,60], and inflammatory cytokines [61]. Further analyses of the cell autonomous functions of SIK3 and of systemic or developmental abnormalities in the organs for energy metabolicsm in *Sik3*$^{-/-}$ mice are needed.

Materials and Methods

Sik3$^{-/-}$ Mice

Embryonic stem cells derived from a C57BL/6N strain (RENKA) were used with the *Sik3*$^{-/-}$ mice. After mating the mice with C57BL/6J mice (CLEA Japan, Tokyo, Japan) for 3 generations, mouse colonies were expanded for experiments under chow and high-fat-diet feeding. After 7 generations of cross breeding, mice colonies were used for cholesterol and cholic acid experiments. *Sik3*$^{+/-}$ mice are now supplied by JCRB Laboratory Animal Resource Bank at the National Institute of Biomedical Innovation (No. nbio157). The experimental mouse protocols were approved by the ethics committee at the National Institute of Biomedical Innovation (assigned No. DS-20-56). The animals were maintained under standard conditions of light (0800–2000) and temperature (23°C, 50% humidity).

For tissue isolation, all mice were fasted for 4 h and then sacrificed within ±1 h of lights out. The chow diet, MF, was purchased from Oriental Yeast (Tokyo, Japan). The high-sucrose (20% cal), high-fat (60% cal), and high-fat (45% cal)/high-sucrose (20% cal) diets were obtained from Research DIET Inc. (NJ, USA). We supplemented 2% cholesterol in the high-fat and high-fat/high-sucrose diets. To prepare the high-cholesterol and high-cholic acid (CA) diets, the chow diet was supplemented with 2% cholesterol or 0.25% CA, respectively. O_2 consumption was monitored using the Oxymax system (Columbus Instruments, Columbus, OH, USA).

The pre-fasting periods for the glucose tolerance test (GTT), insulin tolerance test (ITT), and lactate tolerance test (LTT) were 4, 2, and 24 h, respectively. We administered 1.5 g/kg glucose, 36 μg/kg insulin, and 1.5 g/kg lactate intraperitoneally for these tests, respectively.

Fractionation of Hepatic Parenchymal Cells and Non-parenchymal Cells

Under anesthesia by isoflurane, female C57BL/6J mice (12-week-old) were perfused with Hank's balanced salt solution containing 0.5 mM EGTA via inferior vena cava followed by perfusion with Liver Digestion Medium (Invitorgen). After the digestion, hepatic cells were suspended in Dulbecco's Modified Eagle Medium (DMEM) supplemented with 10% fetal bovine serum and centrifuged at 40×g for 2 minutes. The pellet was used for the parenchymal-cell fraction, and the supernatant was recovered by further centrifuged at 800×g for 5 min and used for non-parenchymal-cell fraction.

Reagents

Blood glucose and β-hydroxybutyrate were measured using a G-meter (Arkray, Kyoto, Japan) and Precision Xceed (Abbott, Abbott Park, IL, USA), respectively. Total cholesterol and triglyceride (TG) in sera were measured using a DryChem7000 (Fujifilm, Tokyo, Japan). Lipids in the liver or feces were extracted in 10 volumes of methanol:chloroform (1:2), dried under N_2 gas, suspended in 300 μL t-butyl alcohol:methanol:-Triton-X 100 (2:1:1, v/v), and quantified using kits (WAKO, Osaka, Japan). Serum insulin, leptin and adiponectin levels were measured using enzyme-linked immunosorbent assay kits from Shibayagi (Gunma, Japan), and low levels of insulin were measured with a low range kit from Morinaga (Tokyo, Japan), while free FA and BA levels were measured using kits from WAKO. Serum lipid separation by fast protein liquid chromatography (FPLC) was contracted to LipiSEARCH (Skylight Biotech, Akita, Japan). The anti-AMPK, anti-phospho-AMPK, and anti-HDAC5 antibodies were purchased from Cell Signaling (Boston, MA, USA), anti-BSEP antibody were from ABGENT (San Diego, CA, USA), while the anti-ALDH1a and anti-CRBP1 antibodies were obtained from Epitomics (Burlingame, CA, USA). The anti-CRTC2 antibody was described previously [29].

Quantitative Real-time PCR

Total RNA was extracted using an EZ1 RNA Universal Tissue Kit (Qiagen, Venlo Park, Netherlands), and cDNA was synthesized using a Transcriptor cDNA First Strand Synthesis Kit (Roche, Branford, CT, USA). PCR amplification was performed using Platinum Quantitative PCR SuperMix (Invitrogen). Since the level of the internal standard RNA, 36B4, was induced by the CA-rich diet, the expression levels of mRNA in the liver of mice fed with diets supplemented with CA or Chol were normalized using glyceraldehyde 3-phosphate dehydrogenase levels. Gene names, abbreviations and primer sequence used in the quantities PCR analysis are listed in Table S2.

Statistical Analysis

Student's *t*-test was used to assess all experimental data in Microsoft Excel. The mean and standard error of the mean (SEM) are shown.

Supporting Information

Figure S1 (A) Most *Sik3*$^{-/-}$ mice died on the first day after birth. The mating system and time of genotyping are indicated. The percentage and number of mice in the first column indicate the sum of neonates at day 1 and embryos at E17.5–E18.5. Neonates prepared by *in vitro* fertilization were delivered by cesarean section and living mice were counted without genotyping. However, ~50% of the mice disappeared by the second day, probably because they were eaten by the foster mice. (B) The difference in the body size of *Sik3*$^{-/-}$ mice became obvious after 2 weeks. (C) HE staining of gonadal fat of 1-year-old mice. (D) Cholesterol (Chol), triglyceride (TG), and carbohydrate (Carbo) content in feces (from 3 cages). Cholesterol and triglycerides were extracted with methanol/chloroform as described in the Materials and Methods. To extract undigested carbohydrates, the feces were re-digested with amylase at 37°C for 12 h, and the debris was removed by centrifugation. Carbohydrates were stained with a solution of 1 volume of 5% phenol and 5 volumes of sulfuric acid and then detected at 490 nm. (E) After fasting for 4-h fasting, the serum levels of free thyroid hormones (FT3 and FT4) were measured with an automated system for clinical assays. Serum thyroid stimulating hormone (TSH) levels were measured with an ELISA kit from Shibayagi Co., Ltd. (F) Insulin tolerance test (ITT). Mice (male n = 5) were fasted for 2 h and then treated intraperitoneally with 36 μg/kg insulin. All data points are $p<0.001$.
(TIF)

Figure S2 (A) Body weight curves of wild-type and *Sik3* heterozygous mice are also shown (n = 12). (B) Levels of *Sik3* mRNA in the livers, brown adipose tissues (BAT), and muscles of wild-type, heterozygous, and *Sik3*$^{-/-}$ mice (n = 3). The error bars indicate SEM. Levels of SIK3 protein in the livers of wild-type, heterozygous, and *Sik3*$^{-/-}$ mice. (C) Hepatic parenchymal and non-parenchymal cells were separated by centrifugation, and *Sik3* mRNA levels were examined by quantitative PCR. *Cyp7α*, *F4/80*, and *Desmin* were used as markers for parenchymal cells, Kupffer's cells (non-parenchymal), and hepatic stellate cells (non-parenchymal), respectively. (n = 3; means and SEM are shown). (D) *In vitro* adipocyte differentiation assay. Preadipocytes were prepared from gonadal fat pads using collagenase and then plated. When the cells reached confluence, the culture medium was changed to Dulbecco's Modified Eagle's Medium (high glucose) supplemented with rosiglitazone (Rosi: indicated concentration), and insulin (1 μg/mL). After 8 days (with changes of medium every 2 days), the cells were fixed with 4% paraformaldehyde and stained with Oil Red O. The high magnification images show cells that were differentiated using 3 μM rosiglitazone. (F) Serum adiponectin levels of the mice examined in Figure 3E. Means and SEM are shown. ### indicates $p<0.001$.
(TIF)

Figure S3 (A) HE staining of embryo livers. The sets in the left and right panels are the same magnification. The lower panels are a higher magnification of the upper panels. (B) Bile acid was extracted with 95% ethanol/0.5% NH_3-water. The numbers of mice (wild-type and *Sik3*$^{-/-}$) used for the assay were: E16.5, 11 and 6; E18.5, 16 and 3; P0, 9 and 5; and 12 weeks, 8 and 5, respectively. Means and SEM are shown. Significant differences

between wild-type and *Sik3*$^{-/-}$ mice are shown by * for $p<0.05$. ## indicates significant differences between P0 and E18.5 or 12 weeks in wild-type mice ($p<0.01$).
(TIF)

Figure S4 (A) Male mice (12 weeks of age, n = 3) were fed diets supplemented with Chol (2%) and cholic acid (0.25%) for 2 days or with fat (60% of calories) for 2 weeks and then sacrificed. The expression of genes for Chol and BA metabolism in the liver was examined using quantitative polymerase chain reaction (normalized by glyceraldehyde 3-phosphate dehydrogenase [GAPDH] levels). Significant differences between wild-type and *Sik3*$^{-/-}$ mice are shown by *, **, and *** for $p<0.05$, <0.01, and <0.001, respectively. # indicates a significant difference between the chow and special diet groups. Means and SEM are shown. (B) Expression levels of nuclear receptors. (C) The expression of genes involved in vitamin A metabolism was examined using the liver cDNA in Figure 3A (1-year-old mice, n = 5).
(TIF)

Figure S5 (A) Effect of 9-cis-RA treatment (0–16 mg $kg^{-1}\cdot d^{-1}$) on the weight gain of wild-type mice (n = 6). (B) Blood glucose levels before and after treatment are indicated by labels as B and A, respectively. (C) The levels of serum ALP and bile acids were measured before (labeled as B) and after (labeled as A) 9-cis-RA treatment (for 9 days: after the analysis shown in Figure 8E). Ethanol (EtOH, 1%) was used as a solvent. Significant differences before and after treatment in the same group (n = 4) are indicated. Although there were no significant fluctuations in the levels of bile acids, their levels decreased in all *Sik3*$^{-/-}$ mice after treatment.

(D) Effect of 9-cis-RA on gene expression in *Sik3*$^{-/-}$ mice. At day 7, *Sik3*$^{-/-}$ mice treated with 9-cis-RA were grouped into sets of 3 (n = 4) and fed a chow, high-Chol, or high-CA diet for an additional 2 days under continuous RA treatment; mRNA levels in the liver were then examined. Significant differences between the chow and special diet groups are indicated.
(TIF)

Table S1 mRNA levels in the liver.
(XLS)

Table S2 List of primers used for quantitative-PCR.
(XLS)

Acknowledgments

We are grateful to Mrs. Junko Morita (NIBIO), Dr. Kazuomi Nakamura (Tottori University), Mrs. Keiko Takeoka (Osaka University), and Mr. Naohiro Hori (Kinki University) for their technical support. We also thank Drs. Mitsuhiro Okamoto (Tezukayama University), Yasuki Nonaka (Osaka Aoyama University), Miho Ohta (Souai University), and Alan F. Hofmann (University of California) for their advice.

Author Contributions

Conceived and designed the experiments: H. Takemori JM NT SI KK AB AS AH MN. Performed the experiments: H. Takemori TU YI OH AK MS TS SS JD KT KM EM TK MK. Analyzed the data: KA TK MO JN H. Takikawa TF JM NT SI KK AB AS AH MN. Contributed reagents/materials/analysis tools: H. Takikawa KK YN HK TT TN. Wrote the paper: H. Takemori.

References

1. Wagner M, Zollner G, Trauner M (2011) Nuclear receptors in liver disease. Hepatology 53: 1023–1034.
2. Willy PJ, Umesono K, Ong ES, Evans RM, Heyman RA, et al. (1995) LXR, a nuclear receptor that defines a distinct retinoid response pathway. Genes Dev 9: 1033–1045.
3. Peet DJ, Turley SD, Ma W, Janowski BA, Lobaccaro JM, et al. (1998) Cholesterol and bile acid metabolism are impaired in mice lacking the nuclear oxysterol receptor LXR alpha. Cell 93: 693–704.
4. Kalaany NY, Gauthier KC, Zavacki AM, Mammen PP, Kitazume T, et al. (2005) LXRs regulate the balance between fat storage and oxidation. Cell Metab 1: 231–244.
5. Makishima M, Okamoto AY, Repa JJ, Tu H, Learned RM, et al. (1999) Identification of a nuclear receptor for bile acids. Science 284: 1362–1365.
6. Sinal CJ, Tohkin M, Miyata M, Ward JM, Lambert G, et al. (2000) Targeted disruption of the nuclear receptor FXR/BAR impairs bile acid and lipid homeostasis. Cell 102: 731–744.
7. Watanabe M, Houten SM, Mataki C, Christoffolete MA, Kim BW, et al. (2006) Bile acids induce energy expenditure by promoting intracellular thyroid hormone activation. Nature 439: 484–489.
8. Watanabe M, Horai Y, Houten SM, Morimoto K, Sugizaki T, et al. (2011) Lowering bile acid pool size with a synthetic farnesoid X receptor (FXR) agonist induces obesity and diabetes through reduced energy expenditure. J Biol Chem 286: 26913–26920.
9. Heyman RA, Mangelsdorf DJ, Dyck JA, Stein RB, Eichele G, et al. (1992) 9-cis retinoic acid is a high affinity ligand for the retinoid X receptor. Cell 68: 397–406.
10. Ziouzenkova O, Orasanu G, Sharlach M, Akiyama TE, Berger JP, et al. (2007) Retinaldehyde represses adipogenesis and diet-induced obesity. Nat Med 13: 695–702.
11. Iqbal J, Hussain MM (2009) Intestinal lipid absorption. Am J Physiol Endocrinol Metab 296: E1183–1194.
12. Takemori H, Okamoto M (2008) Regulation of CREB-mediated gene expression by salt inducible kinase. J Steroid Biochem Mol Biol 108: 287–291.
13. Doi J, Takemori H, Lin X-z, Horike N, Katoh Y, et al. (2002) Salt-inducible kinase represses PKA-mediated activation of human cholesterol side chain cleavage cytochrome promoter through the CREB basic leucine zipper domain. J Biol Chem 277: 15629–15637.
14. Takemori H, Katoh Y, Horike N, Doi J, Okamoto M (2002) ACTH-induced nucleocytoplasmic translocation of salt-inducible kinase. Implication in the protein kinase A-activated gene transcription in mouse adrenocortical tumor cells. J Biol Chem 277: 42334–42343.
15. Koo SH, Flechner L, Qi L, Zhang X, Screaton RA, et al. (2005) The CREB Coactivator TORC2 is a Key Regulator of Fasting Glucose Metabolism. Nature 437: 1109–1111.
16. Uebi T, Tamura M, Horike N, Hashimoto YK, Takemori H (2010) Phosphorylation of the CREB-specific coactivator TORC2 at Ser(307) regulates its intracellular localization in COS-7 cells and in the mouse liver. Am J Physiol Endocrinol Metab 299: E413–425.
17. Muraoka M, Fukushima A, Viengchareun S, Lombes M, Kishi F, et al. (2009) Involvement of SIK2/TORC2 signaling cascade in the regulation of insulin-induced PGC-1alpha and UCP-1 gene expression in brown adipocytes. Am J Physiol Endocrinol Metab 296: E1430–1439.
18. Sasaki T, Takemori H, Yagita Y, Terasaki Y, Uebi T, et al. (2011) SIK2 is a key regulator for neuronal survival after ischemia via TORC1-CREB. Neuron 69: 106–119.
19. Horike N, Kumagai A, Shimono Y, Onishi T, Itoh Y, et al. (2010) Downregulation of SIK2 expression promotes the melanogenic program in mice. Pigment Cell Melanoma Res 23: 809–819.
20. Kumagai A, Horike N, Satoh Y, Uebi T, Sasaki T, et al. (2011) A Potent Inhibitor of SIK2, 3, 3′, 7-Trihydroxy-4′-Methoxyflavon (4′-O-Methylfisetin), Promotes Melanogenesis in B16F10 Melanoma Cells. PLoS One 6: e26148.
21. Altarejos JY, Montminy M (2011) CREB and the CRTC co-activators: sensors for hormonal and metabolic signals. Nat Rev Mol Cell Biol 12: 141–151.
22. Conkright MD, Canettieri G, Screaton R, Guzman E, Miraglia L, et al. (2003) TORCs: transducers of regulated CREB activity. Mol Cell 12: 413–423.
23. Iourgenko V, Zhang W, Mickanin C, Daly I, Jiang C, et al. (2003) Identification of a family of cAMP response element-binding protein coactivators by genome-scale functional analysis in mammalian cells. Proc Natl Acad Sci U S A 100: 12147–12152.
24. Screaton RA, Conkright MD, Katoh Y, Best JL, Canettieri G, et al. (2004) The CREB coactivator TORC2 functions as a calcium- and cAMP-sensitive coincidence detector. Cell 119: 61–74.
25. Katoh Y, Takemori H, Min L, Muraoka M, Doi J, et al. (2004) Salt-inducible kinase-1 represses cAMP response element-binding protein activity both in the nucleus and in the cytoplasm. Eur J Biochem 271: 4307–4319.
26. Bricambert J, Miranda J, Benhamed F, Girard J, Postic C, et al. (2010) Salt-inducible kinase 2 links transcriptional coactivator p300 phosphorylation to the prevention of ChREBP-dependent hepatic steatosis in mice. J Clin Invest 120: 4316–4331.
27. Berdeaux R, Goebel N, Banaszynski L, Takemori H, Wandless T, et al. (2007) SIK1 is a class II HDAC kinase that promotes survival of skeletal myocytes. Nat Med 13: 597–603.
28. Wang B, Moya N, Niessen S, Hoover H, Mihaylova MM, et al. (2011) A hormone-dependent module regulating energy balance. Cell 145: 596–606.
29. Katoh Y, Takemori H, Lin XZ, Tamura M, Muraoka M, et al. (2006) Silencing the constitutive active transcription factor CREB by the LKB1-SIK signaling cascade. Febs J 273: 2730–2748.
30. Hashimoto YK, Satoh T, Okamoto M, Takemori H (2008) Importance of autophosphorylation at Ser186 in the A-loop of salt inducible kinase 1 for its sustained kinase activity. J Cell Biochem 104: 1724–1739.
31. Sasagawa S, Takemori H, Uebi T, Ikegami D, Hiramatsu K, et al. (2012) SIK3 is essential for chondrocyte hypertrophy during skeletal development in mice. Development 139: 1153–1163.
32. Lanjuin A, Sengupta P (2002) Regulation of chemosensory receptor expression and sensory signaling by the KIN-29 Ser/Thr kinase. Neuron 33: 369–381.
33. Wang B, Goode J, Best J, Meltzer J, Schilman PE, et al. (2008) The insulin-regulated CREB coactivator TORC promotes stress resistance in Drosophila. Cell Metab 7: 434–444.
34. Hurov JB, Huang M, White LS, Lennerz J, Choi CS, et al. (2007) Loss of the Par-1b/MARK2 polarity kinase leads to increased metabolic rate, decreased adiposity, and insulin hypersensitivity in vivo. Proc Natl Acad Sci U S A 104: 5680–5685.
35. Lennerz JK, Hurov JB, White LS, Lewandowski KT, Prior JL, et al. (2010) Loss of Par-1a/MARK3/C-TAK1 kinase leads to reduced adiposity, resistance to hepatic steatosis, and defective gluconeogenesis. Mol Cell Biol 30: 5043–5056.
36. Inagaki T, Dutchak P, Zhao G, Ding X, Gautron L, et al. (2007) Endocrine regulation of the fasting response by PPARalpha-mediated induction of fibroblast growth factor 21. Cell Metab 5: 415–425.
37. Mihaylova MM, Vasquez DS, Ravnskjaer K, Denechaud PD, Yu RT, et al. (2011) Class IIa Histone Deacetylases Are Hormone-Activated Regulators of FOXO and Mammalian Glucose Homeostasis. Cell 145: 607–621.
38. Takemori H, Katoh-Hashimoto Y, Nakae J, Olson EN, Okamoto M (2009) Inactivation of HDAC5 by SIK1 in AICAR-treated C2C12 myoblasts. Endocr J 56: 121–130.
39. Kim JY, van de Wall E, Laplante M, Azzara A, Trujillo ME, et al. (2007) Obesity-associated improvements in metabolic profile through expansion of adipose tissue. J Clin Invest 117: 2621–2637.
40. Moschetta A, Bookout AL, Mangelsdorf DJ (2004) Prevention of cholesterol gallstone disease by FXR agonists in a mouse model. Nat Med 10: 1352–1358.
41. Moschetta A, vanBerge-Henegouwen GP, Portincasa P, Renooij W, Groen AK, et al. (2001) Hydrophilic bile salts enhance differential distribution of sphingomyelin and phosphatidylcholine between micellar and vesicular phases: potential implications for their effects in vivo. J Hepatol 34: 492–499.
42. Gyamfi MA, He L, French SW, Damjanov I, Wan YJ (2008) Hepatocyte retinoid X receptor alpha-dependent regulation of lipid homeostasis and inflammatory cytokine expression contributes to alcohol-induced liver injury. J Pharmacol Exp Ther 324: 443–453.
43. Weiss B, Barshack I, Onaca N, Goldberg I, Berkovich Z, et al. (2010) Vitamin A deficiency associated with enhanced proliferation of bile duct epithelial cells in the rat. Isr Med Assoc J 12: 82–86.
44. Schmidt DR, Holmstrom SR, Fon Tacer K, Bookout AL, Kliewer SA, et al. (2010) Regulation of bile acid synthesis by fat-soluble vitamins A and D. J Biol Chem 285: 14486–14494.
45. Hoeke MO, Plass JR, Heegsma J, Geuken M, van Rijsbergen D, et al. (2009) Low retinol levels differentially modulate bile salt-induced expression of human and mouse hepatic bile salt transporters. Hepatology 49: 153–159.
46. Elizondo G, Corchero J, Sterneck E, Gonzalez FJ (2000) Feedback inhibition of the retinaldehyde dehydrogenase gene ALDH1 by retinoic acid through retinoic acid receptor alpha and CCAAT/enhancer-binding protein beta. J Biol Chem 275: 30747–30753.
47. Kane MA, Folias AE, Pingitore A, Perri M, Obrochta KM, et al. (2010) Identification of 9-cis-retinoic acid as a pancreas-specific autacoid that attenuates glucose-stimulated insulin secretion. Proc Natl Acad Sci U S A 107: 21884–21889.
48. Kane MA (2012) Analysis, occurrence, and function of 9-cis-retinoic acid. Biochim Biophys Acta 1821: 10–20, pp 10–20.
49. Erickson JM, Mawson AR (2000) Possible role of endogenous retinoid (Vitamin A) toxicity in the pathophysiology of primary biliary cirrhosis. J Theor Biol 206: 47–54.
50. Kok T, Bloks VW, Wolters H, Havinga R, Jansen PL, et al. (2003) Peroxisome proliferator-activated receptor alpha (PPARalpha)-mediated regulation of multidrug resistance 2 (Mdr2) expression and function in mice. Biochem J 369: 539–547.
51. Chanda D, Lee CH, Kim YH, Noh JR, Kim DK, et al. (2009) Fenofibrate differentially regulates plasminogen activator inhibitor-1 gene expression via adenosine monophosphate-activated protein kinase-dependent induction of orphan nuclear receptor small heterodimer partner. Hepatology 50: 880–892.
52. Lizcano JM, Goransson O, Toth R, Deak M, Morrice NA, et al. (2004) LKB1 is a master kinase that activates 13 kinases of the AMPK subfamily, including MARK/PAR-1. Embo J 23: 833–843.
53. Shaw RJ, Lamia KA, Vasquez D, Koo SH, Bardeesy N, et al. (2005) The kinase LKB1 mediates glucose homeostasis in liver and therapeutic effects of metformin. Science 310: 1642–1646.
54. Woods A, Hedegrave AJ, Muckett PJ, Levene AP, Clements M, et al. (2011) LKB1 is required for hepatic bile acid transport and canalicular membrane integrity in mice. Biochem J 434: 49–60.
55. Yamauchi T, Kamon J, Minokoshi Y, Ito Y, Waki H, et al. (2002) Adiponectin stimulates glucose utilization and fatty-acid oxidation by activating AMP-activated protein kinase. Nat Med 8: 1288–1295.
56. Wu S, Aguilar AL, Ostrow V, De Luca F (2011) Insulin resistance secondary to a high-fat diet stimulates longitudinal bone growth and growth plate chondrogenesis in mice. Endocrinology 152: 468–475.
57. Yadav VK, Oury F, Suda N, Liu ZW, Gao XB, et al. (2009) A serotonin-dependent mechanism explains the leptin regulation of bone mass, appetite, and energy expenditure. Cell 138: 976–989.
58. Maeda T, Jikko A, Abe M, Yokohama-Tamaki T, Akiyama H, et al. (2006) Cartilducin, a paralog of Acrp30/adiponectin, is induced during chondrogenic differentiation and promotes proliferation of chondrogenic precursors and chondrocytes. J Cell Physiol 206: 537–544.
59. Ferron M, Wei J, Yoshizawa T, Del Fattore A, DePinho RA, et al. (2010) Insulin signaling in osteoblasts integrates bone remodeling and energy metabolism. Cell 142: 296–308.
60. Fulzele K, Riddle RC, DiGirolamo DJ, Cao X, Wan C, et al. (2010) Insulin receptor signaling in osteoblasts regulates postnatal bone acquisition and body composition. Cell 142: 309–319.
61. Shikhman AR, Brinson DC, Valbracht J, Lotz MK (2001) Cytokine regulation of facilitated glucose transport in human articular chondrocytes. J Immunol 167: 7001–7008.

Periostin Facilitates Skin Sclerosis via PI3K/Akt Dependent Mechanism in a Mouse Model of Scleroderma

Lingli Yang[1,2], Satoshi Serada[2], Minoru Fujimoto[2], Mika Terao[1], Yorihisa Kotobuki[1,2], Shun Kitaba[1], Saki Matsui[1], Akira Kudo[3], Tetsuji Naka[2], Hiroyuki Murota[1]*, Ichiro Katayama[1]

1 Department of Dermatology, Osaka University Graduate School of Medicine, Osaka, Japan, **2** Laboratory for Immune Signal, National Institute of Biomedical Innovation, Osaka, Japan, **3** Department of Biological Information, Tokyo Institute of Technology, Yokohama, Japan

Abstract

Objective: Periostin, a novel matricellular protein, is recently reported to play a crucial role in tissue remodeling and is highly expressed under fibrotic conditions. This study was undertaken to assess the role of periostin in scleroderma.

Methods: Using skin from patients and healthy donors, the expression of periostin was assessed by immunohistochemistry and immunoblotting analyses. Furthermore, we investigated periostin$^{-/-}$ ($PN^{-/-}$) and wild-type (WT) mice to elucidate the role of periostin in scleroderma. To induce murine cutaneous sclerosis, mice were subcutaneously injected with bleomycin, while untreated control groups were injected with phosphate-buffered saline. Bleomycin-induced fibrotic changes were compared in $PN^{-/-}$ and WT mice by histological analysis as well as by measurements of profibrotic cytokine and extracellular matrix protein expression levels *in vivo* and *in vitro*. To determine the downstream pathway involved in periostin signaling, receptor neutralizing antibody and signal transduction inhibitors were used *in vitro*.

Results: Elevated expression of periostin was observed in the lesional skin of patients with scleroderma compared with healthy donors. Although WT mice showed marked cutaneous sclerosis with increased expression of periostin and increased numbers of myofibroblasts after bleomycin treatment, $PN^{-/-}$ mice showed resistance to these changes. *In vitro*, dermal fibroblasts from $PN^{-/-}$ mice showed reduced transcript expression of alpha smooth actin and procollagen type-I alpha 1 (Col1α1) induced by transforming growth factor beta 1 (TGFβ1). Furthermore, recombinant mouse periostin directly induced Col1α1 expression *in vitro*, and this effect was inhibited by blocking the αv integrin-mediated PI3K/Akt signaling either with anti-αv functional blocking antibody or with the PI3K/Akt kinase inhibitor LY294002.

Conclusion: Periostin plays an essential role in the pathogenesis of Bleomycin-induced scleroderma in mice. Periostin may represent a potential therapeutic target for human scleroderma.

Citation: Yang L, Serada S, Fujimoto M, Terao M, Kotobuki Y, et al. (2012) Periostin Facilitates Skin Sclerosis via PI3K/Akt Dependent Mechanism in a Mouse Model of Scleroderma. PLoS ONE 7(7): e41994. doi:10.1371/journal.pone.0041994

Editor: Alessandra Rossini, Università degli Studi di Milano, Italy

Received March 16, 2012; **Accepted** June 28, 2012; **Published** July 24, 2012

Funding: This study was supported by a grant-in-aid for the Program for Promotion of Fundamental Studies in Health Sciences of the National Institute of Biomedical Innovation and Grant-in-Aid from the Ministry of Health, Labour and Welfare of Japan. The funders had no role in study design, data collection and analysis, decision to publish, or preparation of the manuscript.

Competing Interests: The authors have declared that no competing interests exist.

* E-mail: h-murota@derma.med.osaka-u.ac.jp

Introduction

Scleroderma is a connective tissue disorder with unknown etiology. The disease is characterized by excessive deposition of collagen and other extracellular matrix (ECM) proteins, resulting in fibrosis of skin and other visceral organs [1]. To date, despite much effort, there is still no established treatment for fibrosis in scleroderma.

The ECM of the skin is composed not only of structural proteins such as collagen type-I but of many different proteins that modulate cellular behavior. The interactions among various ECM proteins provide molecular signals to resident cells including dermal fibroblasts and play essential roles in the maintenance and turnover of the ECM. At present, ECM proteins are considered as key players in the pathogenesis of scleroderma.

Among ECM proteins, the cytokine transforming growth factor β1 (TGFβ1) is regarded as a master regulator of the disease process in scleroderma, since it potently accelerates fibrosis in skin by inducing collagen production; various pro-fibrotic ECM proteins such as CCN2 (also known as a connective tissue growth factor or CTGF) are known to induce the transdifferentiation of fibroblasts to myofibroblasts [2,3]. Recently, a class of ECM proteins called matricellular proteins has attracted increasing attention in the field of scleroderma research. These proteins specifically regulate cell-matrix interactions and play critical roles in embryonic development as well as in tissue repair and fibrosis. Indeed, several matricellular proteins, including CCN2 [4], CCN1 (cysteine-rich protein 61) [5], and their cell-adhesive receptor, integrin β1 [6], have been shown to play roles in scleroderma, and such studies are still ongoing. Thus, investigations of the functions of ECM proteins and their signaling networks are urgently needed to elucidate the pathogenesis of scleroderma and develop new therapies.

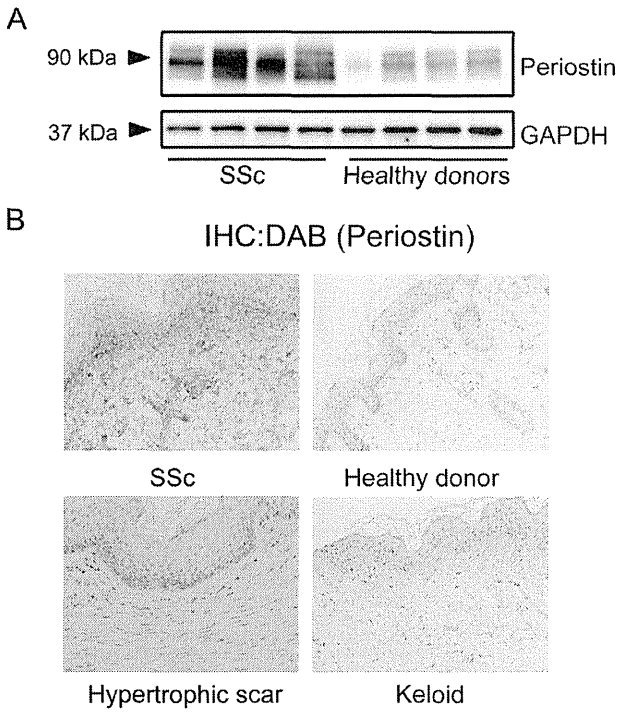

Figure 1. Periostin is overexpressed in lesional skin derived from patients with systemic scleroderma (SSc). A, *Western blotting* analysis for periostin using protein extracts from the skin of SSc patients and healthy donors. B, Representative immunohistochemistry of skin sections of SSc patients, healthy donors, hypertrophic scar and keloid patients. Slides were stained with anti-periostin antibodies (original magnification, ×100).
doi:10.1371/journal.pone.0041994.g001

To investigate the involvement of matricellular proteins in the pathogenesis of scleroderma, we focused on a novel matricellular protein, periostin, a 90-kDa, secreted, homophilic cell adhesion protein. Despite being first identified 15 years ago as osteoblast-specific factor-2 [7], periostin is now classified as a matricellular protein, because it is expressed in many collagen-rich tissues and possesses important biological functions in the ECM [8]. Periostin can bind to collagen during fibrillogenesis, thus affecting the diameter of collagen fibers and the extent of cross-linking [9,10]. Periostin also binds to other ECM proteins, including fibronectin and tenascin-C, thereby organizing the ECM architecture. Like other matricellular proteins, such as CCN1, CCN2, and CCN3 (capable of interacting with αv, β3, and β1 integrins) [11], periostin serves as a ligand for integrins αv, β1, β3, β4, and β5 [12–14]. Such signals can mediate cell adhesion to the ECM and may regulate certain cellular behaviors, including intracellular signaling, proliferation, and differentiation [15].

Analysis on periostin$^{-/-}$ ($PN^{-/-}$) mice revealed that this protein plays a pivotal role in the development of heart, bones, and teeth [16]. Approximately 14% of $PN^{-/-}$ mice die postnatally prior to weaning [17], suggesting a role of periostin in the development of these tissues. In adults, periostin is prominently upregulated during ECM remodeling and fibrosis. The major producers of periostin are fibroblasts [18,19], and its expression is induced by various factors, including TGFβ1, interleukin (IL) 4, and IL13 [19,20]. The prominent expression of periostin has been detected during a number of remodeling processes, including myocardial infarction [21], wound repair [8,22–24], fibrotic scar formation [25], sub-epithelial fibrosis in bronchial asthma [20], and bone marrow fibrosis [26]. Studies of $PN^{-/-}$ mice with experimentally induced diseases have further confirmed that periostin, in many cases, is profoundly involved in the progression of tissue fibrosis [17,27–29]. However, in a model of bronchial asthma, $PN^{-/-}$ mice developed peribronchial fibrosis equivalent